



*nanomaterials*

# The Genetic Changes Induced by Engineered Manufactured Nanomaterials (EMNs)

---

Edited by

Marta Marmiroli

Printed Edition of the Special Issue Published in *Nanomaterials*

# **The Genetic Changes Induced by Engineered Manufactured Nanomaterials (EMNs)**



# The Genetic Changes Induced by Engineered Manufactured Nanomaterials (EMNs)

Editor

**Marta Marmiroli**

MDPI • Basel • Beijing • Wuhan • Barcelona • Belgrade • Manchester • Tokyo • Cluj • Tianjin



*Editor*

Marta Marmiroli  
University of Parma  
Parma  
Italy

*Editorial Office*

MDPI  
St. Alban-Anlage 66  
4052 Basel, Switzerland

This is a reprint of articles from the Special Issue published online in the open access journal *Nanomaterials* (ISSN 2079-4991) (available at: [https://www.mdpi.com/journal/nanomaterials/special\\_issues/genetic\\_engineeredNano](https://www.mdpi.com/journal/nanomaterials/special_issues/genetic_engineeredNano)).

For citation purposes, cite each article independently as indicated on the article page online and as indicated below:

LastName, A.A.; LastName, B.B.; LastName, C.C. Article Title. <i>Journal Name</i> <b>Year</b> , <i>Volume Number</i> , Page Range.
--

**ISBN 978-3-0365-4809-8 (Hbk)**

**ISBN 978-3-0365-4810-4 (PDF)**

© 2022 by the authors. Articles in this book are Open Access and distributed under the Creative Commons Attribution (CC BY) license, which allows users to download, copy and build upon published articles, as long as the author and publisher are properly credited, which ensures maximum dissemination and a wider impact of our publications.

The book as a whole is distributed by MDPI under the terms and conditions of the Creative Commons license CC BY-NC-ND.

# Contents

<b>About the Editor</b> . . . . .	<b>vii</b>
<b>Marta Marmiroli</b>	
Special Issue “The Genetic Changes Induced by Engineered Manufactured Nanomaterials (EMNs)” Reprinted from: <i>Nanomaterials</i> <b>2022</b> , <i>12</i> , 2233, doi:10.3390/nano12132233 . . . . .	<b>1</b>
<b>Chuanxin Ma, Yi Hao, Jian Zhao, Nubia Zuverza-Mena, Ahmed G. Meselhy, Om Parkash Dhankeher, Yukui Rui, Jason C. White and Baoshan Xing</b>	
Graphitic Carbon Nitride (C <sub>3</sub> N <sub>4</sub> ) Reduces Cadmium and Arsenic Phytotoxicity and Accumulation in Rice ( <i>Oryza sativa</i> L.) Reprinted from: <i>Nanomaterials</i> <b>2021</b> , <i>11</i> , 839, doi:10.3390/nano11040839 . . . . .	<b>5</b>
<b>Valentina Gallo, Andrea Zappettini, Marco Villani, Nelson Marmiroli and Marta Marmiroli</b>	
Comparative Analysis of Proteins Regulated during Cadmium Sulfide Quantum Dots Response in <i>Arabidopsis thaliana</i> Wild Type and Tolerant Mutants Reprinted from: <i>Nanomaterials</i> <b>2021</b> , <i>11</i> , 615, doi:10.3390/nano11030615 . . . . .	<b>19</b>
<b>Daniel Lizzi, Alessandro Mattiello, Barbara Piani, Emanuele Gava, Guido Fellet and Luca Marchiol</b>	
Single and Repeated Applications of Cerium Oxide Nanoparticles Differently Affect the Growth and Biomass Accumulation of <i>Silene flos-cuculi</i> L. ( <i>Caryophyllaceae</i> ) Reprinted from: <i>Nanomaterials</i> <b>2021</b> , <i>11</i> , 229, doi:10.3390/nano11010229 . . . . .	<b>39</b>
<b>Marta Marmiroli, Nelson Marmiroli and Luca Pagano</b>	
Nanomaterials Induced Genotoxicity in Plant: Methods and Strategies Reprinted from: <i>Nanomaterials</i> <b>2022</b> , <i>12</i> , 1658, doi:10.3390/nano12101658 . . . . .	<b>53</b>
<b>Kangying Wu, Qixing Zhou and Shaohu Ouyang</b>	
Direct and Indirect Genotoxicity of Graphene Family Nanomaterials on DNA—A Review Reprinted from: <i>Nanomaterials</i> <b>2021</b> , <i>11</i> , 2889, doi:10.3390/nano11112889 . . . . .	<b>63</b>



## About the Editor

### Marta Marmiroli

Marta Marmiroli was born on 8 May 1972.

1998: Master's degree in Physics at Parma University. Thesis title: Crystal field anisotropy in the intermetallic Rare-Earth compounds with aThMn<sub>12</sub> structural type.

2002: Ph.D. in biotechnology, University of Parma, with a thesis about the applications of scanning electron microscopy, microanalysis, microfluorescence, and EXAFS to environmental biotechnology.

2005–2018: Senior Researcher at Parma University.

2018–now: Associate Professor of Plant Biotechnology at Parma University.

From 2009 till 2020: Senior Associated Editor of the *International Journal of Phytoremediation* (<http://www.tandfonline.com/action>). From 2020 till present: Editor-in-Chief of the *International Journal of Phytoremediation*, IF 2021 4.003

Since 2005, I have participated in several EU and NATO projects concerning phytoremediation, food security, and food safety. In 2010 I start working on nanomaterials in the environment and their effects on model organisms such as yeast, *Saccharomyces cerevisiae*, and plants, *Arabidopsis thaliana*. I then moved to studying nanomaterial effects in agriculture in collaboration with the CAES Connecticut Agricultural Experiment Station (CT, USA) and its director, Jason White. I still work with synchrotron-based techniques ( $\mu$ -XRF and XAS) to study nanomaterials' biotransformation in crop and model plants. I also study the effects of nanomaterials on yeast and on human cell lines.





Editorial

# Special Issue “The Genetic Changes Induced by Engineered Manufactured Nanomaterials (EMNs)”

Marta Marmiroli

Department of Chemistry, Life Science, and Environmental Sustainability, University of Parma, Parco Area delle Scienze 33/A, 43124 Parma, Italy; marta.marmiroli@unipr.it

The possibility that engineered manufactured nanomaterials (ENMs) can be harmful to the genetic materials of living individuals has been highlighted in several experiments, but it is still controversial. In fact, there is also evidence that nanoparticles are not genotoxic and do not interfere with the genetic material of organisms. It is of extreme importance to establish which nanomaterials have the potential to exert harmful effects on DNA in different types of living organisms, from simple prokaryotes to complex eukaryotes, starting from model organisms. The aims and scopes of this Special Issue are to (1) highlight the research applications that identify which ENMs are genotoxic, and which are the more susceptible organisms or cell lines, and (2) to pinpoint reliable methods to establish the genotoxicity of ENMs [1].

Because of their large-scale manufacture and widespread application, several studies related to the toxicological assessment of nanomaterials (NMs) have been conducted over the past decade. Notwithstanding the extensive research on the cytotoxicity of NMs, their possible genotoxicity is of concern due to their increased utilization [2]. As explained in one of the reviews included in this Special Issue, the number and quantity of nanomaterials is ever increasing and affecting the environment where humans, bacteria, and plants live, and their genome come in contact with nanomaterials [3]. Although the topic of genotoxicity induced by nanomaterials is important, we had only five contributions for this Special Issue: [3–8].

Marmiroli et al., 2022 [3], contributed a minireview on the methods used to analyze genotoxicity in plants. Many plant species have the capability of being used as systems for genetic assays. Different mechanisms can be utilized according to the different ENM physico-chemical properties, specifically the following: (i) ENMs are able to pass through the cellular membrane lipid bilayer; (ii) endocytosis processes, the Trojan horse mechanism and biotransformation processes drive the accumulation of ENMs in plant cells; (iii) the utilization of membrane transporters mediating the translocation into the plant cell. These phenomena cause the interaction of ENM with DNA and chromatin and standard methods to measure the damages that can be caused are revised [3].

Lizzi et al., 2021 [4], studied the effects of multiple applications of CeO<sub>2</sub> oxide nanoparticles on a wild plant, *Silene flos-cuculi*, instead of a classical crop or model plants. They measured the quantity of nanoparticles in the plants utilising a spICP-MS (Single Particle ICP-MS), and other parameters related to the plant biomass. They found that the CeO<sub>2</sub> nanoparticles translocated from roots to shoots and had adverse effect on the plant health, which indicates possible damage to the organellar DNA. However, the nanoparticles genotoxicity was not measured directly.

Ma et al., 2021 [5], analyzed the consequences of the application of Graphitic carbon nitride nanosheets (C<sub>3</sub>N<sub>4</sub>) on rice plants (*Oryza sativa*) grown on soils contaminated with Cd and As. They found that not only did the nanomaterials increase the yield of the plants, but they abated the genotoxicity caused by Cd. Cd genotoxicity was studied through the application of a random amplified polymorphic DNA (RAPD) analysis. The RAPD primer used in this assay was OPC20 (ACT TCG CCA C). They also analysed the

**Citation:** Marmiroli, M. Special Issue “The Genetic Changes Induced by Engineered Manufactured Nanomaterials (EMNs)”. *Nanomaterials* **2022**, *12*, 2233. <https://doi.org/10.3390/nano12132233>

Received: 4 June 2022

Accepted: 13 June 2022

Published: 29 June 2022

**Publisher’s Note:** MDPI stays neutral with regard to jurisdictional claims in published maps and institutional affiliations.



**Copyright:** © 2022 by the author. Licensee MDPI, Basel, Switzerland. This article is an open access article distributed under the terms and conditions of the Creative Commons Attribution (CC BY) license (<https://creativecommons.org/licenses/by/4.0/>).

expression of many transporters of As and Cd under the effect of  $C_3N_4$ , finding them mostly downregulated thanks to the presence of the nanomaterial. Therefore,  $C_3N_4$  may be a promising material that is sustainable for safe nano-enabled strategies of reducing heavy metal accumulation in key food crops grown in contaminated soils.

Gallo et al., 2021 [6], conducted a proteomic study of two *Arabidopsis thaliana* (L.) Heynh mutants resistant to lethal amounts of CdS Quantum Dot (QD) for the wild type. In fact, in a previous work, two independent *Arabidopsis thaliana* Ac/Ds transposon insertional mutant lines, atnp01 and atnp02, were identified. The tolerance response was completely characterized [7]. In this work, a comparative analysis was performed on protein extracts from plantlets of the two mutants and of wt, each treated with a sublethal concentration of CdS QDs. Two Dimension-PAGE was used to conduct a comparative protein analysis; proteins were characterized by MALDI-TOF/TOF. Ninety eight of the proteins identified showed significant changes in their relative abundance between control and CdS QD-treated plantlets. The two mutants showed a different response to the treatment regarding the type and quantity of up- and downregulated proteins. This difference became more striking when compared to wt. The proteins were analyzed through GO and MapMan to identify functions and pathways. A network analysis of the proteins differentially expressed in the two mutants showed that several of the proteins encoded by putative genes contained transposons, which were responsible for the regulation of some proteins identified in this study. These proteins included complex 3 (Elo3) which is involved in transcriptional elongation; nifu-like protein 3 (Nfu3) which is involved in chloroplast assembly; protein phosphatase 2C (PP2C) which mediates abiotic stress response; magnesium-chelate subunit-2 (Chli2) which is involved in chlorophyll biosynthesis; and other relevant proteins. The change in the protein regulation due to CdS QDs may be due to an interference of the QDs with the DNA and the transcription.

Wu and colleagues, 2021 [8], documented the possible genotoxicity of graphene in all its form to human cells. The graphene nanomaterials family (GFNs) includes graphene, graphene oxide (GO), reduced graphene oxide (rGO), and graphene quantum dots (GQDs). They have a wide range of potential applications, creating the possibility of their release into the environment which implicates exposure to humans and other organisms. However, the genotoxicity of GFNs to DNA remains largely unknown. In their review, the authors studied the interactions between DNA and GFNs and pinpointed the mechanisms of genotoxicity caused by GFNs. In general, genotoxicity can be classified into direct genotoxicity and indirect genotoxicity. The two types of genotoxicity (e.g., direct physical nucleus and DNA damage; and indirect physical destruction, oxidative stress, epigenetic toxicity, and DNA replication) of GFNs were also explored in the paper. Additionally, the influencing factors of the nanoparticles and of the type of experiment (e.g., physicochemical properties, exposure time and dose, the genotoxicity of GFNs) were taken into consideration. The authors conclude that considering the key role of genotoxicity in GFNs' exposure risk assessment, future research is warranted.

**Conflicts of Interest:** The author declares no conflict of interest.

## References

1. Available online: [https://www.mdpi.com/journal/nanomaterials/special\\_issues/genetic\\_engineeredNano](https://www.mdpi.com/journal/nanomaterials/special_issues/genetic_engineeredNano) (accessed on 20 March 2022).
2. Schulte, P.A.; Leso, V.; Niang, M.; Iavicoli, I. Current state of knowledge on the health effects of engineered nanomaterials in workers: a systematic review of human studies and epidemiological investigations. *Scand. J. Work. Environ. Health* **2019**, *45*, 217–238. [[CrossRef](#)] [[PubMed](#)]
3. Marmiroli, M.; Marmiroli, N.; Pagano, L. Nanomaterials Induced Genotoxicity in Plant: Methods and Strategies. *Nanomaterials* **2022**, *12*, 1658. [[CrossRef](#)] [[PubMed](#)]
4. Lizzi, D.; Mattiello, A.; Piani, B.; Gava, E.; Fellet, G.; Marchiol, L. Single and Repeated Applications of Cerium Oxide Nanoparticles Differently Affect the Growth and Biomass Accumulation of *Silene flos-cuculi* L. (*Caryophyllaceae*). *Nanomaterials* **2021**, *11*, 2079–4991. [[CrossRef](#)] [[PubMed](#)]

5. Ma, C.; Hao, Y.; Zhao, J.; Zuverza-Mena, N.; Meselhy, A.G.; Dhankher, O.P.; Rui, Y.; White, J.C.; Xing, B. Graphitic Carbon Nitride (C<sub>3</sub>N<sub>4</sub>) Reduces Cadmium and Arsenic Phytotoxicity and Accumulation in Rice (*Oryza sativa* L.). *Nanomaterials* **2021**, *11*, 839. [[CrossRef](#)] [[PubMed](#)]
6. Gallo, V.; Zappettini, A.; Villani, M.; Marmiroli, N.; Marmiroli, M. Comparative Analysis of Proteins Regulated during Cadmium Sulfide Quantum Dots Response in *Arabidopsis thaliana* Wild Type and Tolerant Mutants. *Nanomaterials* **2021**, *11*, 615. [[CrossRef](#)] [[PubMed](#)]
7. Marmiroli, M.; Pagano, L.; Sardaro, M.L.S.; Villani, M. Genome-Wide Approach in *Arabidopsis thaliana* to Assess the Toxicity of Cadmium Sulfide Quantum Dots. *Environ. Sci. Technol.* **2014**, *48*, 5902–5909. [[CrossRef](#)] [[PubMed](#)]
8. Wu, K.; Zhou, Q.; Ouyang, S. Direct and Indirect Genotoxicity of Graphene Family Nanomaterials on DNA—A Review. *Nanomaterials* **2021**, *11*, 2889. [[CrossRef](#)] [[PubMed](#)]





## Article

# Graphitic Carbon Nitride (C<sub>3</sub>N<sub>4</sub>) Reduces Cadmium and Arsenic Phytotoxicity and Accumulation in Rice (*Oryza sativa* L.)

Chuanxin Ma<sup>1,2</sup>, Yi Hao<sup>1,3</sup>, Jian Zhao<sup>4</sup>, Nubia Zuverza-Mena<sup>2</sup>, Ahmed G. Meselhy<sup>3</sup>, Om Parkash Dhankher<sup>3</sup>, Yukui Rui<sup>5</sup>, Jason C. White<sup>2,\*</sup> and Baoshan Xing<sup>3</sup>

- <sup>1</sup> Key Laboratory for City Cluster Environmental Safety and Green Development of the Ministry of Education, Institute of Environmental and Ecological Engineering, Guangdong University of Technology, Guangzhou 510006, China; chuanxin.ma@gdut.edu.cn (C.M.); hy0305hy@163.com (Y.H.)
  - <sup>2</sup> The Connecticut Agricultural Experiment Station, New Haven, CT 06504, USA; Nubia.Zuverza@ct.gov
  - <sup>3</sup> Stockbridge School of Agriculture, University of Massachusetts Amherst, Amherst, MA 01003, USA; ameselhy@umass.edu (A.G.M.); Parkash@umass.edu (O.P.D.); bx@umass.edu (B.X.)
  - <sup>4</sup> Ministry of Education Key Laboratory of Marine Environment and Ecology, Institute of Coastal Environmental Pollution Control, and Institute for Advanced Ocean Study, Ocean University of China, Qingdao 266100, China; zhaojian047@126.com
  - <sup>5</sup> Beijing Key Laboratory of Farmland Soil Pollution Prevention and Remediation, College of Resources and Environmental Sciences, China Agricultural University, Beijing 100193, China; ruiyukui@163.com
- \* Correspondence: jason.white@ct.gov

**Citation:** Ma, C.; Hao, Y.; Zhao, J.; Zuverza-Mena, N.; Meselhy, A.G.; Dhankher, O.P.; Rui, Y.; White, J.C.; Xing, B. Graphitic Carbon Nitride (C<sub>3</sub>N<sub>4</sub>) Reduces Cadmium and Arsenic Phytotoxicity and Accumulation in Rice (*Oryza sativa* L.). *Nanomaterials* **2021**, *11*, 839. <https://doi.org/10.3390/nano11040839>

Academic Editor: Eleonore Fröhlich

Received: 28 February 2021

Accepted: 22 March 2021

Published: 25 March 2021

**Publisher's Note:** MDPI stays neutral with regard to jurisdictional claims in published maps and institutional affiliations.



**Copyright:** © 2021 by the authors. Licensee MDPI, Basel, Switzerland. This article is an open access article distributed under the terms and conditions of the Creative Commons Attribution (CC BY) license (<https://creativecommons.org/licenses/by/4.0/>).

**Abstract:** The present study investigated the role of graphitic carbon nitride (C<sub>3</sub>N<sub>4</sub>) in alleviating cadmium (Cd)- and arsenic (As)-induced phytotoxicity to rice (*Oryza sativa* L.). A high-temperature pyrolysis was used to synthesize the C<sub>3</sub>N<sub>4</sub>, which was characterized by transmission electron microscopy, Fourier-transform infrared spectroscopy, and dynamic light scattering. Rice seedlings were exposed to C<sub>3</sub>N<sub>4</sub> at 50 and 250 mg/L in half-strength Hoagland's solution amended with or without 10 mg/L Cd or As for 14 days. Both Cd and As alone resulted in 26–38% and 49–56% decreases in rice root and shoot biomass, respectively. Exposure to 250 mg/L C<sub>3</sub>N<sub>4</sub> alone increased the root and shoot fresh biomass by 17.5% and 25.9%, respectively. Upon coexposure, Cd + C<sub>3</sub>N<sub>4</sub> and As + C<sub>3</sub>N<sub>4</sub> alleviated the heavy metal-induced phytotoxicity and increased the fresh weight by 26–38% and 49–56%, respectively. Further, the addition of C<sub>3</sub>N<sub>4</sub> decreased Cd and As accumulation in the roots by 32% and 25%, respectively, whereas the metal contents in the shoots were 30% lower in the presence of C<sub>3</sub>N<sub>4</sub>. Both As and Cd also significantly altered the macronutrient (K, P, Ca, S, and Mg) and micronutrient (Cu, Fe, Zn, and Mn) contents in rice, but these alterations were not evident in plants coexposed to C<sub>3</sub>N<sub>4</sub>. Random amplified polymorphic DNA analysis suggests that Cd significantly altered the genomic DNA of rice roots, while no difference was found in shoots. The presence of C<sub>3</sub>N<sub>4</sub> controlled Cd and As uptake in rice by regulating transport-related genes. For example, the relative expression of the Cd transporter *OsIRT1* in roots was upregulated by approximately threefold with metal exposure, but C<sub>3</sub>N<sub>4</sub> coamendment lowered the expression. Similar results were evident in the expression of the As transporter *OsNIP1;1* in roots. Overall, these findings facilitate the understanding of the underlying mechanisms by which carbon-based nanomaterials alleviate contaminant-induced phyto- and genotoxicity and may provide a new strategy for the reduction of heavy metal contamination in agriculture.

**Keywords:** rice; g-C<sub>3</sub>N<sub>4</sub>; synthesis; cadmium; arsenic; accumulation; metal transporters

## 1. Introduction

Heavy metal contamination in soils has become a major threat to global agriculture due to both direct toxicity to crops and the subsequent impacts on human health [1–3].

Heavy metals in agricultural soils can be derived from both geogenic (soils) and anthropogenic (mining, smelting, solid waste, etc.) sources [4–6]. Cadmium (Cd) and arsenic (As) are two heavy metals that are commonly found in soils [7]. Due to its elemental properties, Cd can replace Ca and cause chronic Cd poisoning, called itai-itai disease [8]. Inorganic As has been classified as a human carcinogen by the United States Environmental Protection Agency (USEPA) [9] and can also cause a series of human diseases [10]. In addition, heavy metals have caused ecotoxicological effects on soil organisms (microorganisms, plants, and animals) due to their toxicity, bioaccumulation, and persistence in environments [11–14]. According to Tóth et al., the average topsoil concentrations of Cd and As in the European Union were  $0.09 \pm 0.11$  and  $3.72 \pm 2.92$  mg/kg, respectively [15]. Similarly, Cd and As concentrations in soils in the United States were 0.2–2 and 0.4–40 mg/kg [16,17]. Heavy metal-induced phytotoxicity to crops has been extensively investigated, with detailed studies addressing metal speciation and accumulation, bioavailability, physiological responses, crop yield, and quality, as well as plant defense mechanisms [18–22]. In addition, efforts have been made to stabilize heavy metal contaminants in agricultural soils using different types of amendments (minerals, organic matters, biofertilizers, rhizosphere microbial community), which have subsequently reduced metal accumulation in crops and risk of human exposure [23–25]. Thus, it is important to not only explore novel, sustainable, and efficient strategies to reduce heavy metal uptake but also reveal the underlying interaction and uptake mechanisms to maximize benefits.

Nano-enabled techniques have been widely used in agriculture for the purposes of monitoring plant health, enhancing crop yield, and suppressing abiotic and biotic stresses [26–29]. A number of recent studies have demonstrated positive impacts of both metal- and carbon-based nanomaterials on alleviating contaminant-induced abiotic stress and toxicity. For example, Ma et al. (2020) reported that zinc oxide (ZnO) nanoparticles (NPs) could significantly reduce the Cd and As accumulation in rice tissues when grown in metal co-contaminated rice paddies, including reduced grain contamination [7]. Similar findings of ZnO NPs alleviating heavy metal toxicity to *Leucaena leucocephala* seedlings were also reported [30]. Other metal-based NPs, such as TiO<sub>2</sub> [31,32] and CuO [33], also exhibited positive impacts by alleviating heavy metal phytotoxicity and enhancing crop growth. With regard to carbon-based nanomaterials, most of the studies have been conducted to facilitate understanding of the interactions between nanomaterials and contaminants [34–37]. Only a small number of studies have evaluated the impacts of carbon-based nanomaterials on alleviating contaminant-induced toxicity to crops. For example, nanoscale biochar reduced Cd accumulation in rice and subsequently ameliorated Cd-induced phytotoxicity as measured by plant growth, pigment production, and lipid peroxidation [38]. In addition, Jia et al. (2020) reported that magnetic carbon nanotubes altered phenanthrene and associated metabolite accumulation in lettuce, suggesting this approach as a novel strategy for soil remediation [39]. Additional investigations exploring the potential of sustainable carbon-based nanomaterials to reduce heavy metal accumulation and phytotoxicity to crops are needed.

Graphitic carbon nitride nanosheets (C<sub>3</sub>N<sub>4</sub>) have attracted attention in recent years due to their unique structure and excellent catalytic properties. Containing only carbon and nitrogen, C<sub>3</sub>N<sub>4</sub> can be easily synthesized using low-cost nitrogen-enriched compounds such as urea and melamine under heat condensation [40–42]. Xiao et al. (2019) reported the superior adsorption performance of C<sub>3</sub>N<sub>4</sub> for heavy metal removal from wastewater; the maximum adsorption capacities of Cd, lead (Pb), and chromium (Cr) were approximately 123, 37, and 684 mg/g, respectively [43]. Similar results were demonstrated for C<sub>3</sub>N<sub>4</sub> quantum dots (QD) removal of mercury chloride (HgCl<sub>2</sub>), with a binding efficiency of 24.63 mg HgCl<sub>2</sub>/10 mg C<sub>3</sub>N<sub>4</sub> [44]. However, biotic and in vivo experiments investigating C<sub>3</sub>N<sub>4</sub> potential for reducing heavy metal accumulation in crops are very limited. Hao et al. (2021) reported that C<sub>3</sub>N<sub>4</sub> not only significantly reduced the Cd content of rice tissues but also increased the nitrogen content to offset the Cd-induced nitrogen deficiency [45].

However, a mechanistic understanding of  $C_3N_4$  regulation of heavy metal transporters at the molecular level remains elusive.

Rice, a semiaquatic annual grass species, is the most important cereal crop in developing countries and the most consumed staple food all over the world [46]. In the present study, rice (*Oryza sativa* L.) seedlings were hydroponically exposed to  $C_3N_4$  and Cd- or As-amended nutrient solutions under greenhouse conditions for 14 days. At harvest, physiological parameters and elemental content of rice tissues were measured across all treatments. In addition, the relative expression of Cd- and As-related transporters was analyzed as affected by  $C_3N_4$  and both Cd and As. The findings provide important information on the role of  $C_3N_4$  in reducing Cd and As bioavailability and subsequent phytotoxicity to crops. More importantly, the work further demonstrates the use of sustainable nano-enabled techniques as a novel strategy for soil remediation to ensure a safe food supply.

## 2. Materials and Methods

### 2.1. $C_3N_4$ Synthesis and Characterization

Graphitic carbon nitride nanosheets ( $C_3N_4$ ) were synthesized with urea (20 g) in a vacuum tube furnace. The ramping rate was  $5\text{ }^\circ\text{C}/\text{min}$ , and the temperature was kept at  $550\text{ }^\circ\text{C}$  under nitrogen flow for 4 h [47]. The synthesized  $C_3N_4$  was cooled down to ambient temperature in the vacuum tube furnace and then washed with deionized water three times. The  $C_3N_4$  yield in each batch was approximately 2% (*w/w*). The procedures were repeated several times to prepare sufficient  $C_3N_4$  for experimentation. All batches of  $C_3N_4$  were mixed thoroughly and then freeze-dried in a lyophilizer ( $<1.5\text{ mbar}$ ,  $-50\text{ }^\circ\text{C}$ , FreeZone<sup>®</sup> Benchtop Freeze Dryers, Model 70020, Labconco Corporation, Kansas City, MO, USA)

For imaging characterization, the synthesized  $C_3N_4$  was dispersed in deionized water and a small volume diluted with methanol (1:1 *v/v*). One drop ( $2\text{ }\mu\text{L}$ ) was deposited onto carbon-coated Cu grids and left to dry at room temperature. Images were taken in a Hitachi model HT7800 transmission electron microscope equipped with a lanthanum hexaboride ( $\text{LaB}_6$ ) filament in high contrast mode at an accelerating voltage (HV) of 80 kV. (Hitachi Incorporation, Tokyo, Japan)

For analysis by Fourier-transform infrared spectroscopy (FTIR, Spectrum One, PerkinElmer Inc, Waltham, MA, USA) equipped with the universal ATR sampling accessory, approximately 50 mg  $C_3N_4$  was pressed into a thin layer and loaded onto the instrument's crystal; the samples were scanned, and spectra of  $C_3N_4$  in the range of  $450\text{--}4000\text{ cm}^{-1}$  were collected [48].

In addition, 50 and 250 mg/L  $C_3N_4$  suspensions were separately prepared in deionized water and half-strength Hoagland's solution. Hydrodynamic diameter and zeta potential were measured by dynamic light scattering (90 Plus Particle Size Analyzer, Brookhaven, Upton, NY, USA) [48].

### 2.2. Hydroponic Experimental Design

Rice seeds (*Oryza sativa* L.) were sterilized with 70% (*v/v*) ethanol for 10 min and rinsed three times with deionized water. The sterilized seeds were germinated and grown in vermiculite for 2 weeks prior to the hydroponic experiment. Vermiculite on the root surfaces was gently removed in tap water, and then plants were transferred into a 100 mL glass jar containing half-strength Hoagland's solution (mg/L: 57.52 ammonium phosphate, monobasic; 1.43 boric acid; 328.2 calcium nitrate; 0.04 cupric sulfate·5H<sub>2</sub>O; 1.68 Na<sub>2</sub>EDTA·2H<sub>2</sub>O; 1.3 ferrous sulfate·7H<sub>2</sub>O; 120.38 magnesium sulfate, anhydrous; 0.91 manganese chloride·4H<sub>2</sub>O; 0.008 molybdenum trioxide; 303.3 potassium nitrate; 0.11 zinc sulfate·7H<sub>2</sub>O, PhytoTechnology Laboratories Inc., Lenexa, KS, USA). After a 5-day acclimation period, rice seedlings were exposed to 50 and 250 mg/L  $C_3N_4$  with or without 10 mg/L As (sodium arsenate, Na<sub>3</sub>AsO<sub>4</sub>) or Cd (cadmium chloride, CdCl<sub>2</sub>); additionally, As and Cd single analyte exposures were established as metal controls. Five biological replicates were established for

each treatment. The plants were grown for 14 days. At harvest, all seedlings were rinsed with deionized water three times to remove the surface-attached  $C_3N_4$  and As and Cd. The fresh biomasses of shoots and roots across all treatments were recorded, and all tissues were stored at  $-80\text{ }^\circ\text{C}$  until further analysis.

### 2.3. Elemental Analysis of Rice Tissues

Shoot and root samples were freeze-dried in a lyophilizer and then ground into fine powder. Approximately 50 and 150 mg of root or shoot tissue were weighed into digestion tubes containing 3 mL concentrated  $HNO_3$ . The mixtures were digested at  $115\text{ }^\circ\text{C}$  for 40 min in a heat block and then cooled to ambient temperature. To complete the digestion, 500  $\mu\text{L}$   $H_2O_2$  was added to each tube for another 20 min of heating at  $115\text{ }^\circ\text{C}$ . The cooled digests were diluted to 25 mL with deionized water. Inductively coupled plasma optical emission spectrometry (ICP-OES; iCAP 6500, Thermo Fisher Scientific, Waltham, MA, USA) was used to determine the As, Cd, and nutrient element (macronutrients (P, S, Ca, Mg, and K) and micronutrients (Cu, Fe, Mn, and Zn)) contents in the acid digested samples [49]. Yttrium (Y) was used as an internal standard, and a sample of known concentration was measured at every 30 samples.

### 2.4. Real-Time Quantitative PCR Analysis of As and Cd Transporters in Rice

Fresh tissues of all five biological replicates in each treatment with 250 mg/L  $C_3N_4$  were ground into a fine powder in liquid nitrogen. A Sigma-Aldrich Spectrum Plant Total RNA kit (Sigma-Aldrich Corp. St. Louis, MO, USA) was used to isolate total RNA from roots and shoots. The total RNA concentration and quality were determined by a Thermo Scientific NanoDrop Lite Spectrophotometer (NanoDrop 2000, Thermo Fisher Scientific, Waltham, MA, USA). One microgram of the extracted RNA was used as template to synthesize complementary DNA (cDNA) with a Verso cDNA synthesis kit. A complete list of primer sequences for As and Cd transporters is provided in Table S1 [50–52]. The synthesized cDNA was diluted to 50 ng/ $\mu\text{L}$ , and was used as the template for the following qPCR analysis. Bio-Rad SsoAdvanced Universal SYBR Green Supermix (Bio-Rad Incorporation, Hercules, CA, USA) was used to run the qPCR, and the working concentration of each primer was 10  $\mu\text{M}$ . The thermal program profile for qPCR amplification was  $95\text{ }^\circ\text{C}$  for 30 s,  $95\text{ }^\circ\text{C}$  for 15 s, and  $63\text{ }^\circ\text{C}$  for 30 s, repeating 40 cycles, melting curve from 65 to  $95\text{ }^\circ\text{C}$ . The total volume of each reaction was 20  $\mu\text{L}$ , and histone H3 was used as a housekeeping gene for normalization. The relative expression of each gene was calculated through the  $2^{-\Delta\Delta C_t}$  method [53].

### 2.5. Random Amplified Polymorphic DNA (RAPD) Analysis

The total DNA of shoots and roots in the treatments with 250 mg/L  $C_3N_4$  with or without the addition of As or Cd and the treatments with As or Cd alone were extracted using a Qiagen DNeasy Plant Mini Kit. Random (Qiagen Incorporation, Germantown, MD, USA) amplified polymorphic DNA (RAPD) analysis was performed using Taq DNA polymerase with a standard Taq buffer. The amplification profile was  $92\text{ }^\circ\text{C}$  for 1 min,  $35\text{ }^\circ\text{C}$  for 1 min, and  $72\text{ }^\circ\text{C}$  for 2 min, and the cycle was repeated 39 times. The RAPD primer used in this assay was OPC20 (ACT TCG CCA C) [54]. PCR products were run in 1% agarose gel, and images were taken under UV light in a gel dock.

### 2.6. Statistical Analysis

For each assay, the means of four to five replicates were calculated; error bars represent the standard error of the mean. A one-way analysis of variance (one-way ANOVA) followed by Duncan's multiple comparison test was used to determine statistical significance at  $p < 0.05$  across all treatments. For gene expression, a Student's *t*-test was used to determine statistical difference ( $p < 0.05$  or  $p < 0.01$ ) between the control and each treatment.

### 3. Results and Discussion

#### 3.1. C<sub>3</sub>N<sub>4</sub> Characterization

Figure 1A,B shows the morphology of the synthesized C<sub>3</sub>N<sub>4</sub>. The FTIR spectra demonstrate characteristic peaks at 810 cm<sup>-1</sup> and 1600–1200 cm<sup>-1</sup> (Figure 1C), corresponding to the breathing mode of triazine units and the stretching mode of CN heterocycles, respectively [55]. All of this indicates successful C<sub>3</sub>N<sub>4</sub> synthesis. The zeta potential value indicates that C<sub>3</sub>N<sub>4</sub> was negatively charged (−18 to −24 mV in both deionized water and nutrient solutions); half-strength Hoagland's solution further decreased the zeta potential as compared with deionized water. The hydrodynamic diameters of C<sub>3</sub>N<sub>4</sub> in half-strength Hoagland's solution and deionized water were similar at 50 mg/L. However, at 250 mg/L, the hydrodynamic diameters of C<sub>3</sub>N<sub>4</sub> in half-strength Hoagland's solution and deionized water were decreased to approximately 600 and 250 nm, respectively (Figure 1D). The possible explanation could be that a high concentration of C<sub>3</sub>N<sub>4</sub> simply formed large aggregates, which could settle faster in the solution.

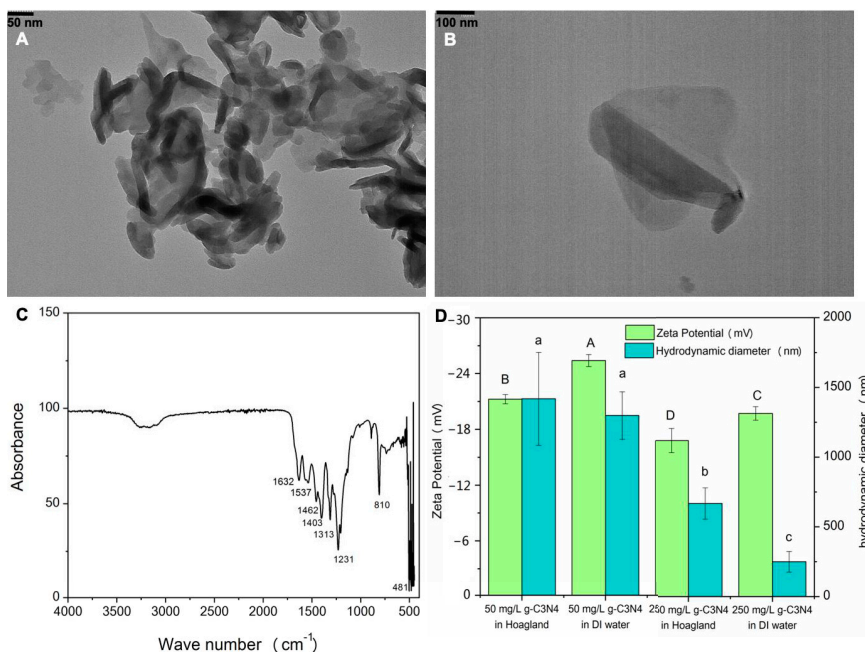


**Figure 1.** Characterization of C<sub>3</sub>N<sub>4</sub> nanosheets. (A,B) represent TEM images of C<sub>3</sub>N<sub>4</sub>; (C) shows FTIR scheme 3, N<sub>4</sub>; (D) shows the hydrodynamic diameter and zeta potential of C<sub>3</sub>N<sub>4</sub> in deionized water (DI) water and half-strength Hoagland's solution. Values of zeta potential followed by different uppercase letters are significantly different at  $p < 0.05$ ; values of hydrodynamic diameter followed by different lowercase letters are significantly different at  $p < 0.05$ .

#### 3.2. Fresh Biomass

After a 14-day exposure, 50 and 250 mg/L C<sub>3</sub>N<sub>4</sub> stimulated the growth of rice as plants grew better than the untreated controls (Figure S1). In the treatments with Cd or As, phenotypic images show overt phytotoxicity to rice in terms of the shoot size; the addition of different concentrations of C<sub>3</sub>N<sub>4</sub> alleviated both As- and Cd-induced toxicity and notably elevated the aboveground biomass (Figure 2A,B). In the C<sub>3</sub>N<sub>4</sub> alone treatment, exposure to 250 mg/L increased the fresh mass of roots and shoots by 17.5% and 25.9%, respectively. Although the presence of 50 mg/L C<sub>3</sub>N<sub>4</sub> also increased the fresh weight of both tissues, large variance across the five biological replicates caused the statistical significance to be

elusive. In the heavy metal alone treatments, both Cd and As resulted in 26–38% and 49–56% decreases in rice root and shoot biomass, respectively, when compared with the corresponding control (Figure 2C,D). It is notable that Cd induced greater phytotoxicity to rice than As. However, the addition of different concentrations of  $C_3N_4$  alleviated the heavy metal-induced toxicity, leading to significant increases in aboveground biomass in a dose-dependent fashion. The addition of 250 mg/L  $C_3N_4$  increased the Cd-treated root and shoot fresh mass by approximately 47% and 50%, respectively, relative to the Cd alone treatment (Figure 2C,D). Similarly, approximately 51% and 29% increases were evident in As-treated roots and shoots upon exposure to 250 mg/L  $C_3N_4$  (Figure 2C,D). Similarly, Hao et al. (2021) reported that the addition of 200 mg/L  $C_3N_4$  increased the shoot height and root length of Cd-treated rice by 14% and 42%, respectively, relative to the Cd alone treatment. Additionally, the authors reported a 20% increase in rice fresh weight upon cotreatment with Cd and  $C_3N_4$ , but a low dose of  $C_3N_4$  (20 mg/L) had no impact on enhancing the biomass of Cd-treated rice [45]. Nanoscale biochar amendment also increased the dry weight of Cd-treated rice tissues by approximately 20–40% relative to the Cd control; the pigment content in the Cd-treated rice showed a dose-dependent increase with greater nanoscale biochar doses [38]. Conversely, although alkaline fertilizer amendment with or without Mn reduced Cd accumulation in rice, the yield was not significantly altered as compared with the Cd control [56]. The coexposure of nanomaterials and an organic contaminant,  $TiO_2$  NPs, also alleviated the tetracycline-induced toxicity to *Arabidopsis* and rice [57,58], suggesting the significant potential of nanoscale materials as amendments for soil remediation, or alleviated heavy metal phytotoxicity.

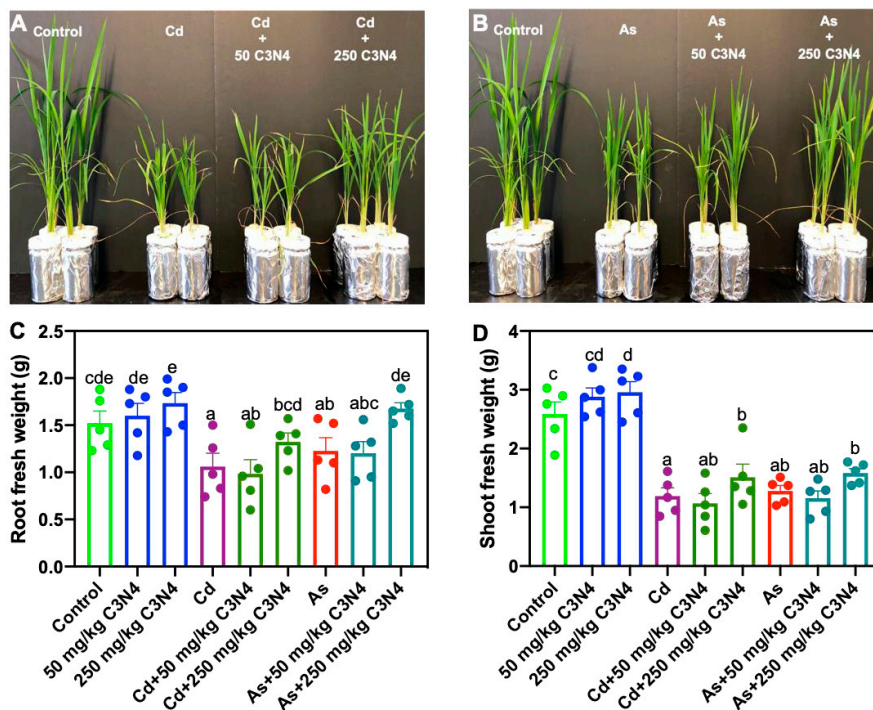


**Figure 2.** Phenotypic images and fresh weight of rice treated with Cd, As, and  $C_3N_4$ . (A,B) represent rice images as affected by Cd  $\times$   $C_3N_4$  and As  $\times$   $C_3N_4$  for 14 days, respectively. (C,D) show the fresh biomass of rice roots and shoots across all the treatments, respectively. Values of fresh weight followed by different letters are significantly different at  $p < 0.05$ .

### 3.3. Cd and As Content in Rice Tissues

In the As and Cd alone treatments, the shoot and root Cd contents were 105 and 1643 mg/kg, which were 3.5- and 2.3-fold of the As contents in shoot and root tissues, respectively (Figure 3). The Cd and As contents in rice tissues were reduced upon exposure to 250 mg/L  $C_3N_4$ , particularly the roots (Figure 3). For example, addition of 250 mg/L  $C_3N_4$  decreased the Cd contents in roots and shoots by 32% and 35%, respectively, as compared with the control. However, due to large variance of the shoot Cd content, the decrease was statistically insignificant as compared with the Cd alone treatment (Figure 3A). Similarly, 250 mg/L  $C_3N_4$  resulted in approximately 25% and 36% decrease in As in the roots and shoots, respectively (Figure 3B), clearly demonstrating the potential of  $C_3N_4$  to alter the heavy metal and metalloid uptake and distribution in rice. It is worth noting that the Cd and As translocation factors were not significantly altered as compared with the respective metal controls (data not shown). Exposure to 50 mg/L  $C_3N_4$  had no impact on Cd and As contents. Yue et al. (2020) also reported that nanoscale biochar beyond 500 mg/kg reduced the Cd content in rice tissues by more than 50% and significantly outperformed bulk-sized biochar [38]. Metal-based NPs have also been shown to decrease the bioavailability of heavy metals to crop species. Sharifan et al. (2019) demonstrated that ZnO NPs' exposure reduced the Cd contents in lettuce roots and shoots by 49% and 30%, respectively [59]. Similarly, both bulk- and nano-sized  $TiO_2$  NPs reduced the Pb accumulation in rice [60]. In the current study, we hypothesize that the adsorption of As and Cd onto the  $C_3N_4$  surface in the rhizosphere subsequently reduces metal bioavailability [43].

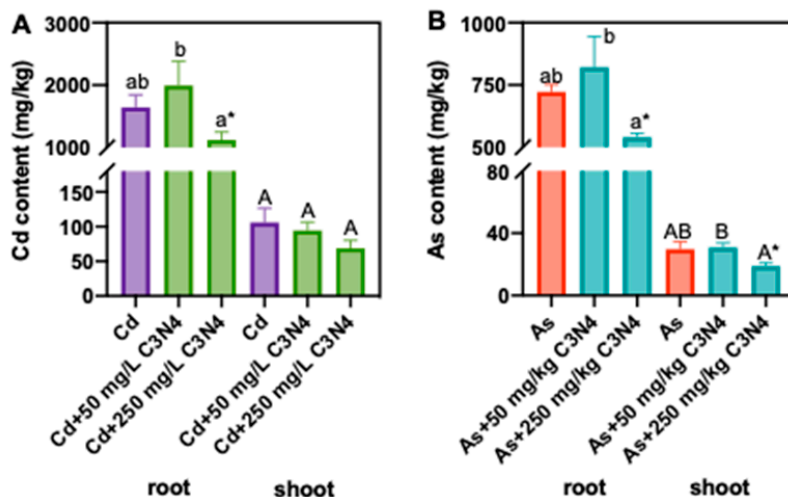


**Figure 3.** The Cd (A) and As (B) contents in rice roots and shoots upon exposure to As or Cd with or without the addition of  $C_3N_4$ . Values of As or Cd contents in roots followed by different lowercase letters are significantly different at  $p < 0.05$ ; values of As or Cd contents in shoots followed by different uppercase letters are significantly different at  $p < 0.05$ . Single asterisk “\*” indicates the significant difference between control and each treatment at  $p < 0.05$  using a Student’s *t*-test.

### 3.4. Macro- and Micronutrient Content Analysis in Rice Tissues

Both macro- and micronutrients are involved in critical metabolism and development processes throughout the plant life cycle [61]. Upon exposure to abiotic stressors, such as heavy metals, displacement of nutrient uptake and distribution in rice could result in phytotoxicity and may trigger plant defense mechanisms. Consequently, the macro- and micronutrient contents of rice tissues upon coexposure to Cd or As and  $C_3N_4$  were measured. Exposure to both Cd and As significantly altered rice root and shoot macronutrients, although the observed changes were metal specific (Figure 4 and Figure S2). For example,

exposure to Cd increased shoot P content by more than 90% as compared with controls, regardless of the  $C_3N_4$  presence (Figure 4B), whereas no difference was found with As treatments (Figure 4B). Similarly, the shoot S content was increased by more than 40% and 60% upon Cd treatments as compared with the control and the As treatments, respectively (Figure 4D). Exposure to As led to decreases in the tissue macronutrient content relative to the Cd treatments. For example, the lowest K contents in both roots and shoots were evident in the As-treated tissues, regardless of the presence of  $C_3N_4$  (Figure S2C,D). Similar results were also observed for the shoot S, Ca, and Mg contents (Figure 4D,F and Figure S2B). Importantly, the addition of  $C_3N_4$  had little impact on macronutrient content, the exception being shoot S and Ca in the 250 mg/L  $C_3N_4$  treatment, where the contents were significantly higher than those in the control (Figure 4D,F).

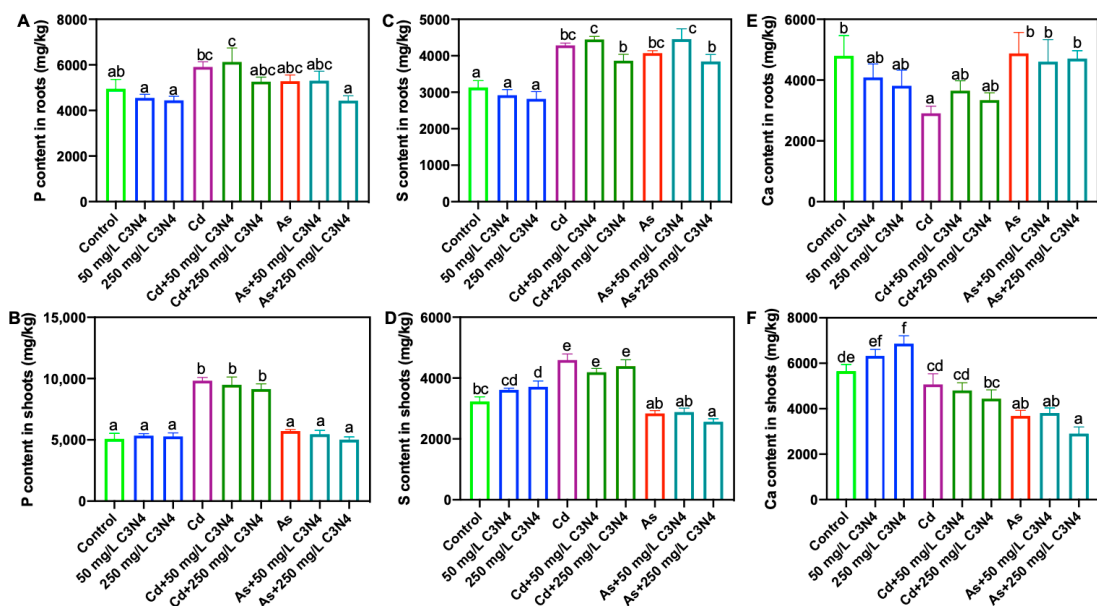


**Figure 4.** The contents of macronutrients in rice roots and shoots upon exposure to As and Cd with or without the addition of  $C_3N_4$ . (A,C,E) represent the P, S, and Ca contents in rice roots across all treatments, respectively. (B,D,F) represent the P, S, and Ca contents in rice shoots across all treatments, respectively. Values of each nutrient content in shoots followed by different letters are significantly different at  $p < 0.05$ .

In general, changes to the tissue micronutrient content were of a lesser magnitude than those to the macronutrient content, although some statistically significant changes were evident (Figure 5). For example, the Cu contents in roots cotreated with As and  $C_3N_4$  were significantly lower than those in the control (Figure 5A). Similarly, root Fe content in the Cd treatments with or without  $C_3N_4$  was increased by more than 100% relative to the control (Figure 5C); additionally, 50–80% increases in the shoot Zn contents were found in the Cd treatments, regardless of  $C_3N_4$  exposure (Figure 5G). In comparison with Cd, As exerted less impact on micronutrient displacement in rice, the exception being shoot Fe, where the Fe content was decreased by 20% relative to the control (Figure 5D). Overall, the nutrient analysis demonstrates that heavy metal exposure can induce nutrient displacement in rice and that  $C_3N_4$  amendment has little impact on these alterations.

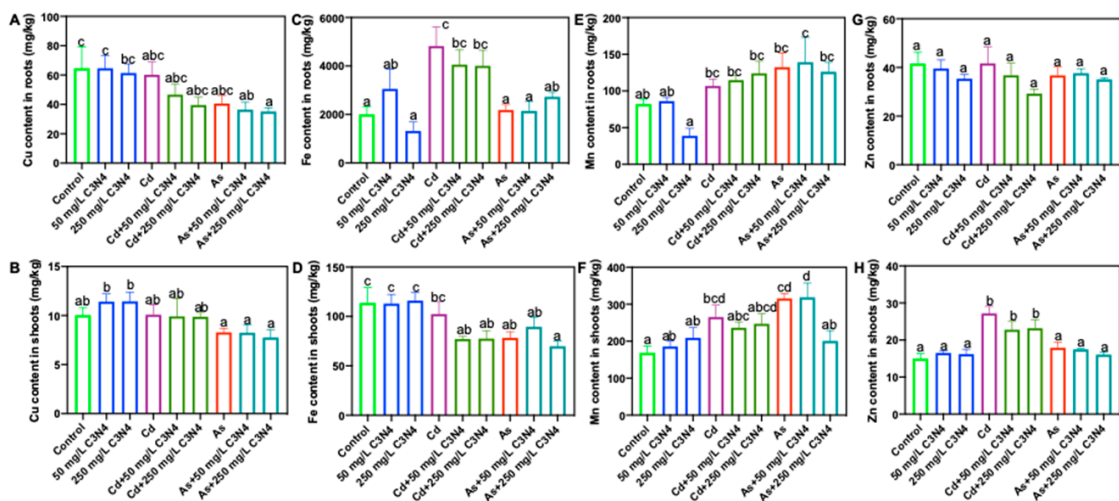


**Figure 5.** The contents of micronutrients in rice roots and shoots upon exposure to As and Cd with or without the addition of  $C_3N_4$ . (A,C,E,G) represent the Cu, Fe, Mn, and Zn contents in rice roots across all treatments, respectively. (B,D,F,H) represent the Cu, Fe, Mn, and Zn contents in rice shoots across all treatments, respectively. Values of each nutrient content in roots followed by different letters are significantly different at  $p < 0.05$ .

Nutrient displacement and dysfunction induced by exposure to heavy metals or other contaminants can severely compromise crop health. For example, tetracycline reduced the macronutrient (K, P, and S) contents of rice by approximately 20% relative to the control [58]. High doses of metal-based NPs, such as Ag,  $CeO_2$ , and  $In_2O_3$ , can significantly decrease Fe content and subsequently compromise plant metabolism [49,62]. No published studies have reported on the levels of mineral nutrients in crops affected by  $C_3N_4$  exposure. It is worth noting that the addition of  $C_3N_4$  had little impact on nutrient accumulation in rice, suggesting that the mode of action may be through stabilization of heavy metals in soils.

### 3.5. Plant Molecular Response

#### 3.5.1. RAPD Analysis upon Exposure to $C_3N_4$ and Heavy Metals

RAPD was employed to assess the potential of both  $C_3N_4$  and heavy metals to induce DNA damages in rice. In shoot tissues, the amplicon sizes of all bands were between 500–1500 bp, and there were no significant changes in the total number of DNA bands across all  $C_3N_4$  and heavy metal treatments relative to the control. In root tissues, the presence of Cd significantly altered the total number of DNA bands. Two additional DNA bands (>1500 bp) were evident in the Cd alone treatment, and one band (>1500 bp) was found in the cotreatment with Cd and  $C_3N_4$ . Conversely, the total number of DNA bands was unchanged upon As treatment (Figure S3), indicating that Cd had more negative impact on rice DNA than As.  $C_3N_4$  had no significant impact on the total number of DNA bands in rice tissues. These findings align with those of Venkatachalam et al., who reported that 50 mg/L Cd caused an additional band at 1100 bp in exposed *Leucaena leucocephala* seedlings; conversely, ZnO NPs alone had no impact relative to the control [30]. Mosa et al. (2018) used three different primers (OPA7, OPA8, and OPA9) in cucumber to demonstrate that copper NPs induced additional bands as compared with the corresponding control, suggesting that copper NPs can also cause genomic alteration [63].

#### 3.5.2. Relative Expression of Cd and As Transporters

In order to explore the underlying mechanisms by which  $C_3N_4$  altered heavy metal accumulation in rice, the relative expressions of Cd- and As-related transporters in root and shoot tissues were evaluated (Figure 6, Figure 7, Figure S4 and S5). The relative expression

of rice iron-regulated transporter 1, *OsIRT1*, in roots in the Cd alone treatment was upregulated by approximately threefold of the control; however, the addition of  $C_3N_4$  reduced this expression by 25% (Figure 6A). No difference was noted in the expression of the other IRT gene (*OsIRT2*) in the roots with Cd alone or with coexposure to  $C_3N_4$  (Figure 6B). However, the addition of  $C_3N_4$  significantly reduced the Cd-related transporter expression of rice heavy metal P-type ATPases (*OsHMA2* and *OsHMA3*) and natural resistance-associated macrophage protein 5 (*OsNramp5*) in metal-treated roots (Figure 6C,D,F). The expression of *OsNramp1* was rather insensitive to Cd exposure, with an expression increase less than 50% of the control. Although  $C_3N_4$  slightly increased the *OsNramp1* expression, the increase was also less than 50% as compared with the control and the Cd alone treatment (Figure 6E). In the shoots, the relative expression of Cd-related transporters was not significantly upregulated upon exposure relative to the control (Figure S4A–E), with the exception being *OsNramp5*, whose level was approximately 50% higher than that of the control (Figure S4F).

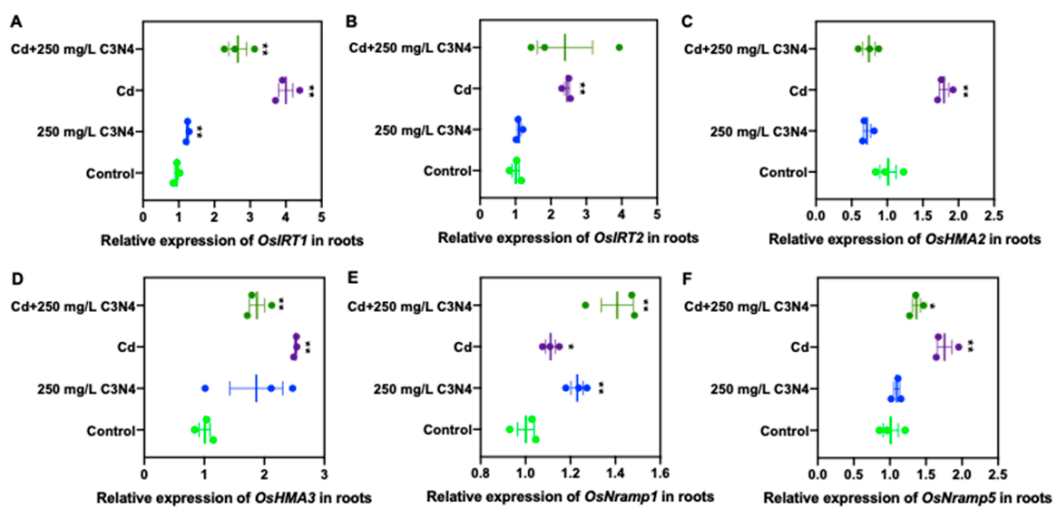


**Figure 6.** The relative expression of Cd transport-associated genes in rice roots upon exposure to Cd with or without the addition of  $C_3N_4$ . (A,B) represent the relative expression of Fe-regulated transporters *IRT1* and *IRT2*, respectively, in roots. (C,D) represent the relative expression of heavy metal ATPases *HMA2* and *HMA3*, which mediate the Cd loading and translocation from roots to shoots, in roots. (E,F) show the relative expression of the natural resistance-associated macrophage proteins *Nramp1* and *Nramp5*, respectively, in rice roots affected by As and  $C_3N_4$ . Single asterisk “\*” indicates the significant difference between control and each treatment at  $p < 0.05$ ; double asterisks “\*\*” indicate the significant difference between control and each treatment at  $p < 0.01$  using a Student’s *t*-test.

With regard to As-related transporters (both arsenite and arsenate), exposure to As induced upregulation of rice nodulin 26-like intrinsic proteins, *OsNIP1;1*, and phosphate transporter, *OsPT4*, in the roots relative to the control (Figure 7D,E). Either the expression of the remaining genes was increased by less than 50% of the control, or no change was evident upon exposure to As and  $C_3N_4$  (Figure 7A–C). Downregulation of the *OsPT8* expression was evident in both the As alone and cotreatment with  $C_3N_4$  (Figure 7F). Similarly, in shoots the regulation of As-related transporters in the As treatments was similar to the control (<50% change) (Figure S5). However, the addition of  $C_3N_4$  downregulated the expression of low silica transporters, *Lsi1* and *Lsi2*, and *OsPT4* in shoot tissues (Figure S5A,B,E).

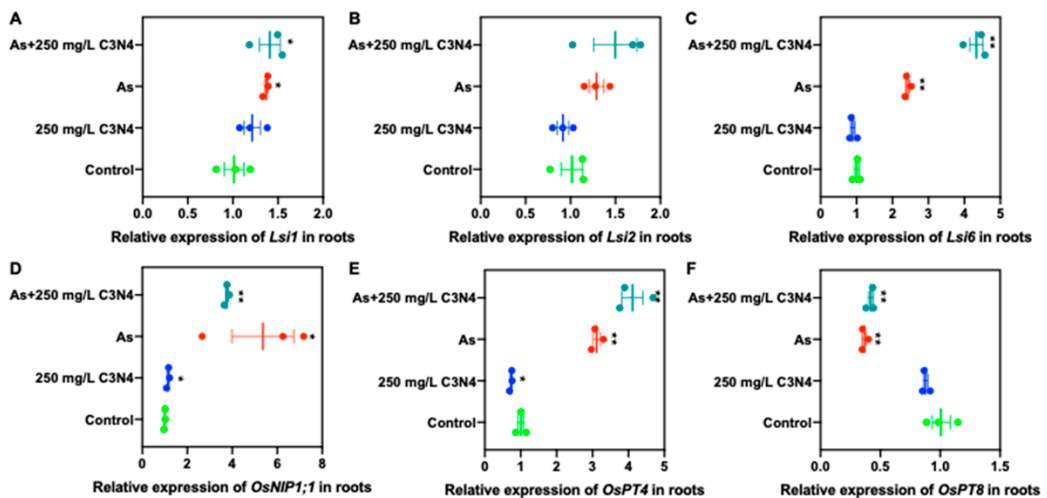


**Figure 7.** The relative expression of As transport-associated genes in rice roots upon exposure to As with or without the addition of C<sub>3</sub>N<sub>4</sub>. (A–C) represent the relative expression of the Si transport-related genes (*Lsi1*, 2, and 6), which have a demonstrated association with arsenite transport in roots. (D) shows the relative expression of nodulin 26-like intrinsic proteins (*NIPs1;1*) associated with arsenite uptake in roots. (E,F) show the relative expression of the Pht1 family genes, *OsPT1* and *OsPT8*, involving arsenate uptake, respectively, in rice roots as affected by As and C<sub>3</sub>N<sub>4</sub>. Single asterisk “\*” indicates the significant difference between control and each treatment at  $p < 0.05$ ; double asterisks “\*\*” indicate the significant difference between control and each treatment at  $p < 0.01$  using a Student’s *t*-test.

The expression and function of genes involved in Cd and As transport in rice have been extensively studied. In the present work, exposure to Cd upregulated both *OsIRTs* in rice, which is consistent with the amounts of Fe and Cd detected in rice tissues. Similar results were reported by Jiang et al. (2020), who demonstrated that Cd transporter-related genes were elevated in rice upon exposure to Cd, while the presence of glutamate lowered their expression and consequently reduced the Cd uptake [52]. Ma et al. (2016) also demonstrated that the expression of Fe-related transporters in *Arabidopsis* was downregulated upon CeO<sub>2</sub> NP treatment, which could explain the reduced Fe content as compared with the control [49]. Regarding As, aquaporin-related genes in wheat and tomato were notably upregulated upon exposure to graphene and As; additionally, coexposure to these two analytes could result in relatively higher expression of these genes relative to the single analyte treatments [64].

#### 4. Conclusions

In summary, C<sub>3</sub>N<sub>4</sub> significantly alleviated Cd- and As-induced phytotoxicity to rice without exerting any additional or unique negative impact on plant growth as determined by phenotype and biomass. In addition, C<sub>3</sub>N<sub>4</sub> modulated the expression of Cd and As transporter genes and subsequently reduced contaminant accumulation or bioavailability, offering one of the mechanistic insights into the observed effects. Further investigation evaluating grain yield and quality in rice coexposed to heavy metals and C<sub>3</sub>N<sub>4</sub> is warranted. Overall, the present work demonstrates that C<sub>3</sub>N<sub>4</sub> nanosheets are able to alleviate the phytotoxicity and reduce the accumulation of Cd and As in rice. Therefore, the use of C<sub>3</sub>N<sub>4</sub> is a promising material to be studied as a sustainable and safe nano-enabled strategy for reducing heavy metal accumulation in important food crops grown in contaminated soils.

**Supplementary Materials:** The following are available online at <https://www.mdpi.com/2079-4991/11/11/839/s1>, Figure S1: Phenotypic image of rice treated with 50 and 250 mg/L C<sub>3</sub>N<sub>4</sub> for 14 days; Figure S2: The content of macronutrients (Mg and K) in rice roots and shoots upon exposure to

As, Cd with or without the addition of C3N4; Figure S3: Random Amplified Polymorphic DNA (RAPD) analysis with random oligonucleotide primer OPC20; Figure S4: The relative expression of Cd transport-associated genes in rice shoots upon exposure to Cd with or without the addition of C3N4; Figure S5: The relative expression of As transport-associated genes in rice shoots upon exposure to As with or without the addition of C3N4; Table S1: A list of used primers.

**Author Contributions:** Conceptualization, C.M., J.C.W. and B.X.; methodology, C.M. and Y.H.; formal analysis, C.M., Y.H. and J.C.W.; investigation, C.M., Y.H., J.Z., N.Z.-M. and A.G.M.; resources, J.C.W. and B.X.; data curation, C.M. and J.C.W.; writing—original draft preparation, C.M.; writing—review and editing, C.M., O.P.D., Y.R., J.C.W. and B.X.; supervision, J.C.W. and B.X.; project administration, J.C.W. and B.X.; funding acquisition, J.C.W. and B.X. All authors have read and agreed to the published version of the manuscript.

**Funding:** This research was supported by the Program for Guangdong Introducing Innovative and Entrepreneurial Teams (2019ZT08L213) and USDA NIFA and Hatch Programs (MAS 00549 and CONH00147).

**Institutional Review Board Statement:** Not applicable.

**Informed Consent Statement:** Not applicable.

**Data Availability Statement:** Data is contained within the article or supplementary material.

**Acknowledgments:** This work is supported by the Program for Guangdong Introducing Innovative and Entrepreneurial Teams (2019ZT08L213) and USDA NIFA and Hatch Programs (MAS 00549 and CONH00147).

**Conflicts of Interest:** The authors declare no conflict of interest.

## References

- Hou, D.; O'Connor, D.; Igalavithana, A.D.; Alessi, D.S.; Luo, J.; Tsang, D.C.W.; Sparks, D.L.; Yamauchi, Y.; Rinklebe, J.; Ok, Y.S. Metal contamination and bioremediation of agricultural soils for food safety and sustainability. *Nat. Rev. Earth Environ.* **2020**, *1*, 366–381. [CrossRef]
- Podgorski, J.; Berg, M.J.S. Global threat of arsenic in groundwater. *Science* **2020**, *368*, 845–850. [CrossRef]
- Li, S.W.; Sun, H.J.; Li, H.B.; Luo, J.; Ma, L.Q. Assessment of cadmium bioaccessibility to predict its bioavailability in contaminated soils. *Environ. Int.* **2016**, *94*, 600–606. [CrossRef]
- Marrugo-Negrete, J.; Pinedo-Hernández, J.; Diez, S. Assessment of heavy metal pollution, spatial distribution and origin in agricultural soils along the Sinú River Basin, Colombia. *Environ. Res.* **2017**, *154*, 380–388. [CrossRef]
- Shi, G.; Chen, Z.; Bi, C.; Li, Y.; Teng, J.; Wang, L.; Xu, S. Comprehensive assessment of toxic metals in urban and suburban street deposited sediments (SDSs) in the biggest metropolitan area of China. *Environ. Pollut.* **2010**, *158*, 694–703. [CrossRef]
- Guadie, A.; Yesigat, A.; Gatew, S.; Worku, A.; Liu, W.; Ajibade, F.O.; Wang, A. Evaluating the health risks of heavy metals from vegetables grown on soil irrigated with untreated and treated wastewater in Arba Minch, Ethiopia. *Sci. Total Environ.* **2021**, *761*, 143302. [CrossRef] [PubMed]
- Ma, X.; Sharifan, H.; Dou, F.; Sun, W. Simultaneous reduction of arsenic (As) and cadmium (Cd) accumulation in rice by zinc oxide nanoparticles. *Chem. Eng. J.* **2020**, *384*, 123802. [CrossRef]
- Kubier, A.; Wilkin, R.T.; Pichler, T. Cadmium in soils and groundwater: A review. *Appl. Geochem.* **2019**, *108*, 1–16. [CrossRef] [PubMed]
- Arsenic Compounds. Available online: <https://www.epa.gov/sites/production/files/2016-09/documents/arsenic-compounds.pdf> (accessed on 20 March 2021).
- Kumarathilaka, P.; Seneweera, S.; Meharg, A.; Bundschuh, J. Arsenic speciation dynamics in paddy rice soil-water environment: Sources, physico-chemical, and biological factors—A review. *Water Res.* **2018**, *140*, 403–414. [CrossRef] [PubMed]
- Li, X.; Cui, X.; Zhang, X.; Liu, W.; Cui, Z. Combined toxicity and detoxification of lead, cadmium and arsenic in *Solanum nigrum* L. *J. Hazard. Mater.* **2020**, *389*, 121874. [CrossRef] [PubMed]
- Baderna, D.; Lomazzi, E.; Pogliaghi, A.; Ciaccia, G.; Lodi, M.; Benfenati, E. Acute phytotoxicity of seven metals alone and in mixture: Are Italian soil threshold concentrations suitable for plant protection? *Environ. Res.* **2015**, *140*, 102–111. [CrossRef] [PubMed]
- Tang, R.; Lan, P.; Ding, C.; Wang, J.; Zhang, T.; Wang, X. A new perspective on the toxicity of arsenic-contaminated soil: Tandem mass tag proteomics and metabolomics in earthworms. *J. Hazard. Mater.* **2020**, *398*, 122825. [CrossRef] [PubMed]
- Raiesi, F.; Sadeghi, E. Interactive effect of salinity and cadmium toxicity on soil microbial properties and enzyme activities. *Ecotoxicol. Environ. Saf.* **2019**, *168*, 221–229. [CrossRef]
- Toth, G.; Hermann, T.; Szatmari, G.; Pasztor, L. Maps of heavy metals in the soils of the European Union and proposed priority areas for detailed assessment. *Sci. Total Environ.* **2016**, *565*, 1054–1062. [CrossRef]

16. Rossi, L.; Sharifan, H.; Zhang, W.; Schwab, A.P.; Ma, X. Mutual effects and in planta accumulation of co-existing cerium oxide nanoparticles and cadmium in hydroponically grown soybean (*Glycine max* (L.) Merr.). *Environ. Sci. Nano* **2018**, *5*, 150–157. [[CrossRef](#)]
17. Carey, A.M.; Scheckel, K.G.; Lombi, E.; Newville, M.; Choi, Y.; Norton, G.J.; Charnock, J.M.; Feldmann, J.; Price, A.H.; Meharg, A.A. Grain unloading of arsenic species in rice. *Plant Physiol.* **2010**, *152*, 309–319. [[CrossRef](#)] [[PubMed](#)]
18. Cai, C.; Zhao, M.; Yu, Z.; Rong, H.; Zhang, C. Utilization of nanomaterials for in-situ remediation of heavy metal(loid) contaminated sediments: A review. *Sci. Total Environ.* **2019**, *662*, 205–217. [[CrossRef](#)]
19. Riaz, M.; Kamran, M.; Fang, Y.; Wang, Q.; Cao, H.; Yang, G.; Deng, L.; Wang, Y.; Zhou, Y.; Anastopoulos, I.; et al. Arbuscular mycorrhizal fungi-induced mitigation of heavy metal phytotoxicity in metal contaminated soils: A critical review. *J. Hazard. Mater.* **2021**, *402*, 123919. [[CrossRef](#)]
20. Suriyagoda, L.D.B.; Dittert, K.; Lambers, H. Arsenic in Rice Soils and Potential Agronomic Mitigation Strategies to Reduce Arsenic Bioavailability: A Review. *Pedosphere* **2018**, *28*, 363–382. [[CrossRef](#)]
21. Vaculik, M.; Lukacova, Z.; Bokor, B.; Martinka, M.; Tripathi, D.K.; Lux, A. Alleviation mechanisms of metal(loid) stress in plants by silicon: A review. *J. Exp. Bot.* **2020**, *71*, 6744–6757. [[CrossRef](#)]
22. Zhao, F.-J.; Wang, P. Arsenic and cadmium accumulation in rice and mitigation strategies. *Plant Soil* **2019**, *446*, 1–21. [[CrossRef](#)]
23. Wu, J.; Li, Z.; Huang, D.; Liu, X.; Tang, C.; Parikh, S.J.; Xu, J. A novel calcium-based magnetic biochar is effective in stabilization of arsenic and cadmium co-contamination in aerobic soils. *J. Hazard. Mater.* **2020**, *387*, 122010. [[CrossRef](#)]
24. Pramanik, K.; Mitra, S.; Sarkar, A.; Soren, T.; Maiti, T.K. Characterization of cadmium-resistant *Klebsiella pneumoniae* MCC 3091 promoted rice seedling growth by alleviating phytotoxicity of cadmium. *Environ. Sci. Pollut. Res. Int.* **2017**, *24*, 24419–24437. [[CrossRef](#)]
25. Kamran, M.; Malik, Z.; Parveen, A.; Zong, Y.; Abbasi, G.H.; Rafiq, M.T.; Shaaban, M.; Mustafa, A.; Bashir, S.; Rafay, M.; et al. Biochar alleviates Cd phytotoxicity by minimizing bioavailability and oxidative stress in pak choi (*Brassica chinensis* L.) cultivated in Cd-polluted soil. *J. Environ. Manag.* **2019**, *250*, 109500. [[CrossRef](#)] [[PubMed](#)]
26. White, J.C.; Gardea-Torresdey, J. Achieving food security through the very small. *Nat. Nanotechnol.* **2018**, *13*, 627–629. [[CrossRef](#)]
27. Kah, M.; Tufenkji, N.; White, J.C. Nano-enabled strategies to enhance crop nutrition and protection. *Nat. Nanotechnol.* **2019**, *14*, 532–540. [[CrossRef](#)] [[PubMed](#)]
28. Servin, A.D.; White, J.C. Nanotechnology in agriculture: Next steps for understanding engineered nanoparticle exposure and risk. *NanoImpact* **2016**, *1*, 9–12. [[CrossRef](#)]
29. Giraldo, J.P.; Wu, H.; Newkirk, G.M.; Kruss, S. Nanobiotechnology approaches for engineering smart plant sensors. *Nat. Nanotechnol.* **2019**, *14*, 541–553. [[CrossRef](#)]
30. Venkatachalam, P.; Jayaraj, M.; Manikandan, R.; Geetha, N.; Rene, E.R.; Sharma, N.C.; Sahi, S.V. Zinc oxide nanoparticles (ZnONPs) alleviate heavy metal-induced toxicity in *Leucaena leucocephala* seedlings: A physiochemical analysis. *Plant Physiol. Biochem.* **2017**, *110*, 59–69. [[CrossRef](#)]
31. Rizwan, M.; Ali, S.; ur Rehman, M.Z.; Malik, S.; Adrees, M.; Qayyum, M.F.; Alamri, S.A.; Alyemeni, M.N.; Ahmad, P. Effect of foliar applications of silicon and titanium dioxide nanoparticles on growth, oxidative stress, and cadmium accumulation by rice (*Oryza sativa*). *Acta Physiol. Plant.* **2019**, *41*, 35. [[CrossRef](#)]
32. Lian, J.; Zhao, L.; Wu, J.; Xiong, H.; Bao, Y.; Zeb, A.; Tang, J.; Liu, W. Foliar spray of TiO<sub>2</sub> nanoparticles prevails over root application in reducing Cd accumulation and mitigating Cd-induced phytotoxicity in maize (*Zea mays* L.). *Chemosphere* **2020**, *239*, 124794. [[CrossRef](#)] [[PubMed](#)]
33. Liu, J.; Dhungana, B.; Cobb, G.P. Copper oxide nanoparticles and arsenic interact to alter seedling growth of rice (*Oryza sativa* japonica). *Chemosphere* **2018**, *206*, 330–337. [[CrossRef](#)] [[PubMed](#)]
34. Fiyadh, S.S.; AlSaadi, M.A.; Jaafar, W.Z.; AlOmar, M.K.; Fayaed, S.S.; Mohd, N.S.; Hin, L.S.; El-Shafie, A. Review on heavy metal adsorption processes by carbon nanotubes. *J. Clean. Prod.* **2019**, *230*, 783–793. [[CrossRef](#)]
35. Ihsanullah; Abbas, A.; Al-Amer, A.M.; Laoui, T.; Al-Marri, M.J.; Nasser, M.S.; Khraisheh, M.; Atieh, M.A. Heavy metal removal from aqueous solution by advanced carbon nanotubes: Critical review of adsorption applications. *Sep. Purif. Technol.* **2016**, *157*, 141–161. [[CrossRef](#)]
36. Xu, J.; Cao, Z.; Zhang, Y.; Yuan, Z.; Lou, Z.; Xu, X.; Wang, X. A review of functionalized carbon nanotubes and graphene for heavy metal adsorption from water: Preparation, application, and mechanism. *Chemosphere* **2018**, *195*, 351–364. [[CrossRef](#)]
37. Matos, M.P.S.R.; Correia, A.A.S.; Rasteiro, M.G. Application of carbon nanotubes to immobilize heavy metals in contaminated soils. *J. Nanopart. Res.* **2017**, *19*. [[CrossRef](#)]
38. Yue, L.; Lian, F.; Han, Y.; Bao, Q.; Wang, Z.; Xing, B. The effect of biochar nanoparticles on rice plant growth and the uptake of heavy metals: Implications for agronomic benefits and potential risk. *Sci. Total Environ.* **2019**, *656*, 9–18. [[CrossRef](#)] [[PubMed](#)]
39. Jia, W.; Ma, C.; Yin, M.; Sun, H.; Zhao, Q.; White, J.C.; Wang, C.; Xing, B. Accumulation of phenanthrene and its metabolites in lettuce (*Lactuca sativa* L.) as affected by magnetic carbon nanotubes and dissolved humic acids. *Environ. Sci. Nano* **2020**, *7*, 3759–3772. [[CrossRef](#)]
40. Zheng, Y.; Lin, L.; Wang, B.; Wang, X. Graphitic Carbon Nitride Polymers toward Sustainable Photoredox Catalysis. *Angew. Chem. Int. Ed. Engl.* **2015**, *54*, 12868–12884. [[CrossRef](#)]
41. Inagaki, M.; Tsumura, T.; Kinumoto, T.; Toyoda, M. Graphitic carbon nitrides (g-C<sub>3</sub>N<sub>4</sub>) with comparative discussion to carbon materials. *Carbon* **2019**, *141*, 580–607. [[CrossRef](#)]

42. Praus, P.; Svoboda, L.; Ritz, M.; Troppová, I.; Šihor, M.; Kočí, K. Graphitic carbon nitride: Synthesis, characterization and photocatalytic decomposition of nitrous oxide. *Mater. Chem. Phys.* **2017**, *193*, 438–446. [[CrossRef](#)]
43. Xiao, G.; Wang, Y.; Xu, S.; Li, P.; Yang, C.; Jin, Y.; Sun, Q.; Su, H. Superior adsorption performance of graphitic carbon nitride nanosheets for both cationic and anionic heavy metals from wastewater. *Chin. J. Chem. Eng.* **2019**, *27*, 305–313. [[CrossRef](#)]
44. Shorie, M.; Kaur, H.; Chadha, G.; Singh, K.; Sabherwal, P. Graphitic carbon nitride QDs impregnated biocompatible agarose cartridge for removal of heavy metals from contaminated water samples. *J. Hazard. Mater.* **2019**, *367*, 629–638. [[CrossRef](#)]
45. Hao, Y.; Lv, R.; Ma, C.; Adeel, M.; Zhao, Z.; Rao, Y.; Rui, Y. Graphitic carbon nitride (g-C<sub>3</sub>N<sub>4</sub>) alleviates cadmium-induced phytotoxicity to rice (*Oryza sativa* L.). *Environ. Sci. Pollut. Res. Int.* **2021**. [[CrossRef](#)]
46. Introduction to Rice. Available online: [https://archive.gramene.org/species/oryza/rice\\_intro.html](https://archive.gramene.org/species/oryza/rice_intro.html) (accessed on 20 March 2021).
47. Qi, Y.; Liang, Q.; Lv, R.; Shen, W.; Kang, F.; Huang, Z.H. Synthesis and photocatalytic activity of mesoporous g-C<sub>3</sub>N<sub>4</sub>/MoS<sub>2</sub> hybrid catalysts. *R. Soc. Open Sci.* **2018**, *5*, 180187. [[CrossRef](#)] [[PubMed](#)]
48. Shang, H.; Guo, H.; Ma, C.; Li, C.; Chefetz, B.; Polubesova, T.; Xing, B. Maize (*Zea mays* L.) root exudates modify the surface chemistry of CuO nanoparticles: Altered aggregation, dissolution and toxicity. *Sci. Total Environ.* **2019**, *690*, 502–510. [[CrossRef](#)]
49. Ma, C.; Liu, H.; Guo, H.; Musante, C.; Coskun, S.H.; Nelson, B.C.; White, J.C.; Xing, B.; Dhankher, O.P. Defense mechanisms and nutrient displacement in Arabidopsis thaliana upon exposure to CeO<sub>2</sub> and In<sub>2</sub>O<sub>3</sub> nanoparticles. *Environ. Sci. Nano* **2016**, *3*, 1369–1379. [[CrossRef](#)]
50. Ma, J.F.; Yamaji, N.; Mitani, N.; Xu, X.-Y.; Su, Y.-H.; McGrath, S.P.; Zhao, F.-J. Transporters of arsenite in rice and their role in arsenic accumulation in rice grain. *Proc. Natl. Acad. Sci. USA* **2008**, *105*, 9931–9935. [[CrossRef](#)]
51. Ye, Y.; Li, P.; Xu, T.; Zeng, L.; Cheng, D.; Yang, M.; Luo, J.; Lian, X. OsPT4 Contributes to Arsenate Uptake and Transport in Rice. *Front. Plant Sci.* **2017**, *8*, 2197. [[CrossRef](#)]
52. Jiang, M.; Jiang, J.; Li, S.; Li, M.; Tan, Y.; Song, S.; Shu, Q.; Huang, J. Glutamate alleviates cadmium toxicity in rice via suppressing cadmium uptake and translocation. *J. Hazard. Mater.* **2020**, *384*, 121319. [[CrossRef](#)] [[PubMed](#)]
53. Ma, C.; Chhikara, S.; Xing, B.; Musante, C.; White, J.C.; Dhankher, O.P. Physiological and Molecular Response of Arabidopsis thaliana (L.) to Nanoparticle Cerium and Indium Oxide Exposure. *ACS Sustain. Chem. Eng.* **2013**, *1*, 768–778. [[CrossRef](#)]
54. Cao, D.; Oard, J.H. Pedigree and RAPD-based DNA analysis of commercial US rice cultivars. *Crop Sci.* **1997**, *37*, 1630–1635. [[CrossRef](#)]
55. Yu, H.; Chen, F.; Chen, F.; Wang, X. In situ self-transformation synthesis of g-C<sub>3</sub>N<sub>4</sub>-modified CdS heterostructure with enhanced photocatalytic activity. *Appl. Surf. Sci.* **2015**, *358*, 385–392. [[CrossRef](#)]
56. Deng, X.; Chen, Y.; Yang, Y.; Lu, L.; Yuan, X.; Zeng, H.; Zeng, Q. Cadmium accumulation in rice (*Oryza sativa* L.) alleviated by basal alkaline fertilizers followed by topdressing of manganese fertilizer. *Environ. Pollut.* **2020**, *262*, 114289. [[CrossRef](#)] [[PubMed](#)]
57. Liu, H.; Ma, C.; Chen, G.; White, J.C.; Wang, Z.; Xing, B.; Dhankher, O.P. Titanium Dioxide Nanoparticles Alleviate Tetracycline Toxicity to Arabidopsis thaliana (L.). *ACS Sustain. Chem. Eng.* **2017**, *5*, 3204–3213. [[CrossRef](#)]
58. Ma, C.; Liu, H.; Chen, G.; Zhao, Q.; Eitzer, B.; Wang, Z.; Cai, W.; Newman, L.A.; White, J.C.; Dhankher, O.P.; et al. Effects of titanium oxide nanoparticles on tetracycline accumulation and toxicity in *Oryza sativa* (L.). *Environ. Sci. Nano* **2017**, *4*, 1827–1839. [[CrossRef](#)]
59. Sharifan, H.; Ma, X.; Moore, J.M.; Habib, M.R.; Evans, C. Zinc Oxide Nanoparticles Alleviated the Bioavailability of Cadmium and Lead and Changed the Uptake of Iron in Hydroponically Grown Lettuce (*Lactuca sativa* L. var. *Longifolia*). *ACS Sustain. Chem. Eng.* **2019**, *7*, 16401–16409. [[CrossRef](#)]
60. Cai, F.; Wu, X.; Zhang, H.; Shen, X.; Zhang, M.; Chen, W.; Gao, Q.; White, J.C.; Tao, S.; Wang, X. Impact of TiO<sub>2</sub> nanoparticles on lead uptake and bioaccumulation in rice (*Oryza sativa* L.). *NanoImpact* **2017**, *5*, 101–108. [[CrossRef](#)]
61. Marschner, H.; Römheld, V.; Horst, W.J.; Martin, P. Root-induced changes in the rhizosphere: Importance for the mineral nutrition of plants. *Z. Pflanzenernähr. Bodenkd.* **1986**, *149*, 441–456. [[CrossRef](#)]
62. Ma, C.; Chhikara, S.; Minocha, R.; Long, S.; Musante, C.; White, J.C.; Xing, B.; Dhankher, O.P. Reduced Silver Nanoparticle Phytotoxicity in Crambe abyssinica with Enhanced Glutathione Production by Overexpressing Bacterial gamma-Glutamylcysteine Synthase. *Environ. Sci. Technol.* **2015**, *49*, 10117–10126. [[CrossRef](#)] [[PubMed](#)]
63. Mosa, K.A.; El-Naggar, M.; Ramamoorthy, K.; Alawadhi, H.; Elnaggar, A.; Wartanian, S.; Ibrahim, E.; Hani, H. Copper Nanoparticles Induced Genotoxicity, Oxidative Stress, and Changes in Superoxide Dismutase (SOD) Gene Expression in Cucumber (*Cucumis sativus*) Plants. *Front. Plant Sci.* **2018**, *9*, 872. [[CrossRef](#)] [[PubMed](#)]
64. Cao, X.; Ma, C.; Chen, F.; Luo, X.; Musante, C.; White, J.C.; Zhao, X.; Wang, Z.; Xing, B. New insight into the mechanism of graphene oxide-enhanced phytotoxicity of arsenic species. *J. Hazard. Mater.* **2020**, *410*, 124959. [[CrossRef](#)] [[PubMed](#)]



## Article

# Comparative Analysis of Proteins Regulated during Cadmium Sulfide Quantum Dots Response in *Arabidopsis thaliana* Wild Type and Tolerant Mutants

Valentina Gallo <sup>1</sup>, Andrea Zappettini <sup>2</sup>, Marco Villani <sup>2</sup>, Nelson Marmiroli <sup>1,3</sup> and Marta Marmiroli <sup>1,\*</sup>

<sup>1</sup> Department of Chemistry, Life Sciences and Environmental Sustainability, University of Parma, 43123 Parma, Italy; valentina.gallo@unipr.it (V.G.); nelson.marmiroli@unipr.it (N.M.)

<sup>2</sup> Institute of Materials for Electronics and Magnetism (IMEM), National Research Council (CNR), 43124 Parma, Italy; andrea.zappettini@imem.cnr.it (A.Z.); marco.villani@imem.cnr.it (M.V.)

<sup>3</sup> The Italian National Interuniversity Consortium for Environmental Sciences (CINSA), 43123 Parma, Italy

\* Correspondence: marta.marmiroli@unipr.it; Tel.: +39-0521-905698

**Abstract:** In previous work, two independent *Arabidopsis thaliana* Ac/Ds transposon insertional mutant lines, *atnp01* and *atnp02*, were identified that showed a higher level of tolerance than the wild type (wt) line to cadmium sulfide quantum dots (CdS QDs). The tolerance response was characterized at physiological, genetic and transcriptomic levels. In this work, a comparative analysis was performed on protein extracts from plantlets of the two mutants and of wt, each treated with 80 mg L<sup>-1</sup> CdS QDs. A comparative protein analysis was performed by 2D-PAGE, and proteins were characterized by MALDI-TOF/TOF mass spectrometry. Of 250 proteins identified from all three lines, 98 showed significant changes in relative abundance between control and CdS QD-treated plantlets. The wt, *atnp01*, and *atnp02* control-treated pairs respectively showed 61, 31, and 31 proteins with differential expression. The two mutants had a different response to treatment in terms of type and quantity of up- and downregulated proteins. This difference became more striking when compared to wt. A network analysis of the proteins differentially expressed in *atnp01* and *atnp02* included several of those encoded by putative genes accommodating the transposons, which were responsible for regulation of some proteins identified in this study. These included nifu-like protein 3 (Nfu3), involved in chloroplast assembly, elongator complex 3 (Elo3), involved in transcriptional elongation, magnesium-chelate subunit-2 (Chl2), involved in chlorophyll biosynthesis, and protein phosphatase 2C (PP2C) which mediates abiotic stress response.

**Citation:** Gallo, V.; Zappettini, A.; Villani, M.; Marmiroli, N.; Marmiroli, M. Comparative Analysis of Proteins Regulated during Cadmium Sulfide Quantum Dots Response in *Arabidopsis thaliana* Wild Type and Tolerant Mutants. *Nanomaterials* **2021**, *11*, 615. <https://doi.org/10.3390/nano11030615>

Academic Editor: Thierry Rabilloud

Received: 7 February 2021

Accepted: 25 February 2021

Published: 1 March 2021

**Keywords:** proteomics; engineered nanomaterials; mutants; 2D-PAGE; stress response proteins; network analysis

**Publisher's Note:** MDPI stays neutral with regard to jurisdictional claims in published maps and institutional affiliations.



**Copyright:** © 2021 by the authors. Licensee MDPI, Basel, Switzerland. This article is an open access article distributed under the terms and conditions of the Creative Commons Attribution (CC BY) license (<https://creativecommons.org/licenses/by/4.0/>).

## 1. Introduction

One result of the expansion of nanotechnology has been the large-scale production of engineered nanomaterials (ENMs), which are becoming widely diffused as industrial products for everyday use. However, ENMs can be released into the environment through the recycling of waste, manufacturing, and deliberate or accidental environmental release [1]. Soil is becoming more frequently contaminated with released ENMs, some types of which, due to their small size and high surface reactivity, may enter into plant cells, where both detrimental and positive effects have been noted [2]. Among the smallest ENMs are colloidal cadmium sulfide quantum dots (CdS QDs). The market for colloidal quantum dots (QDs) alone is projected to increase from the current \$3 billion to \$8.5 billion by 2023, an almost three-fold increase in production and marketing (<https://www.marketsandmarkets.com/Market> (accessed on 2 February 2021)). QDs are semiconductor nanocrystals measuring around 2–10 nm [3], and their chemical and physical properties are closely size-dependent. Based on their excellent optical properties, QDs have important applications, with development of platforms for simultaneous

imaging, sensing, and therapy [4,5]. Indeed, QDs are pivotal constituents of innovative nanotechnology-enabled tools for medical diagnostic and ex vivo imaging [6,7]. QDs have also been used to improve resolution in TVs, digital cameras, computers, and smartphone displays and to increase energy conversion efficiency in quantum dot light-emitting diodes (QLEDs) and in quantum solar cells (QDSSCs) [8,9]. Consequently, the increasing use of QDs-enabled products is expected to result in larger releases of these materials into the environment [10,11]. CdS QDs are very stable and have high reactivity and high surface charge [12]. However, different properties have been connected with CdS QDs toxicity; some studies have implicated Cd release as the main toxicity factor, but under other circumstances, particle properties like shape and size seem to be more relevant [13,14]. Our previous work showed that only about 2% of CdS QDs dissolved in MS medium in 21 days [14]. The main toxicity mechanisms of CdS QDs nanoparticles within a cell or an organism are the generation of reactive oxygen species (ROS), which damage cell membranes, proteins and DNA; the production of protein coronas, removing proteins important to normal cell metabolism [15]; inhibition of the functionality of chloroplasts and mitochondria [16,17]; and the induction of apoptosis through the activation of post-translational regulatory mechanisms such as miRNA [18].

Generally, the influence of exposure duration on Cd-based QDs toxicity is insufficiently understood [19,20]. Only a limited number of studies have analyzed and compared the impacts of CdS QDs and Cd ions on whole organism development, as well as on organ, tissue or cellular structure [21–24]. Marmioli et al. [14,25] characterized the transcriptomic and changes associated with exposure to CdS QDs in *A. thaliana*; two mutants (*atnp01* and *atnp02*) of Landsberg *erecta*, collection Soll-Jonson, with Ac/Ds maize transposon insertion, were identified as tolerant to CdS QDs but not to Cd<sup>2+</sup>. Genotypic characterization of *atnp01* and *atnp02* was performed; Southern hybridization profiles based on either EcoRI or BamHI digestion identified two hybridizing fragments in *atnp01*, and a single different one in *atnp02*, demonstrating that the two mutants harbored three different Ds elements. The number of Ds elements inserted in each mutant and their genomic locations were determined by genome walking. Upon sequencing the amplicons produced in the genome walking, a BLAST-based alignment with the full genome sequence identified that the candidate genes potentially affected by the Ds transposition events in *atnp01* were *At3g46880*, coding an unknown chloroplast-localized protein, *At1g13870* (*DRL1*, deformed roots and leaves) coding a cytoplasm-localized calmodulin-binding protein possibly involved in leaf development and meristem structural organization, and *At1g13880* (*ELM2*), a member of the MYB transcription factors category. The *atnp02* event could have affected either *At3g24330*, which encodes an O-glycosyl hydrolase localizing to the endomembrane, or *At3g24430* (*HCF101*), coding for a chloroplast-localizing ATP-binding protein. The Ds element lay within the *At3g24400* pseudogene (*AtPERK2*), which may code for a proline-rich extensin-like receptor kinase.

These mutants were characterized at physiological, genetic, and transcriptomic levels, and a comparison with the response to Cd<sup>2+</sup> demonstrated the nano-specific nature of the molecular mechanisms and the pathways involved in the tolerance. It was proved by Marmioli et al. [26] that CdS QDs once inside the plant cell undergo biotransformation rendering them less active and diminishing their power to hamper photosynthesis, respiration, and DNA transcription; this occurs through the inactivation of specific enzymes and by the chaperone action of hard corona proteins, including some heat shock proteins (Hsp70) [15]. The correspondence between transcriptomics and proteomics results for the same toxicant is typically in the range 20–80% [25,27], but proteomics furnishes important information about the cellular response to toxicants, protein–protein interactions, and post-translational modifications that cannot be detected by transcriptomics. Proteins differentially expressed in the presence and absence of CdS QDs were identified by 2D-PAGE. Image analysis was used to compare spots between gels of treated and untreated wt and mutants (*atnp01*, *atnp02*), and those with different intensities were excised and fingerprinted using MALDI-TOF/TOF mass spectrometry. Results obtained with 2D-PAGE were then compared with

those obtained in previous work [25], which used the same conditions of treatment but a different separation technique: two-dimensional protein fractionation (ProteomeLab PF2D), employing a gradient isoelectric focusing (IEF) separation in the first dimension, and high-performance liquid chromatography (HPLC) in the second dimension. These two techniques use a different pH range (5–8 vs. 4–8.5), a different solubilization for proteins (SDS vs. urea), and a different quantity of proteins (4 mg vs. 400 µg); therefore, they are often seen as complementary [28]. However, other proteomic techniques, like iTRAQ, have been shown to give a greater number of identifications [29].

## 2. Materials and Methods

### 2.1. Plant Material

*A. thaliana* accession Landsberg *erecta* (L. Heyn) mutants *atnp01* and *atnp02* were previously isolated by screening for resistance to CdS QDs 378 transposon insertional lines obtained from the Nottingham Arabidopsis Stock Centre (uNAS; <http://arabidopsis.info/> (accessed on 2 February 2021)). Marmioli et al., [14] reported the conditions of isolation and characterization of the two mutants when treated with CdS QDs and CdSO<sub>4</sub>. All reagents and standards were purchased from Sigma-Aldrich (St. Louis, MO, USA) unless otherwise stated.

### 2.2. Synthesis and Characterization of the CdS QDs

The synthesis and characterization of CdS QDs are reported in “Supplementary Materials S.1” (Figures S1 and S2). X-ray diffraction (XRD) (XRD Empirean alpha1, Malvern Panalytical, UK) and high-resolution transmission electron microscopy (HR-TEM) (Hitachi HT7700, Hitachi High Technologies America, Pleasanton, CA, US) demonstrated that the average static diameter of the CdS QD NPs (nanoparticles) was 5 nm; the crystal structure was hexagonal wurtzite (ZnS) with about 78% Cd. The average particle size of the aggregates measured by dynamic light scattering, and zeta potential (ζ) estimated in ddH<sub>2</sub>O, were 178.7 nm and + 15.0 mV, respectively [14].

### 2.3. Seed Germination, Growth, and Treatments

Twenty-five seeds of *A. thaliana* wild type (wt) and two mutants, *atnp01* and *atnp02*, were sown on Petri dishes containing Murashige and Skoog (MS) nutrient medium (Duchefa Biochemie, Haarlem, Netherlands) containing 1% *w/v* sucrose and 0.8% *w/v* agar, then placed in the dark, under controlled conditions in a growth chamber. After germination, seedlings were grown at 24 °C, with a relative humidity of 30%, and under a 16-h photoperiod (light intensity 120 µM m<sup>-2</sup> s<sup>-1</sup> photosynthetic photon flux) in the MS medium in the absence of treatment for 14 days. After that time span, seedlings were transferred to a fresh MS medium containing 80 mg L<sup>-1</sup> CdS QDs (treatment) or without CdS QDs (control) and grown for a further 21 days in the same conditions as above. Because 80 mg L<sup>-1</sup> CdS QDs is a sub-inhibitory concentration, the stocks of seeds of both mutants and wt plants were checked for their capacity to grow in the presence of CdS QDs up to 250 mg L<sup>-1</sup>, which was totally inhibiting for wt. All six samples were collected after 21 days by removing them carefully from the medium; they were gently washed with distilled H<sub>2</sub>O, frozen in liquid nitrogen and then stored at −80 °C until use for protein extraction.

### 2.4. Protein Extraction and Quantification

Proteins of wt and of the two mutant lines, untreated and treated (80 mg L<sup>-1</sup> CdS QDs), were extracted. Frozen samples were ground to powder in liquid nitrogen using a mortar and pestle; 1 g aliquot was suspended in 6 mL of extraction buffer: 700 mM sucrose, 500 mM Tris-HCl, pH 7.5, 50 mM ethylenediaminetetraacetic acid (EDTA), 100 mM KCl, 2% dithiothreitol (DTT), 0.1% Protease Inhibitor Cocktail (Sigma-Aldrich), vortexed and mixed for 10 min on ice. An equal volume of 500 mM Tris-HCl buffered phenol was added, and the solution was mixed at room temperature for 10 min [30,31]. The samples were

centrifuged for 10 min at  $5500\times g$  and at  $4\text{ }^{\circ}\text{C}$ . The phenolic phase was collected in a new tube and back-extracted with 3 mL of extraction buffer. Proteins were precipitated from the phenolic phase overnight at  $-20\text{ }^{\circ}\text{C}$  by adding five volumes of 0.1 M ammonium acetate (J.T. Baker, Deventer, The Netherlands) saturated in methanol. Precipitated proteins were centrifuged for 30 min at  $5500\times g$  and at  $4\text{ }^{\circ}\text{C}$ , the pellet was washed with cooled methanol and then with cooled acetone. After each washing step, the sample was centrifuged for 5 min at  $5500\times g$  and at  $4\text{ }^{\circ}\text{C}$ . Finally, the pellet was dried using a Speed Vac Concentrator 5301 (Eppendorf AG, Barkhausenweg, Hamburg, Germany).

The pellet was dissolved in 300  $\mu\text{L}$  of isoelectrofocusing (IEF) buffer containing 9 M urea, 4% 3-[(3-cholamidopropyl) dimethylamino]-1-propanesulfonate (CHAPS), 50 mM DTT, 0.001% protease inhibitor cocktail, 1% carrier ampholyte mixtures (pH 3–10, BioRad, CA, USA). Protein quantification was evaluated according to a modified Bradford assay [32] based on the acidification of the sample buffer with 20 mM HCl. Bovine serum albumin (BSA) was used as standard.

### 2.5. 2D Gel Electrophoresis

The proteins mixtures were resolved by two-dimensional polyacrylamide gel electrophoresis (2D-PAGE). For proteins separation in the first dimension (IEF), 400  $\mu\text{g}$  of proteins of each sample were loaded onto 11-cm ReadyStrip pH 5-8 IPG strips (BioRad, CA, USA) which had been rehydrated overnight with 250  $\mu\text{L}$  IEF buffer containing the sample. Proteins were focused by PROTEAN<sup>®</sup> i12<sup>™</sup> IEF System (BioRad, CA, USA) applying 250 V (60 min), 1000 V (60 min), 8000 V (2 h) and 8000 V up to 35,000 V/h.

After IEF, the strips were incubated 15 min in 3 mL of reducing buffer containing 6 M urea, 2% *w/v* DTT, 0.375 M Tris-HCl (pH 8.8), 20% *w/v* glycerol, 2% *w/v* SDS and for 15 min in 3 mL of alkylating buffer containing 6 M urea, 2.5% *w/v* iodoacetamide, 0.375 M Tris-HCl (pH 8.8), 2% *w/v* glycerol. The second dimension (SDS-PAGE) was performed using a Criterion<sup>™</sup> Dodeca<sup>™</sup> cell (BioRad, CA, USA) and 12% Criterion<sup>™</sup> XT Bis-Tris gels (BioRad, USA) in 1 M MOPS (3-(*N*-morpholino)-propanesulfonic acid) buffer (1 M Tris, 20 mM EDTA and 2% *w/v* SDS).

2D gels were stained with QC Colloidal Coomassie G-250 (BioRad, CA, USA) and were scanned with a ChemiDoc<sup>™</sup> Imaging System (BioRad, CA, USA). Gel analysis was performed using PDQuest software (BioRad, CA, USA). Spot detection and matching between gels were performed automatically, followed by manual verification. The spot densities were normalized by local regression method and followed by a calculation against the whole gel densities. The percentage density of every spot was averaged over three replicate gels, and Student's *t*-test analysis ( $p < 0.05$ ) was carried out to find statistically significant differences in protein abundances. Statistically significant spots were then excised from the gels using an EXQuest Spot Cutter (BioRad, CA, USA), destained by soaking the pieces of acrylamide in a 1:1 solution of 100 mM ammonium bicarbonate/ acetonitrile for 30 min, and the proteins were hydrolyzed with trypsin at  $37\text{ }^{\circ}\text{C}$  overnight [33].

### 2.6. MALDI-TOF/TOF Mass Spectrometry

The solutions containing the tryptic peptides were desalted and concentrated to a final volume of 4  $\mu\text{L}$  with Zip-Tip C18 (Millipore Corporation, Billerica, MA, USA), according to the manufacturer's protocol, then dispersed into an  $\alpha$ -cyano-4-hydroxycinnamic acid (4-HCCA) matrix, prepared by dissolving 4-HCCA in 50% acetonitrile/0.05% trifluoroacetic acid and spotted on a MALDI plate. The analysis was performed through a model 4800 MALDI-TOF/TOF<sup>™</sup> MS analyzer (Applied Biosystems, Foster City, CA, USA). Peptide mass spectra were acquired in reflectron mode (500–4000 *m/z* range) and analyzed with the help of mMass v5.5 open-source software (<http://www.mmass.org/> (accessed on 2 February 2021)). A peak list was created for each feature, and then manually controlled for the presence of signal from the matrix complex, human keratin peptides and trypsin. The main parameters were set as follows: digestion enzyme trypsin with one missed cleavage, mass type monoisotopic, 100 ppm peptide tolerance, methionine oxidation

and cysteine carbamidomethylation were set to enzymatic cleavage as fixed and variable modifications respectively.

Peptide mass fingerprinting analysis was performed with the software Mascot (<http://www.matrixscience.com> (accessed on 2 February 2021)) and proteins were identified with the Swiss-Prot data base of *A. thaliana* (thale cress). The information about gene loci was found in the UniProt and in TAIR database (<https://www.arabidopsis.org/> (accessed on 2 February 2021)) for the corresponding *A. thaliana* proteins names and description.

### 2.7. Data Mining and Analysis

Heat maps of significant proteins were generated by R v3.3.1 ([www.r-project.org](http://www.r-project.org) (accessed on 2 February 2021)). The Gene Ontology enrichment analysis was performed through the Panther database ([pantherdb.org/](http://pantherdb.org/)). The pathway analysis was performed using the GoMapMan tool based on ITAG Release 2.3 234 (2011-04-26) of the *A. thaliana* genome sequence. MapMan 3.6.0RC1 software ([mapman.gabipd.org/web/guest/mapman-download](http://mapman.gabipd.org/web/guest/mapman-download)) was used to place proteins within a likely pathway (BIN). Protein–protein interactions (PPIs) of differentially expressed proteins from *A. thaliana* were performed using STRING v11.0 (<https://string-db.org/> (accessed on 2 February 2021)).

## 3. Results and Discussion

### 3.1. *A. Thaliana* Proteome after CdS QDs Treatment

2D-PAGE profiling (technical triplicates) of the plant proteomes of *A. thaliana* generated overall about 600 visible protein features for each of the wt and two mutants, exposed or not exposed to CdS QDs. After minor spots were eliminated to allow consistent MALDI-TOF/TOF analysis, about 250 reproducible spots remained (Figure S3). For the control samples, we had a total of 103 reproducible spots, of which 79 were present in all three plants; 2 were found only in wt, and 1 only in *atnp01*, with no unique spots for *atnp02* (Figure S4A). For the treated samples, we had 105 reproducible spots, of which 81 were common to all the plant types. A further 4, 0 and 3 were unique to wt, *atnp01*, and *atnp02* respectively (Figure S4B). The proteins in common between wt and mutants are shown in Figure S4 and explained in the Figure caption. Of these spots, 98 were designated as ‘differentially abundant’, meaning that they varied in intensity with  $p$ -value  $\leq 0.05$  between the treated (trt) and untreated (ctr) plant pairs. Of these, 61 were from the wt pair, 31 from the *atnp01* pair and 31 from the *atnp02* pair (Figure 1A). The numbers of commonalities and up- and downregulated proteins between wt and mutants and between mutants are listed in the caption to Figure 1.

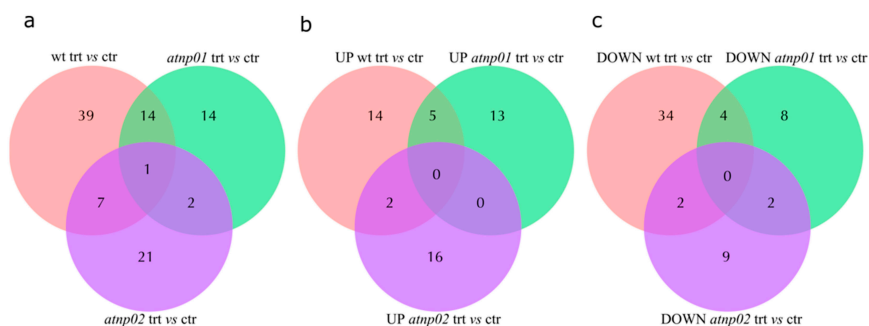


**Figure 1.** Venn diagrams showing proteins common and non-common to wt and *atnp01*, to wt and *atnp02*, to *atnp01* and *atnp02* and to all treatment conditions. (a) There were 15 proteins common between wt and *atnp01*, 8 between wt and *atnp02*, and 3 between the two mutants; (b) The proteins upregulated in wt, *atnp01* and *atnp02* lines between control and treatment conditions. There were four upregulated proteins in common between wt and *atnp01*, two between wt and *atnp02*, and none between the two mutants; (c) The proteins downregulated in wt, *atnp01* and *atnp02* mutant lines between control and treatment conditions. There were four downregulated proteins in common between wt and *atnp01*, two between wt and *atnp02*, and two between the two mutants.

The identities of the differentially abundant proteins are reported in Table S1, and the associated heat map is shown in Figure 2. The heat map was obtained after the computation of the protein abundances in the control and treated samples for all the plant types, and by dividing the treated by the control to obtain the final differential heat map. Figure S4 shows the heat maps for all the treatments and controls of wt, *atnp01*, and *atnp02*. For all 98 proteins, the MapMan ontology BIN assignments are listed in Table S2. Most of the proteins in wt were downregulated, annotating in processes such as biotic and abiotic stress responses, protein folding, and protein degradation (Figure 2). Conversely, in both mutants, there is a balance between the numbers of up- and downregulated proteins (Figure 2). Comparing the heat map of treated vs. control, it can be observed that, whereas the treatment for the wt led to a general down-regulation of proteins, for the two mutants *atnp01* and *atnp02* there was also a significant number of proteins upregulated (Figure 2). The proteome of each mutant differed from that of the wt, both when the plants were grown under control conditions and when they were exposed to CdS QDs. Only one of the variable features was in common among all comparisons, namely putative protein phosphatase 2C 58 (At4g28400), downregulated in both mutants and upregulated in wt (Figures 1A and 2). This is a protein phosphatase known to mediate abiotic stress pathways and it is a member of major phosphatase class PP2C [34,35]. The phytohormone abscisic acid (ABA) is a major player in the regulation of responses to abiotic stresses, in particular drought and salinity. In Arabidopsis, ABA signaling, triggered particularly under abiotic stresses, involve various PP2Cs members as key regulators [36]. Two proteins were common to both mutants in the treatment condition, namely bifunctional enolase 2/transcriptional activator (Eno2) and putative pectinesterase/pectinesterase inhibitor VGDH2 (Vgdh2) (Figure 1A). Eno2, downregulated in the mutants (Figure 2), is the key glycolytic enzyme and encoded by LOS2 (Low expression of osmotically responsive genes 2). The ENO2 locus is highly expressed throughout plant development and is on average 10-fold more abundant than ENO1 and ENO3 in all tissues and organs [37]. Interestingly, Eno2 is a key protein in glycolysis and might be involved in the response to CdS QDs which can include impaired glycolysis. Vgdh2, downregulated in *atnp01* and upregulated in *atnp02* (Figure 2), acts in the modification of cell walls via demethylesterification of cell wall pectin [38].

Separately considering the up- and downregulated proteins, we constructed two new Venn diagrams (Figure 1B,C). The diagram for the upregulated proteins indicates that there are five proteins in common between treated wt and treated *atnp01*: pathogenesis-related protein 5 (At1g75040), F-box only protein 7 (Fbx7), oxygen-evolving enhancer protein 1-1, chloroplastic (Psbo1), probable fatty acyl-CoA reductase 4 (Far4), and gamma carbonic anhydrase 2 (Gammaca2). Pathogenesis-related protein 5 is partially responsible for acquired pathogen resistance [39]. Fbx7 is required for protein synthesis during temperature stress. [40]. Psbo1 stabilizes the manganese cluster which is the primary site of water splitting [41]. Far4 provides the fatty alcohols required for the synthesis of suberin in roots, seed coat, and wound-induced leaf tissue [42]. Gammaca2 mediates complex I assembly in mitochondria and respiration [43]. There are two proteins in common between treated wt and treated *atnp02*: vacuolar protein sorting-associated protein 24 homolog 1 (Vps24-1) and 30S ribosomal protein S5, chloroplastic (At2g33800). Vps24-1 is required for multivesicular body (MVB) formation and sorting of endosomal cargo proteins into MVBs. [44]. At2g33800 binds directly to 16S ribosomal RNA [45]. In the groups considered, there are no proteins in common between the two treated mutants. Among the downregulated proteins we found four proteins in common between treated wt and treated *atnp01*: heat shock 70 kDa protein 3 (Hsp70-3), histone H2B.7 (At3g46030), L-ascorbate peroxidase 1 (Apx1), and filament-like plant protein 6 (Fpp6). Hsp70-3, in collaboration with other chaperone proteins, assists translocation of precursor proteins into organelles, facilitates folding of de novo synthesized proteins, and is responsible for the degradation of damaged proteins undergoing stress conditions such as from Cd [46]; At3g46030 is a core component of the nucleosome [39]; Apx1 is a key component of the reactive oxygen species gene network, moreover, its synthesis can be induced by Cd exposure [46].

The function of Fpp6 is unknown. We found two proteins in common between treated wt and treated *atnp02*: glycine-rich RNA-binding protein 8 (Rbg8) and Ras-related protein RABF1(Rabf1). Rbg8 plays a role in RNA transcription or processing during stress [47]. Rabf1 is an endosomal protein probably involved in endocytosis [48]. There are two proteins in common between the two treated mutant lines: probable protein phosphatase 2C 58 and enolase 2. The first of these proteins was found in common between the wt and two mutants (Figure 1A), but it was upregulated in the wt while being downregulated in the two mutants (Figure 2). The second protein was found in common between the two mutants and was downregulated.

From the lower part of the heat map (Figure 2), it seems that the majority of the downregulated proteins are specific to the mutant *atnp01*, with the exception of Sap1, a zinc-finger protein and Scl28, a serine-arginine-like splicing factor, both upregulated. The most strongly downregulated proteins are: Pcmp-E25, a pentatricopeptide; Hsp70-3, a heat shock protein; Sam1, a S-adenosylmethionine synthetase; Xi-J, myosine 16; Far4, fatty-acyl-CoA reductase, At3g46030, histone H2B.7, VHA-B1, V-type proton ATPase, SEN1, t-RNA splicing endonuclease, and FPP6, filament like plant protein. Instead, ENO2 and PP2C were downregulated in both mutants. For the proteins Vgdh, Gapa1, Aba3, Pux10, and At4g05080, we found that they are strongly downregulated in the mutant *atnp01*, but strongly upregulated in *atnp02* (Figure 2). This behavior indicates that this group of proteins is involved in an opposite manner within the response pathways that the two different mutants display towards the treatment. In the upper part of the heatmap in Figure 2, it is possible to observe several strongly upregulated proteins only in the mutant *atnp02*. These proteins are: Hsp70-10, a mitochondrial heat shock protein involved in the response to stress, Cat2, catalase 2, involved in the detoxification of hydrogen peroxide, Clpc2, a chloroplast chaperon protein with ATPase activity, Gldp2, a glycine dehydrogenase involved in the degradation of glycine in the mitochondrion, Cul3-B, cullin 3B, active in protein ubiquitination, and Atk5, kinesin 5, with microtubule-binding activity in the cytoskeleton. These proteins reflect the activity of the plant to control the oxidative stress and damage to mitochondria brought about by the CdS QDs.

In wt, the set of reprogrammed proteins was associated with the following major MapMan bins: protein synthesis, protein degradation and protein post-transcriptional modification; RNA regulation of transcription; DNA synthesis and chromatin structure; amino acid metabolism; hormone metabolism; redox ascorbate and glutathione biosynthesis; photosynthesis and photorespiration and abiotic and biotic stresses (Figure 3). In *atnp01*, the set of reprogrammed proteins was associated with protein degradation, RNA regulation of transcription, abiotic and biotic stress, and mitochondrial electron transport and ATP synthesis (Figure 3). In *atnp02*, the set of reprogrammed proteins was associated with protein folding, protein degradation, RNA regulation of transcription, photosynthesis (PS), secondary metabolism, mitochondrial electron transport/ATP synthesis, hormone metabolism, abiotic and biotic stress (Figure 3).

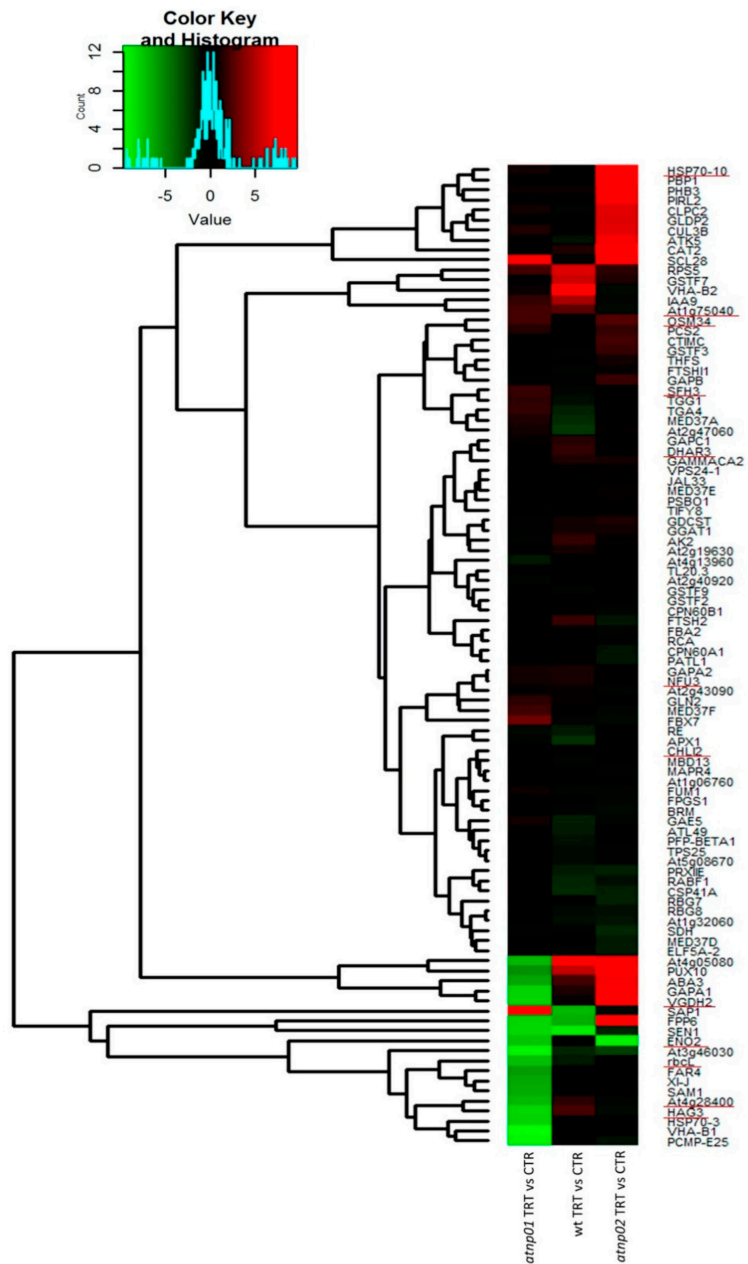


**Figure 2.** Heat map representing the effect on the *A. thaliana* proteome of CdS QDs ( $80 \text{ mg L}^{-1}$ ) for wt and for the mutant lines *atnp01* and *atnp02*. This heat map was obtained, similarly to Figure S5, by dividing the abundances of treated samples by the control samples. The proteins underlined in red are those in common among the wt and the two mutants *atnp01* and *atnp02*, those that were found in the networks related to the mutated genes in the two mutants and those in common with the proteomic study with PF2D and the transcriptome.

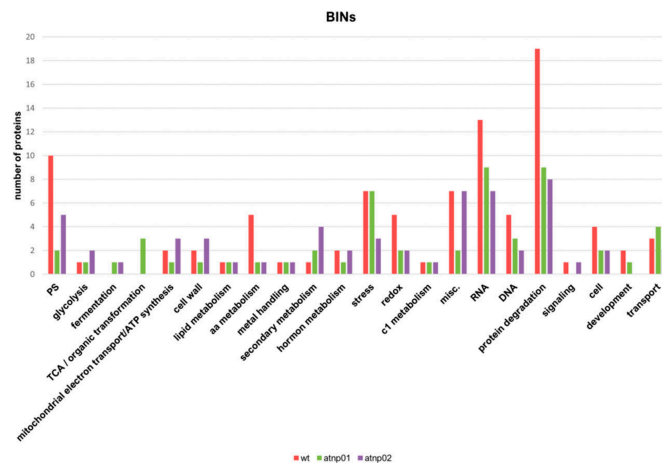


**Figure 3.** The distribution of differentially abundant proteins in wt, atnp01 and atnp02 according to MapMan ontology classification (BINs). The horizontal axis shows the different MapMan bin types, with the number of proteins for each bin on the vertical axis.

### 3.2. Ontology Analysis of the Identified Proteins

We classified each protein into one of three ontology categories: biological processes, molecular function, and cell components. For the proteins significant when comparing treated wt vs. control wt, the biological processes that were found more enriched were: carbon fixation, response to zinc ion, detoxification, response to cadmium ion, response to abiotic stimulus, and response to stress (Figure 4A). Molecular function categories enriched for this comparison were: glutathione binding, oligopeptide binding, and glutathione transferase activity, while the cell compartments were: apoplast, plastoglobule, chloroplast stroma, thylakoid, photosynthetic membrane, cell wall, organelle envelope, cytosol, and plastid (Figure S5A). The biological processes showed a strong response to stress in general and to metals in particular, including cadmium, which is a component of CdS QDs. In the enriched molecular functions, we found a predominant role of glutathione, which suggests a general response to oxidative stress caused by CdS QDs exposure [24]. The cell compartment pinpoints the role of the chloroplast in the response to CdS QDs, as already found by Pagano et al. [16]. (Figure S5B). This is in keeping with the oxidative stress response prominent in molecular function, as found by Ruotolo et al. [15]. For the protein differences emerging in the comparison of treated *atnp01* vs. control *atnp01*, the biological processes that were found most enriched were: protein refolding, response to cadmium ion, response to heat and temperature and response to stress (Figure 4B). For this pair, the enriched molecular function categories were: misfolded protein binding, protein folding chaperone and heat shock protein binding, while the cell components were: endoplasmic reticulum chaperon complex, secretory vesicle, apoplast, cell wall, and cytosol (Figure S5C). Here, it is possible to recognize in the biological process not only responses to abiotic stress and metals, but also a protein folding response which is again predominant in the molecular function. Therefore, it can be summarized that treatment of the mutant line *atnp01* potentiated several proteolytic mechanisms. Thus, the cellular components affected by the treatment were the endoplasmic reticulum and cell wall where proteolysis is carried out by the cell (Figure S5D). For the proteins emerging in the comparison of treated *atnp02* vs. control *atnp02*, the biological processes that were found more enriched were: protein refolding, response to cadmium ion, response to metal ion, response to catabolic process and response to abiotic stimulus (Figure 4C). Laware and colleagues [49] found that in seedlings of *Alium cepa* treated with TiO<sub>2</sub> nanoparticles there was a strong dose-dependent proteolytic activity. For the molecular function of the same comparison the

enriched categories were: misfolded protein binding, protein folding chaperone, heat shock protein binding, and nucleoside-triphosphate activity (Figure S5E), while the cell components were: apoplast, plastid envelope, thylakoid, chloroplast envelope and stroma, vacuole, bounding membrane of organelles and cell-cell junction (Figure S5F). Treated *atnp02* responded in the biological function category with a general stress response and one category of protein folding which is similar to the response of the *atnp01*. Similarly, in terms of molecular function the categories were predominantly related to protein readjustment. In this case, the chloroplast (*Gapa1* and *Gapa2*) and the vacuole (*Vps24-1*) were involved in the treatment response, which indicates the presence of oxidative stress [16].

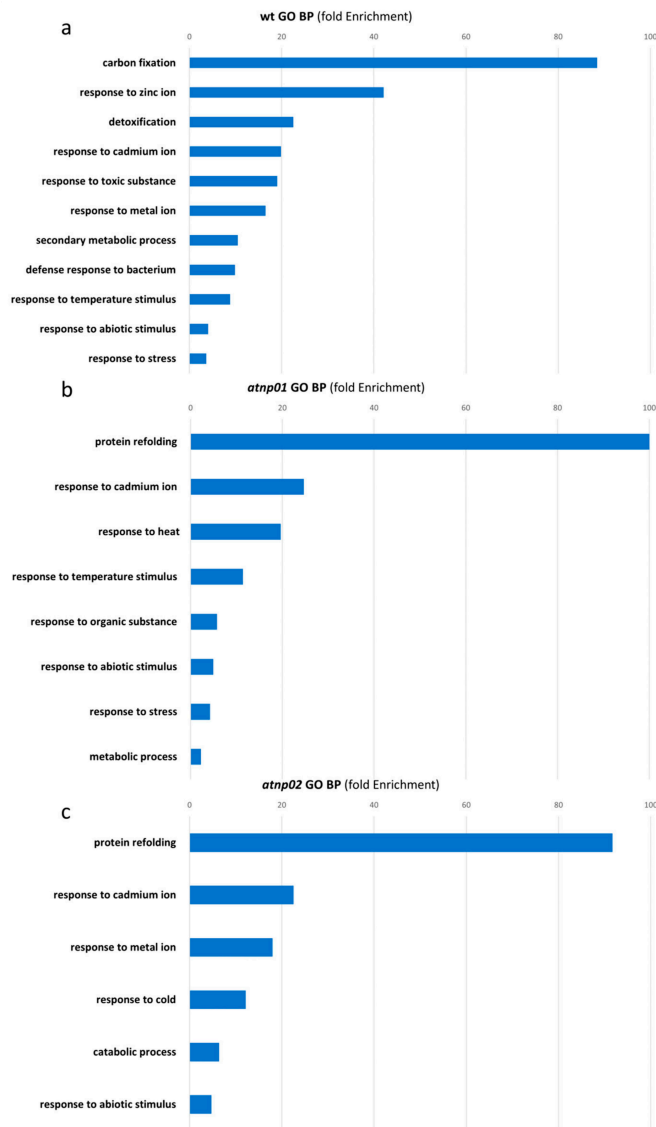


**Figure 4.** Gene ontology and analyses with  $n$ -fold enrichment =  $-\log_{10}$  (Fisher's exact  $p$ -value) for Biological process in wt (a), *atnp01* (b) and *atnp02* (c).

### 3.3. Pathways Analysis in Response to CdS QDs Treatment

Several pathways were identified by Mapman ontology as being particularly involved in the response to CdS QDs. In wt and both mutants, proteins from cellular metabolism such as glyceraldehyde-3-phosphate dehydrogenase (Gapc1, Gapb, Gapa1 and Gapa2), pyrophosphate fructose6-phosph1-phosphotransferase subunit beta1 (Pep-beta1), 30S ribosomal protein S5, glycine dehydrogenase decarboxylating 2 (Glpd2) and bifunctional enolase 2/transcriptional activator (Eno2) were modulated (Figures 2 and 3 and Table S2). Arabidopsis has four different GAPDH isoforms, with seven phosphorylating types and one non-phosphorylating. These include cytosolic glycolytic GAPDHs (GAPC1 and GAPC2), chloroplastic photosynthetic GAPDHs (GAPA1, GAPA2, and GAPB), plastidic glycolytic GAPDHs (GAPCp1 and GAPCp2), and the NADP-dependent non-phosphorylating cytosolic GAPDH (NP-GAPDH) [50]. Substrate conversion by glycolytic GAPDHs catalyzes a simultaneous reduction of  $\text{NAD}^+$  to NADH [51]. Arabidopsis GAPA1/2 and GAPB use NADPH to generate  $\text{NADP}^+$ , which buffers free radical generation from the electron transport chain by dissipating the  $\text{H}^+$  gradient in the thylakoid membrane [52,53]. Therefore, by contributing to the maintenance of the  $\text{NAD(P)}^+/\text{NAD(P)H}$  ratio of the cell, plant GAPDHs influence cellular redox and general metabolism. In particular, Gapc1 plays a role in the glycolytic pathway, but at the same time, it can interact with  $\text{H}_2\text{O}_2$  thus becoming part of the ROS signaling cascade [51]. The regulation of several proteins involved in primary metabolism suggests that CdS QDs exposure had moderately influenced carbon metabolism. These include two proteins involved in the glycolytic pathway: the upregulation in wt of Gapc1 and the downregulation in two mutants of Eno2 (Figures 2, 3 and 5 and Table S2). This observation further supports the concept that CdS QDs exerts oxidative stress by reacting with cellular proteins and enzymes and subsequently generated free radicals [54]. As hypothesized by Tiwari et al. [55], the disruption or malfunction of the electron transport system in mitochondria and chloroplast by QDs, once they are inside the cell, could lead to ROS production [55]. In wt and the two mutants many proteins are involved in mitochondrial electron transport including V-type proton ATPase subunit B1 and B2 (Vha-b1, Vha-b2), prohibitin-3 (Phb3), and gamma carbonic anhydrase 2 (Gammaca2), with, in the chloroplast Calvin cycle, phosphoribulokinase (At1g32060) and chaperonin 60 subunit beta 1 (Cpn60b1) (Figure 3 and Table S2). It has been demonstrated that physical interaction with ENMs disrupts the normal function of organelles in cells. For example, mitochondrial damage is thought to be one of the possible mechanisms of ENMs cytotoxicity by inducing oxidative stress through the destruction and redistribution of normal electron transport by respiratory complexes [56]. V-type proton ATPase subunit B1 was downregulated in wt and in *atnp01*, while V-type proton ATPase subunit B2 was downregulated in *atnp02* (Figures 2 and 5). A study on Arabidopsis mitochondrial proteomics identified enolase among the enzymes associated with the outer mitochondrial membrane [57], and enolase is also proven to interact with the tonoplast through direct association with V-ATPase subunits, specifically the regulatory subunit Vha-b [58]. According to Ruotolo et al. [15], CdS QD treatment decreases respiratory efficiency and chlorophyll content in Arabidopsis [15]. Therefore, our findings support the involvement of the mitochondria respiratory process in CdS QDs responses in wt and both mutants. Interestingly, in the two mutants, respiration and photosynthesis were less sensitive to QDs than wt. Most of the studies carried out so far have dealt primarily with the overall plant stress response towards specific groups of ENMs, showing a differential abundance of proteins involved in oxidation-reduction, reactive oxygen species (ROS) detoxification, stress signaling, and hormonal pathways [59].

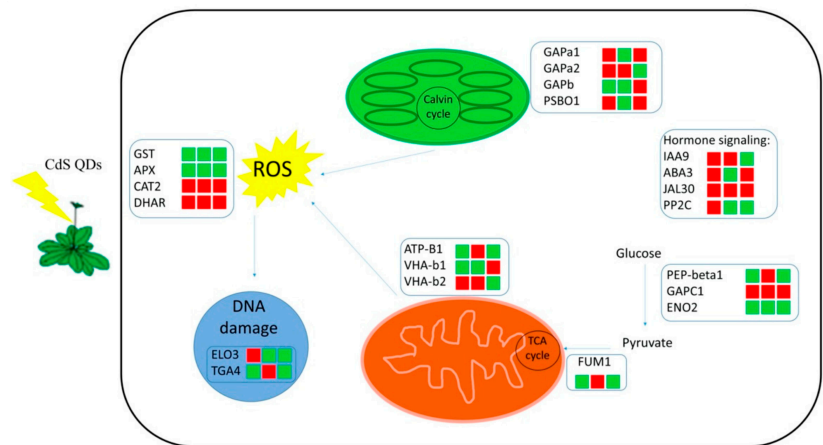


**Figure 5.** Model depicting the main *A. thaliana* proteome pathways responsive to CdS QDs treatment. For each protein the colored bars indicate up- (red) or downregulation (green). The first column indicates the up- and downregulated proteins in wt, while the second and third columns similarly show those in mutants *atnp01* and *atnp02*.

Interestingly, five glutathione S-transferases (GSTs), representative of  $\lambda$  and  $\phi$  classes of the GST family, have been identified in the proteome analysis (Figure 2 and Table S2). In wt, two GST family members, Gst F2 and F9, decreased under treatment, while GstF7 and Gst-darh3 increased; conversely, in *atnp02*, GstF3 was upregulated (Figures 2 and 5). The GST family in plants is notable for its structural and functional diversity, but the biochemical and physiological functions of each specific member remain to be clarified. As well as, or instead of, catalyzing conjugase reactions, some GSTs have antioxidative functions. The DHAR type of GST is one example. In addition, several subclasses of GST have peroxidase activity [60,61]. The detection of a large number of GSTs in the *A. thaliana* proteome is quite interesting; the functions of GSTs in the maintenance of the cell's redox balance, in xenobiotic detoxification and flavonoids subcellular transport is well known. GST expression is induced by a broad swathe of stressing conditions [62], including ENMs [63,64]. In *Arabidopsis*, ENMs induce an oxidative stress response by producing ROS, as has also been reported in crop plants [64,65]. Genes encoding for proteins of the NADPH oxidase and superoxide dismutase (SODs) families, and particularly peroxidases (PODs) and glutathione S-transferase (GST) families, involved in antioxidant pathways that promote ROS detoxification, become significantly modulated under CdS QD and CuO and ZnO NP treatments [24,66,67].

Exposure to ENMs may result in the change of transcription of genes involved in hormone signaling pathways, e.g., of auxin repressor or auxin response genes, abscisic acid (ABA) biosynthetic genes, or ethylene signaling components [68]. The present study, shows that in *A. thaliana* wt CdS QDs caused upregulation of the protein involved in the biosynthesis of auxins (auxin-responsive protein IAA9); in *atnp01* there was downregulation of proteins involved in the biosynthesis of ABA (molybdenum cofactor sulfurase), and in *atnp02* there was upregulation of a protein involved in the biosynthesis of jasmonate (JA) (PYK10-binding protein 1) and downregulation of the protein involved in the biosynthesis of auxin (IAA9) (Figures 2 and 5 and Table S2). ABA plays a key role in lateral root formation inhibition in plants exposed to environmental stress [69], and it is also an antagonist of brassicosteroids-promoted growth. Genes induced by ABA are upregulated by CdS QDs [14], CuO [66], and ZnO [67] NPs. In plants, protein phosphatase 2C 58 (PP2C) has been connected with the negative regulation of protein kinase cascades that are activated because of stress. Members of the PP2C family, such as ABI1 and ABI2, are involved in ABA signal transduction. ABA is a plant hormone crucial in mediating the

plant responses to environmental stresses [70]. In this work, we found that ABI1 and ABI2 are upregulated in the wt and downregulated in both mutants when treated with CdS QDs (Figures 2 and 5). These proteins are downregulated in both mutants probably because the signal transduction carried out by the hormone ABA is impaired in both mutants by the nanoparticles. The major role of JA (jasmonic acid) is defense against pathogens. However, this hormone plays a role in plant growth control [71]; the transcription of some JA responsive genes increased upon exposure to certain ENMs. Several genes involved in SA (salicylic acid) pathways, a signaling molecule that is important in general plant stress response, were downregulated by early exposure to Ag and TiO<sub>2</sub>; however, they were upregulated by exposure to CdS QD, CuO, and ZnO NPs [14,66,67]. The modulation of these proteins by CdS QDs treatment highlights the importance of hormones and signaling in the response mechanisms to these nanoparticles. Figure 5 gives an overview of all the above-mentioned pathways responsive to treatment with CdS QDs.

#### 3.4. Network Analysis

Starting from the molecular structure of the two mutants *atnp01* and *atnp02*, and using a network analysis, we tried to find any among the identified proteins which showed variations that could be correlated with the mutations. Three candidate genes were potentially affected by the mutagenic events in *atnp01* [14]. Two of these genes (At1g13880 and DLR1) are positioned on chromosome 1, the other (At3g46880) is on chromosome 3 (Figure 6) and encodes an unknown protein localized in the chloroplast, which does not interact with any other protein. DRL1 encodes a cytoplasm-localized calmodulin binding protein involved in leaf development and meristem structural organization. DLR1 is a homolog of the yeast TOT4/KTI12 protein which associates with elongator, a multisubunit complex binding to RNA polymerase II transcription elongation complex [72]. DRL1 interacts with two differentially abundant proteins found with 2D-PAGE: elongator complex protein 3 (Elo3) and magnesium-chelatase subunit Chli-2 (Chli2) (Figure 6A), which are respectively down- and upregulated in *atnp01*. Elo3 is one of the six subunits of Arabidopsis Elongator Complex (AtELP) [73]. *Atelp/elo* mutants display pleiotropic phenotypes, including resistance to oxidative stress, hypersensitivity to abscisic acid, severely aberrant auxin phenotypes, altered cell cycle progression, abnormal root development, and disease susceptibility [74–76]. Recent studies have shown that AtELP3, together with AtELP2, regulates the kinetics of pathogen-induced transcriptome reprogramming [77]. CHLI isoforms in Arabidopsis are encoded by two genes: Chli1 (At4g18480) and Chli2 (At5g45930). Chli1 seems to be the major functional form since chlorophyll levels in *chli1*-null mutants are reduced to 10% to 17% of the wild-type level [78]. It has been hypothesized that Chli2 could support some chlorophyll biosynthesis in the complete absence of Chli1 [79]. At1g13880 (Elm2) is a member of the MYB class of transcription factors. Elm2 has only a limited role in mitochondrial fission, but it is a 54% paralog with ELM1 which has a fundamental function in mitochondrial fission [80]. Elm2 interacts with one differentially abundant upregulated protein, NifU-like protein 3 (Nfu3), which is involved [81] in the cluster assembly of chloroplastic Fe-S proteins (Figure 6A).

The *atnp02* mutagenic event affected genes on chromosome 3, potentially At3g24330, encoding an O-glycosyl hydrolase localized in the endomembrane, and At3g24430 (Hcf101) encoding an ATP binding protein localized in the chloroplast. The mutagenic element lay within the At3g24400 pseudogene (AtPERK2), which possibly encodes a proline-rich extensin-like receptor kinase [14]. Hcf101 results were bound in the network with Nfu3, which in this case is downregulated (Figure 6B). The gene *Perk2* interacts with the downregulated protein phosphatase 2C (At4g28400) (Figure 6B). This protein has already been described in Sections 3.1 and 3.3 and is the only one in common among the wt and the two mutants. The hypothesis is that the proteins related to these mutated genes were also the main targets in the signal cascade deriving from interaction with CdS QDs during the treatment.

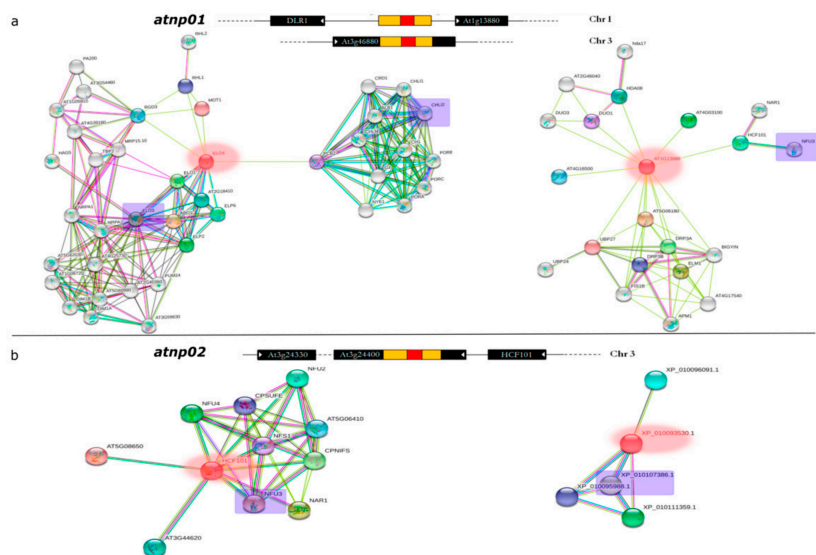


**Figure 6.** Molecular interaction network of differentially abundant proteins. The mutated genes in the two mutant lines are shown in red in all the networks. A schematic above each network shows the structure of the mutated genes as in [14]. The segment in red and yellow is the insertion element (Ac), the segments in black are the mutated genes and Chr indicates the chromosomes on which these genes are positioned. The putative proteins that were found in the protein analysis and that connect in the network are indicated with blue rectangles. Networks for mutant *atnp01* (a) and mutant *atnp02* (b). Colored lines and dots indicate different types of interaction evidence (cyan, from curated databases; green, gene neighborhood; blue, gene co-occurrence; pink, experimentally determined; black, co-expression; light blue, protein homology).

### 3.5. Comparison between 2D-PAGE, Pf2D, and Transcriptomics

Marmiroli et al. [25] compared the proteomes of wt and the two mutants, treated with 80 mg/L CdS QDs, using a gel-less technique based on liquid IEF in the first dimension and HPLC in the second dimension, performed with a ProteomeLab<sup>TM</sup> PF2D (Beckman Coulter) [25]. The IEF gradient was pH 4–8.5 and the most water-soluble proteins were separated with this method. In our experiments we found four proteins in common with Marmiroli et al. [25]. For the wild type: ribulose biphosphate carboxylase large chain (rbcl) (Rubisco large chain) [82], (downregulated in both cases); glutathione S-transferase DHAR3 (Dhar3) and pathogenesis-related protein 5 (At1g75040) (both proteins upregulated in all cases); for the mutant *atnp02*: heat shock 70 kDa protein 10 mitochondrial (Hsp70-10) (upregulated). For the mutant *atnp01* there were no common proteins.

Plant pathogenesis-related (PR) proteins are expressed in response to pathogen attack, developmental processes and environmental stresses; some of these proteins are constitutively expressed [83]. Hsp70-10 was required for transport of secretory proteins from the Golgi complex [84]. Comparing our data with the transcriptomics results reported in Marmiroli et al. [14], we found three proteins in common: osmotin-like protein OSM34 (Osm34), pathogenesis-related protein 5 (At1g75040) and phosphatidylinositol/phosphatidylcholine transfer protein SFH3 (Sfh3). OSM34 was always upregulated both in the transcriptomics and in the proteomics in the wt and in the two mutants. This protein is usually considered a response protein to osmotic stress [85]. Pathogenesis-related protein 5 was upregulated in the transcriptomics, and in the proteomics was also upregulated in both wt and mutant *atnp01*. This protein was in common with the gel-less proteomic study performed with PF2D (see above). For all lines Sfh3 was found downregulated in the transcriptomic, while in our study was upregulated in *atnp01* and downregulated in wt

and in *atnp02*. These common proteins are mostly related to the oxidative stress response, which seems to be the driving stress arising from the interactions with CdS QDs [15].

Figure 7 shows the levels of correlation between proteomics (2D-PAGE)/transcriptomics, proteomics (PF2D)/transcriptomics, and proteomics (2D-PAGE)/proteomic (PF2D) markers. The figure was obtained by comparing 98 significant proteins obtained with 2D-PAGE with 88 selected proteins obtained with PF2D and the significant group of transcripts obtained with an Arabidopsis microarray platform. It is well known that the correlation between proteomics and transcriptomics is moderate to low [25,29], and in this case is also strongly biased by the difference between the higher number of transcripts and the lower number of proteins. Therefore, the proteins/transcripts considered as molecular markers showing this degree of correlation in the three comparisons are viewed as robust enough to be considered candidate “-omics” CdS QDs exposure markers.

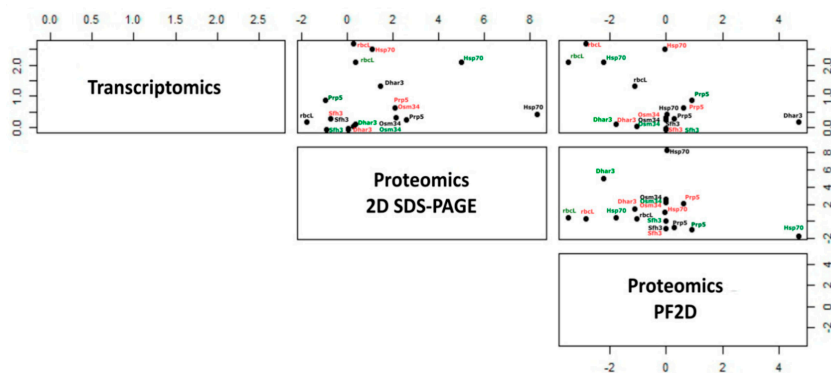


**Figure 7.** Scatterplot matrix of the independent variables: transcriptome, proteome with 2D-PAGE, and proteome with PF2D. The three-dimensional scatterplot represents the correlation among gene expression, protein abundance with 2D-PAGE and protein abundance with Pf2D. The lines are represented in black for wt, in red for *atnp01*, and in green for *atnp02*. Transcriptomics data are taken from array analysis in Marmioli et al. [14], and proteomic with PF2D data from Marmioli et al. [25]. Each point represents a protein/transcript for the different plant lines using colors as above.

#### 4. Conclusions

The majority of the differential abundance proteins in the wt were downregulated on exposure to CdS QDs and in Mapman bins annotated to processes like protein folding, biotic and abiotic stress responses, and protein degradation. Conversely, in both mutants, there was a balance in numbers between reprogrammed up- and downregulated proteins (Figure 2). Mapman bins for the mutant *atnp01* were protein degradation, abiotic stress and mitochondrial electron transport. These pathways are all typical of the responses to nanomaterials [86]. For the mutant *atnp02*, the main Mapman bins were glycolysis, mitochondrial electron transport, photosynthesis and hormone metabolism [15,86]. These results indicate that in *atnp02* the photosynthetic apparatus was impaired by treatment with CdS QDs, in addition to the other categories, especially hormone metabolism and mitochondrial electron transport chain, which were common to both mutants.

Network analysis showed that in the two mutants, the genes affected by the transposons are responsible for regulation of four proteins: *Nfu*, *Elo3*, *Chli2* and *PP2c*, involved respectively in chloroplast assembly, transcription elongation, chlorophyll biosynthesis and abiotic stress response. The reprogramming of these particular proteins demonstrates the importance of the chloroplast and of photosynthesis in the responses to CdS QDs of the mutants.

The authors are perfectly aware that there are more powerful proteomic tools available for plants (i.e., iTRAQ) which can give higher resolution and better quantification than

2D-PAGE. The purpose of this paper was to compare protein variations resulting from samples treated with CdS QDs vs. untreated controls, which certainly may benefit from powerful proteomic tools, but at the same time to probe these variations with the aid of a genetic tool, two CdS QDs-tolerant mutants. The use of the two mutants allowed refining the protein comparison from a large systematic and almost taxonomic level to a comparison in which a small proportion of proteins were objectively important. The two mutants consistently narrowed the proteomic range, allowing focus on those proteins specific for the tolerant phenotype rather than attention being dispersed on a plethora of proteins that were more aligned to networking effects. This approach is suitable not only following treatment with CdS QDs, but also for many other stressed conditions.

**Supplementary Materials:** The following are available online at <https://www.mdpi.com/2079-4991/11//615/s1>, Supplementary File 1: S.1. Supplementary methods related to nanoparticles synthesis and characterization. S.2. MapMan pathways identified under QDs treatment. Figure S1. HRTEM image of ligand-free QDs assembly and X-ray diffraction pattern. Figure S2. (A) ESEM image of the CdS QDs agglomerates. (B) X ray spectra corresponding to the red rectangle in figure S2A. Figure S3. 2D SDS-PAGE. Figure S4. Venn diagrams for common and non-common proteins to wt and *atnp01*, to wt and *atnp02*, to *atnp01* and *atnp02* (a) in the control and (b) in treatment conditions. Figure S5. Heat map of *A. thaliana* wt and mutant lines *atnp01* and *atnp02* not treated and treated with 80 mg L<sup>-1</sup> CdS QDs. Figure S6. Gene Ontology and enrichment analyses with fold enrichment =  $-\log_{10}$  (Fisher's exact *p* value) for molecular function wt (a); cellular component wt (b); molecular function *atnp01* (c); cellular component *atnp01* (d); molecular function *atnp02* (e), cellular component *atnp02* (f). Figure S7. Cell function overview map after CdS QDs exposure. Cell functions associated with the proteomic changes affecting *Arabidopsis thaliana* after CdS QDs exposure in wt (a) *atnp01* (b) and in *atnp02* (c) using MapMan software. Figure S8. Biotic stress overview map after CdS QDs exposure. Stress response associated with the proteomic changes affecting *A. thaliana* after CdS QDs exposure in wt (a) *atnp01* (b) and in *atnp02* (c) using MapMan software. Table S2. MapMan BIN assignment and description of differentially expressed proteins in *Arabidopsis thaliana*. Supplementary File 2: Table S1. MALDI-TOF/TOF data associated with differentially expressed proteins identified by 2D-PAGE.

**Author Contributions:** N.M., V.G., M.M. organized the experimental setup and collaborated in writing the manuscript. V.G. performed the experiment, analyzed the data and helped in writing the manuscript. M.V. and A.Z. provided the CdS QDs and their physico-chemical characterization. All authors have read and agreed to the published version of the manuscript.

**Funding:** This research received no external funding.

**Informed Consent Statement:** Not applicable.

**Data Availability Statement:** Publicly available datasets were analyzed in this study. This data can be found here: [doi:10.1021/es404958r; doi.org/10.3389/fpls.2015.01104].

**Acknowledgments:** The authors acknowledge the assistance of Gianluca Paredi (Department of Pharmacy, University of Parma) for MS analysis, of CIM (Parma, Italy) for access to MALDI-TOF-MS facilities. Martin Shepherd is acknowledged for helpful suggestions and language revision.

**Conflicts of Interest:** The authors declare no conflict of interest.

## References

1. Cota-Ruiz, K.; Delgado-Rios, M.; Martínez-Martínez, A.; Núñez-Gastelum, J.A.; Peralta-Videa, J.R.; Gardea-Torresdey, J.L. Current findings on terrestrial plants—Engineered nanomaterial interactions: Are plants capable of phytoremediating nanomaterials from soil? *Curr. Opin. Environ. Sci. Health* **2018**, *6*, 9–15. [[CrossRef](#)]
2. Hatami, M.; Kariman, K.; Ghorbanpour, M. Engineered nanomaterial-mediated changes in the metabolism of terrestrial plants. *Sci. Total. Environ.* **2016**, *571*, 275–291. [[CrossRef](#)]
3. Alivisatos, A.P. Semiconductor Clusters, Nanocrystals, and Quantum Dots. *Science* **1996**, *271*, 933–937. [[CrossRef](#)]
4. Matea, C.T.; Mocan, T.; Tabaran, F.; Pop, T.; Mosteanu, O.; Puia, C.; Iancu, C.; Mocan, L. Quantum dots in imaging, drug delivery and sensor applications. *Int. J. Nanomed.* **2017**, *12*, 5421–5431. [[CrossRef](#)] [[PubMed](#)]
5. Pang, C.; Gong, Y. Current Status and Future Prospects of Semiconductor Quantum Dots in Botany. *J. Agric. Food Chem.* **2019**, *67*, 7561–7568. [[CrossRef](#)] [[PubMed](#)]

6. Padmanabhan, P.; Kumar, A.; Kumar, S.; Chaudhary, R.K.; Gulyás, B. Nanoparticles in practice for molecular-imaging applications: An overview. *Acta Biomater.* **2016**, *41*, 1–16. [[CrossRef](#)]
7. Wang, Z.-G.; Liu, S.-L.; Hu, Y.-J.; Tian, Z.-Q.; Hu, B.; Zhang, Z.-L.; Pang, D.-W. Dissecting the Factors Affecting the Fluorescence Stability of Quantum Dots in Live Cells. *ACS Appl. Mater. Interfaces* **2016**, *8*, 8401–8408. [[CrossRef](#)] [[PubMed](#)]
8. Qiu, Q.; Wang, P.; Xu, L.; Wang, D.; Lin, Y.; Xie, T. Photoelectrical properties of CdS/CdSe core/shell QDs modified anatase TiO<sub>2</sub> nanowires and their application for solar cells. *Phys. Chem. Chem. Phys.* **2017**, *19*, 15724–15733. [[CrossRef](#)]
9. Moon, H.; Lee, C.; Lee, W.; Kim, J.; Chae, H. Stability of Quantum Dots, Quantum Dot Films, and Quantum Dot Light-Emitting Diodes for Display Applications. *Adv. Mater.* **2019**, *31*, e1804294. [[CrossRef](#)]
10. Matos, B.; Martins, M.; Samamed, A.C.; Sousa, D.; Ferreira, I.; Diniz, M.S. Toxicity Evaluation of Quantum Dots (ZnS and CdS) Singly and Combined in Zebrafish (*Danio rerio*). *Int. J. Environ. Res. Public Health* **2019**, *17*, 232. [[CrossRef](#)] [[PubMed](#)]
11. Modlitbová, P.; Pořízka, P.; Novotný, K.; Drbohlavová, J.; Chamradová, I.; Farka, Z.; Zlámalová-Gargošová, H.; Romih, T.; Kaiser, J. Short-term assessment of cadmium toxicity and uptake from different types of Cd-based Quantum Dots in the model plant *Allium cepa* L. *Ecotoxicol. Environ. Saf.* **2018**, *153*, 23–31. [[CrossRef](#)]
12. Favero, P.P.; de Souza-Parise, M.; Fernandez, J.L.R.; Miotto, R.; Ferraz, A.C. Surface properties of CdS nanoparticles. *Braz. J. Phys.* **2006**, *36*, 1032–1034. [[CrossRef](#)]
13. Wu, T.; Tang, M. Toxicity of quantum dots on respiratory system. *Inhal. Toxicol.* **2014**, *26*, 128–139. [[CrossRef](#)]
14. Marmioli, M.; Pagano, L.; Sardaro, M.L.S.; Villani, M. Genome-Wide Approach in *Arabidopsis thaliana* to Assess the Toxicity of Cadmium Sulfide Quantum Dots. *Environ. Sci. Technol.* **2014**, *48*, 5902–5909. [[CrossRef](#)] [[PubMed](#)]
15. Ruotolo, R.; Maestri, E.; Pagano, L.; Marmioli, M.; White, J.C.; Marmioli, N. Plant Response to Metal-Containing Engineered Nanomaterials: An Omics-Based Perspective. *Environ. Sci. Technol.* **2018**, *52*, 2451–2467. [[CrossRef](#)] [[PubMed](#)]
16. Pagano, L.; Maestri, E.; Caldara, M.; White, J.C.; Marmioli, N.; Marmioli, M. Engineered Nanomaterial Activity at the Organelle Level: Impacts on the Chloroplasts and Mitochondria. *ACS Sustain. Chem. Eng.* **2018**, *6*, 12562–12579. [[CrossRef](#)]
17. Pasquali, F.; Agrimonti, C.; Pagano, L.; Zappettini, A.; Villani, M.; Marmioli, M.; White, J.C.; Marmioli, N. Nucleo-mitochondrial interaction of yeast in response to cadmium sulfide quantum dot exposure. *J. Hazard. Mater.* **2017**, *324*, 744–752. [[CrossRef](#)]
18. Paesano, L.; Marmioli, M.; Bianchi, M.G.; White, J.C.; Bussolati, O.; Zappettini, A.; Villani, M.; Marmioli, N. Differences in toxicity, mitochondrial function and miRNome in human cells exposed in vitro to Cd as CdS quantum dots or ionic Cd. *J. Hazard. Mater.* **2020**, *393*, 122430. [[CrossRef](#)]
19. Oh, E.; Liu, R.; Nel, A.; Gemill, K.B.; Bilal, M.; Cohen, Y.; Medintz, I.L. Meta-analysis of cellular toxicity for cadmium-containing quantum dots. *Nat. Nanotechnol.* **2016**, *11*, 479–486. [[CrossRef](#)] [[PubMed](#)]
20. Yan, Y.; Gong, J.; Chen, J.; Zeng, Z.; Huang, W.; Pu, K.; Liu, J.; Chen, P. Recent advances on Graphene Quantum Dots: From chemistry and physics to applications. *Adv. Mater.* **2019**, *31*, e1808283. [[CrossRef](#)] [[PubMed](#)]
21. Wang, Y.; Tang, M. Dysfunction of various organelles provokes multiple cell death after quantum dot exposure. *Int. J. Nanomed.* **2018**, *13*, 2729–2742. [[CrossRef](#)] [[PubMed](#)]
22. Rocha, T.L.; Bilbao, E.; Cardoso, C.; Soto, M.; Bebianno, M.J. Changes in metallothionein transcription levels in the mussel *Mytilus galloprovincialis* exposed to CdTe quantum dots. *Ecotoxicology* **2018**, *27*, 402–410. [[CrossRef](#)]
23. Majumdar, S.; Ma, C.; Villani, M.; Zuverza-Mena, N.; Pagano, L.; Huang, Y.; Zappettini, A.; Keller, A.A.; Marmioli, N.; Dhankher, O.P.; et al. Surface coating determines the response of soybean plants to cadmium sulfide quantum dots. *NanoImpact* **2019**, *14*, 100151. [[CrossRef](#)]
24. Marmioli, M.; Mussi, F.; Pagano, L.; Imperiale, D.; Lencioni, G.; Villani, M.; Zappettini, A.; White, J.C.; Marmioli, N. Cadmium sulfide quantum dots impact *Arabidopsis thaliana* physiology and morphology. *Chemosphere* **2020**, *240*, 124856. [[CrossRef](#)]
25. Marmioli, M.; Imperiale, D.; Pagano, L.; Villani, M.; Zappettini, A.; Marmioli, N. The proteomic response of *Arabidopsis thaliana* to cadmium sulfide quantum dots, and its correlation with the transcriptomic response. *Front. Plant Sci.* **2015**, *6*, 1104. [[CrossRef](#)]
26. Marmioli, M.; Lepore, G.O.; Pagano, L.; D'Acapito, F.; Gianoncelli, A.; Villani, M.; Lazzarini, L.; White, J.C.; Marmioli, N. The fate of CdS quantum dots in plants as revealed by extended X-ray absorption fine structure (EXAFS) analysis. *Environ. Sci. Nano* **2020**, *7*, 1150–1162. [[CrossRef](#)]
27. Hajduch, M.; Hearne, L.B.; Mierny, J.A.; Casteel, J.E.; Joshi, T.; Agrawal, G.K.; Song, Z.; Zhou, M.; Xu, D.; Thelen, J.J. Systems Analysis of Seed Filling in *Arabidopsis*: Using General Linear Modeling to Assess Concordance of Transcript and Protein Expression. *Plant Physiol.* **2010**, *152*, 2078–2087. [[CrossRef](#)] [[PubMed](#)]
28. Pütz, S.M.; Boehm, A.M.; Stiewe, T.; Sickmann, A. iTRAQ Analysis of a Cell Culture Model for Malignant Transformation, Including Comparison with 2D-PAGE and SILAC. *J. Proteome Res.* **2012**, *11*, 2140–2153. [[CrossRef](#)]
29. Gallo, V.; Srivastava, V.; Bulone, V.; Zappettini, A.; Villani, M.; Marmioli, N.; Marmioli, M. Proteomic analysis identifies markers of exposure to Cadmium Sulfide Quantum Dots (CdS QDs). *Nanomaterials* **2020**, *10*, 1214. [[CrossRef](#)]
30. Rocco, M.; D'Ambrosio, C.; Arena, S.; Faurobert, M.; Scaloni, A.; Marra, M. Proteomic analysis of tomato fruits from two ecotypes during ripening. *Proteomics* **2006**, *6*, 3781–3791. [[CrossRef](#)]
31. Faurobert, M.; Mihr, C.; Bertin, N.; Pawlowski, T.; Negroni, L.; Sommerer, N.; Causse, M. Major Proteome Variations Associated with Cherry Tomato Pericarp Development and Ripening. *Plant Physiol.* **2007**, *143*, 1327–1346. [[CrossRef](#)] [[PubMed](#)]
32. Ramagli, L.S.; Rodriguez, L.V. Quantitation of microgram amounts of protein in SDS-mercaptoethanol-tris electrophoresis sample buffer. *Electrophoresis* **1985**, *6*, 559–563. [[CrossRef](#)]

33. Shevchenko, A.; Tomas, H.; Havlis, J.; Olsen, J.V.; Mann, M.J. In-gel digestion for mass spectrometric characterization of proteins and proteomes. *Nat. Protoc.* **2006**, *1*, 2856–2860. [[CrossRef](#)]
34. Singh, A.; Giri, J.; Kapoor, S.; Tyagi, A.K.; Pandey, G.K. Protein phosphatase complement in rice: Genome-wide identification and transcriptional analysis under abiotic stress conditions and reproductive development. *BMC Genom.* **2010**, *11*, 435. [[CrossRef](#)]
35. Yoshida, T.; Nishimura, N.; Kitahata, N.; Kuromori, T.; Ito, T.; Asami, T.; Shinozaki, K.; Hirayama, T. ABA-hypersensitive germination3 encodes a protein phosphatase 2C (AtPP2CA) that strongly regulates abscisic acid signaling during germination in Arabidopsis protein phosphatase 2Cs. *Plant Physiol.* **2006**, *140*, 115–126. [[CrossRef](#)] [[PubMed](#)]
36. Singh, A.; Jha, S.K.; Bagri, J. ABA inducible rice protein phosphatase 2C confers ABA insensitivity and abiotic stress tolerance in Arabidopsis. *PLoS ONE* **2015**, *10*, e0125168.
37. Andriotis, V.M.E.; Kruger, N.J.; Pike, M.J.; Smith, A.M. Plastidial glycolysis in developing Arabidopsis embryos. *New Phytol.* **2009**, *185*, 649–662. [[CrossRef](#)]
38. Jiang, L.; Yang, S.-L.; Xie, L.-F.; Puah, C.S.; Zhang, X.-Q.; Yang, W.-C.; Sundaresan, V.; Ye, D. VANGUARD1 Encodes a Pectin Methyltransferase That Enhances Pollen Tube Growth in the Arabidopsis Style and Transmitting Tract. *Plant Cell* **2005**, *17*, 584–596. [[CrossRef](#)]
39. Semane, B.; Dupae, J.; Cuyper, A.; Noben, J.P.; Tuomainen, M.; Karenlampi, S.; Van Belleghem, F.; Smeets, K.; Vangrosveld, J. Leaf proteome responses of *Arabidopsis thaliana* exposed to mild Cadmium stress. *J. Plant Physiol.* **2010**, *167*, 247–254. [[CrossRef](#)] [[PubMed](#)]
40. Calderon-Villalobos, L.I.A.; Nill, C.; Marrocco, K.; Kretsch, T.; Schweichheimer, C. The evolutionarily conserved Arabidopsis thaliana F-box protein AtFBP7 is required for efficient translation during temperature stress. *Gene* **2007**, *392*, 106–116. [[CrossRef](#)]
41. Yi, X.; McChargue, M.; Laborde, S.; Frankel, L.K.; Bricker, T.M. The manganese-stabilizing protein is required for photosystem II assembly/stability and photoautotrophy in higher plants. *J. Biol. Chem.* **2005**, *280*, 16170–16174. [[CrossRef](#)]
42. Kosma, D.K.; Molina, I.; Ohlrogge, J.B.; Pollard, M. Identification of an Arabidopsis Fatty Alcohol:Caffeoyl-Coenzyme A Acyltransferase Required for the Synthesis of Alkyl Hydroxycinnamates in Root Waxes. *Plant Physiol.* **2012**, *160*, 237–248. [[CrossRef](#)] [[PubMed](#)]
43. Perales, M.; Eubel, H.; Heinemeyer, J.; Colaneri, A.; Zabaleta, E.; Braun, H.-P. Disruption of a Nuclear Gene Encoding a Mitochondrial Gamma Carbonic Anhydrase Reduces Complex I and Supercomplex I+III2 Levels and Alters Mitochondrial Physiology in Arabidopsis. *J. Mol. Biol.* **2005**, *350*, 263–277. [[CrossRef](#)] [[PubMed](#)]
44. Gaudet, P.; Livstone, M.S.; Lewis, S.E.; Thomas, P.D. Phylogenetic-based propagation of functional annotations within the Gene Ontology consortium. *Briefings Bioinform.* **2011**, *12*, 449–462. [[CrossRef](#)] [[PubMed](#)]
45. Bach-Pages, M.; Homma, F.; Kourelis, J.; Kaschani, F.; Mohammed, S.; Kaiser, M.; Van Der Hoorn, R.A.L.; Castello, A.; Preston, G.M. Discovering the RNA-Binding Proteome of plant leaves with an improved RNA interactome capture method. *Biomolecules* **2020**, *10*, 661. [[CrossRef](#)] [[PubMed](#)]
46. Sarry, J.-E.; Kuhn, L.; Ducruix, C.; Lafaye, A.; Junot, C.; Hugouvieux, V.; Jourdain, A.; Bastien, O.; Fievet, J.B.; Vailhen, D.; et al. The early responses of Arabidopsis thaliana cells to cadmium exposure explored by protein and metabolite profiling analyses. *Proteomics* **2006**, *6*, 2180–2198. [[CrossRef](#)]
47. Kwak, K.J.; Kim, Y.O.; Kang, H. Characterization of transgenic Arabidopsis plants overexpressing GR-RBP4 under high salinity, dehydration, or cold stress. *J. Exp. Bot.* **2005**, *56*, 3007–3016. [[CrossRef](#)]
48. Lawere, S.L.; Raskar, S. Effect of titanium dioxide nanoparticles on hydrolytic and antioxidant enzymes during seed germination in onion. *Int. J. Curr. Microbiol. App. Sci.* **2014**, *3*, 749–760.
49. Ueda, T.; Yamaguchi, M.; Uchimiya, H.; Nakano, A. Ara6, a plant-unique novel type Rab GTPase, functions in the endocytic pathway of Arabidopsis thaliana. *EMBO J.* **2001**, *20*, 4730–4741. [[CrossRef](#)]
50. Zaffagnini, M.; Fermani, S.; Costa, A.; Lemaire, S.D.; Trost, P. Plant cytoplasmic GAPDH: Redox post-translational modifications and moonlighting properties. *Front. Plant Sci.* **2013**, *4*, 450. [[CrossRef](#)] [[PubMed](#)]
51. Rius, S.P.; Casati, P.; Iglesias, A.A.; Gomez-Casati, D.F. Characterization of Arabidopsis Lines Deficient in GAPC-1, a Cytosolic NAD-Dependent Glyceraldehyde-3-Phosphate Dehydrogenase. *Plant Physiol.* **2008**, *148*, 1655–1667. [[CrossRef](#)] [[PubMed](#)]
52. Baalman, E.; Backhausen, J.E.; Rak, C.; Vetter, S.; Scheibe, R. Reductive modification and nonreductive activation of purified spinach chloroplast NADP-dependent glyceraldehyde-3-phosphate dehydrogenase. *Arch. Biochem. Biophys.* **1995**, *324*, 201–208. [[CrossRef](#)] [[PubMed](#)]
53. Price, G.D.; Evans, J.; Caemmerer, S.; Yu, J.-W.; Badger, M. Specific reduction of chloroplast glyceraldehyde-3-phosphate dehydrogenase activity by antisense RNA reduces CO<sub>2</sub> assimilation via a reduction in ribulose biphosphate regeneration in transgenic tobacco plants. *Planta* **1995**, *195*, 369–378. [[CrossRef](#)] [[PubMed](#)]
54. Garcia-Sánchez, S.; Bernales, I.; Cristobal, S. Early response to nanoparticles in the Arabidopsis transcriptome compromises plant defence and root-hair development through salicylic acid signaling. *BMC Genom.* **2015**, *16*, 341. [[CrossRef](#)]
55. Tiwari, M.; Krishnamurthy, S.; Shukla, D.; Kiiskila, J.; Jain, A.; Datta, R.; Sharma, N.; Sahi, S.V. Comparative transcriptome and proteome analysis to reveal the biosynthesis of gold nanoparticles in Arabidopsis. *Sci. Rep.* **2016**, *6*, 21733. [[CrossRef](#)]
56. Marmiroli, M.; Maestri, E.; Pagano, L.; Robinson, B.H.; Ruotolo, R.; Marmiroli, N. Toxicology assessment of engineered nanomaterials: Innovation and tradition. In *Exposure to Engineered Nanomaterials in the Environment*; Elsevier BV: Amsterdam, The Netherlands, 2019; Volume 8, pp. 209–234.

57. Giegé, P.; Heazlewood, J.L.; Roessner-Tunali, U.; Millar, A.H.; Fernie, A.R.; Leaver, C.J.; Sweetlove, L.J. Enzymes of glycolysis are functionally associated with the mitochondrion in Arabidopsis cells. *Plant Cell* **2003**, *15*, 2140–2151. [[CrossRef](#)]
58. Barkla, B.J.; Vera-Estrella, R.; Hernández-Coronado, M.; Pantoja, O. Quantitative proteomics of the tonoplast Reveals a Role for Glycolytic Enzymes in Salt Tolerance. *Plant Cell* **2009**, *21*, 4044–4058. [[CrossRef](#)]
59. Hossain, Z.; Mustafa, G.; Komatsu, S. Plant Responses to Nanoparticle Stress. *Int. J. Mol. Sci.* **2015**, *16*, 26644–26653. [[CrossRef](#)]
60. Wagner, U.; Edwards, R.; Dixon, D.P.; Mauch, F. Probing the Diversity of the Arabidopsis glutathione S-Transferase Gene Family. *Plant Mol. Biol.* **2002**, *49*, 515–532. [[CrossRef](#)]
61. Dixon, D.P.; Edwards, R. Glutathione Transferases. *Arab. Book* **2010**, *8*, e0131. [[CrossRef](#)]
62. Moons, A. Regulatory and Functional Interactions of Plant Growth Regulators and Plant Glutathione S-Transferases (GSTs). *Vitam. Horm.* **2005**, *72*, 155–202. [[CrossRef](#)] [[PubMed](#)]
63. Nair, P.M.G.; Park, S.Y.; Choi, J. Evaluation of the effect of silver nanoparticles and silver ions using stress responsive gene expression in *Chironomus riparius*. *Chemosphere* **2013**, *92*, 592–599. [[CrossRef](#)] [[PubMed](#)]
64. Tiwari, M.; Sharma, N.C.; Fleischmann, P.; Burbage, J.; Venkatachalam, P.; Sahi, S.V. Nanotitania Exposure Causes Alterations in Physiological, Nutritional and Stress Responses in Tomato (*Solanum lycopersicum*). *Front. Plant Sci.* **2017**, *8*, 633. [[CrossRef](#)]
65. Pagano, L.; Pasquali, F.; Majumdar, S.; De La Torre-Roche, R.; Zuverza-Mena, N.; Villani, M.; Zappettini, A.; Marra, R.E.; Isch, S.M.; Marmiroli, M.; et al. Exposure of Cucurbita pepo to binary combinations of engineered nanomaterials: Physiological and molecular response. *Environ. Sci. Nano* **2017**, *4*, 1579–1590. [[CrossRef](#)]
66. Tang, Y.; He, R.; Zhao, J.; Nie, G.; Xu, L.; Xing, B. Oxidative stress-induced toxicity of CuO nanoparticles and related toxicogenomic responses in Arabidopsis thaliana. *Environ. Pollut.* **2016**, *212*, 605–614. [[CrossRef](#)] [[PubMed](#)]
67. Landa, P.; Prerostova, S.; Petrova, S.; Knirsch, V.; Vankova, R.; Vanek, T. The transcriptomic response of Arabidopsis thaliana to Zinc Oxide: A comparison of the impact of Nanoparticle, Bulk, and Ionic Zinc. *Environ. Sci. Technol.* **2015**, *49*, 14537–14545. [[CrossRef](#)]
68. Syu, Y.-Y.; Hung, J.-H.; Chen, J.-C.; Chuang, H.-W. Impacts of size and shape of silver nanoparticles on Arabidopsis plant growth and gene expression. *Plant Physiol. Biochem.* **2014**, *83*, 57–64. [[CrossRef](#)]
69. De Smet, I.; Signora, L.; Beeckman, T.; Inzé, D.; Foyer, C.H.; Zhang, H. An abscisic acid-sensitive checkpoint in lateral root development of Arabidopsis. *Plant J.* **2003**, *33*, 543–555. [[CrossRef](#)]
70. Chandler, P.M.; Robertson, M. Gene Expression Regulated by Abscisic Acid and its Relation to Stress Tolerance. *Annu. Rev. Plant Biol.* **1994**, *45*, 113–141. [[CrossRef](#)]
71. Jaillais, Y.; Chory, J. Unraveling the paradoxes of plant hormone signaling integration. *Nat. Struct. Mol. Biol.* **2010**, *17*, 642–645. [[CrossRef](#)]
72. Mehlgarten, C.; Prochaska, H.; Hammermeister, A.; Abdel-Fattah, W.; Wagner, M.; Krutyholowa, R.; Jun, S.E.; Kim, G.-T.; Glatt, S.; Breunig, K.D.; et al. Use of a Yeast tRNase Killer Toxin to Diagnose Kti12 Motifs Required for tRNA Modification by Elongator. *Toxins* **2017**, *9*, 272. [[CrossRef](#)] [[PubMed](#)]
73. Woloszyńska, M.; Le Gall, S.; Van Lijsebettens, M. Plant Elongator-mediated transcriptional control in a chromatin and epigenetic context. *Biochim. Biophys. Acta (BBA)-Gene Regul. Mech.* **2016**, *1859*, 1025–1033. [[CrossRef](#)]
74. Chen, Z.; Zhang, H.; Jablonowski, D.; Zhou, X.; Ren, X.; Hong, X.; Schaffrath, R.; Zhu, J.-K.; Gong, Z. Mutations in ABO1/ELO2, a Subunit of Holo-Elongator, Increase Abscisic Acid Sensitivity and Drought Tolerance in Arabidopsis thaliana. *Mol. Cell. Biol.* **2006**, *26*, 6902–6912. [[CrossRef](#)]
75. Zhou, X.; Hua, D.; Chen, Z.; Zhou, Z.; Gong, Z. Elongator mediates ABA responses, oxidative stress resistance and anthocyanin biosynthesis in Arabidopsis. *Plant J.* **2009**, *60*, 79–90. [[CrossRef](#)] [[PubMed](#)]
76. Xu, D.; Huang, W.; Li, Y.; Wang, H.; Huang, H.; Cui, X. Elongator complex is critical for cell cycle progression and leaf patterning in Arabidopsis. *Plant J.* **2011**, *69*, 792–808. [[CrossRef](#)]
77. DeFraia, C.T.; Wang, Y.; Yao, J.; Mou, Z. Elongator subunit 3 positively regulates plant immunity through its histone acetyltransferase and radical S-adenosylmethionine domains. *BMC Plant Biol.* **2013**, *13*, 102. [[CrossRef](#)]
78. Rissler, H.M.; Collakova, E.; Della Penna, D.; Whelan, J.; Pogson, B.J. Chlorophyll biosynthesis. Expression of a second chl I gene of magnesium chelatase in Arabidopsis supports only limited chlorophyll synthesis. *Plant Physiol.* **2002**, *128*, 770–779. [[CrossRef](#)] [[PubMed](#)]
79. Huang, Y.-S.; Li, H.-M. Arabidopsis CHLI2 Can Substitute for CHLI1. *Plant Physiol.* **2009**, *150*, 636–645. [[CrossRef](#)]
80. Arimura, S.-I.; Kurisu, R.; Sugaya, H.; Kadoya, N.; Tsutsumi, N. Cold Treatment Induces Transient Mitochondrial Fragmentation in Arabidopsis thaliana in a Way that Requires DRP3A but not ELM1 or an ELM1-Like Homologue, ELM2. *Int. J. Mol. Sci.* **2017**, *18*, 2161. [[CrossRef](#)] [[PubMed](#)]
81. Couturier, J.; Touraine, B.; Briat, J.F.; Gaymard, F.; Rouhier, N. The iron-sulfur cluster assembly machineries in plants: Current knowledge and open questions. *Front. Plant Sci.* **2013**, *4*, 259. [[CrossRef](#)]
82. Bayer, E.M.; Bottrill, A.R.; Walshaw, J.; Vigouroux, M.; Naldrett, M.J.; Thomas, C.L.; Maule, A.J. Arabidopsis cell wall proteome defined using multidimensional protein identification technology. *Proteomics* **2006**, *6*, 301–311. [[CrossRef](#)] [[PubMed](#)]
83. Huang, L.-F.; Lin, K.-H.; He, S.-L.; Chen, J.-L.; Jiang, J.-Z.; Chen, B.-H.; Hou, Y.-S.; Chen, R.-S.; Hong, C.-Y.; Ho, S.-L. Multiple Patterns of Regulation and Overexpression of a Ribonuclease-Like Pathogenesis-Related Protein Gene, OsPR10a, Conferring Disease Resistance in Rice and Arabidopsis. *PLoS ONE* **2016**, *11*, e0156414. [[CrossRef](#)] [[PubMed](#)]

84. Mo, P.; Zhu, Y.; Liu, X.; Zhang, A.; Yan, C.; Wang, D. Identification of two phosphatidylinositol/phosphatidylcholine transfer protein genes that are predominately transcribed in the flowers of *Arabidopsis thaliana*. *J. Plant Physiol.* **2007**, *164*, 478–486. [[CrossRef](#)] [[PubMed](#)]
85. Capelli, N.; Diogon, T.; Greppin, H.; Simon, P. Isolation and characterization of a cDNA clone encoding an osmotin-like protein from *Arabidopsis thaliana*. *Gene* **1997**, *191*, 51–56. [[CrossRef](#)]
86. Tumburu, L.; Andersen, C.P.; Rygiewicz, P.T.; Reichman, J.R. Molecular and Physiological Responses to Titanium dioxide and Cerium Oxide nanoparticles in *Arabidopsis*. *Environ. Toxicol. Chem.* **2017**, *36*, 71–82. [[CrossRef](#)] [[PubMed](#)]



## Article

# Single and Repeated Applications of Cerium Oxide Nanoparticles Differently Affect the Growth and Biomass Accumulation of *Silene flos-cuculi* L. (Caryophyllaceae)

Daniel Lizzi <sup>1,2</sup>, Alessandro Mattiello <sup>1</sup>, Barbara Piani <sup>1</sup>, Emanuele Gava <sup>3</sup>, Guido Fellet <sup>1</sup> and Luca Marchiol <sup>1,\*</sup>

<sup>1</sup> Department of AgriFood, Environmental and Animal Science, University of Udine, via delle Scienze 206, 33100 Udine, Italy; lizzi.daniel.1@spes.uniud.it (D.L.); alessandro.mattiello@uniud.it (A.M.); barbara.piani@uniud.it (B.P.); guido.fellet@uniud.it (G.F.)

<sup>2</sup> Department of Life Sciences, University of Trieste, Via Licio Giorgieri 10, 34127 Trieste, Italy

<sup>3</sup> Laboratory of Inorganic Micro-Pollutants Regional Environmental Protection Agency of Friuli Venezia Giulia (ARPA-FVG), Via Colugna 42, 33100 Udine, Italy; emanuele.gava@arpa.fvg.it

\* Correspondence: marchiol@uniud.it

**Abstract:** Cerium oxide nanoparticles ( $n\text{CeO}_2$ ) have a wide variety of applications in industry. Models demonstrated that  $n\text{CeO}_2$  can reach environmental compartments. Studies regarding the relationships between plants and  $n\text{CeO}_2$  considered only crop species, whereas a relevant knowledge gap exists regarding wild plant species. Specimens of *Silene flos-cuculi* (Caryophyllaceae) were grown in greenhouse conditions in a substrate amended with a single dose (D1) and two and three doses (D2 and D3) of 20 mg kg<sup>-1</sup> and 200 mg kg<sup>-1</sup>  $n\text{CeO}_2$  suspensions, respectively. sp-ICP-MS and ICP-MS data demonstrated that  $n\text{CeO}_2$  was taken up by plant roots and translocated towards aerial plant fractions. Biometric variables showed that plants responded negatively to the treatments with a shortage in biomass of roots and stems. Although not at relevant concentrations, Ce was accumulated mainly in roots and plant leaves.

**Citation:** Lizzi, D.; Mattiello, A.; Piani, B.; Gava, E.; Fellet, G.; Marchiol, L. Single and Repeated Applications of Cerium Oxide Nanoparticles Differently Affect the Growth and Biomass Accumulation of *Silene flos-cuculi* L. (Caryophyllaceae). *Nanomaterials* **2021**, *11*, 229. <https://doi.org/10.3390/nano11010229>

Received: 16 December 2020

Accepted: 13 January 2021

Published: 16 January 2021

**Publisher's Note:** MDPI stays neutral with regard to jurisdictional claims in published maps and institutional affiliations.



**Copyright:** © 2021 by the authors. Licensee MDPI, Basel, Switzerland. This article is an open access article distributed under the terms and conditions of the Creative Commons Attribution (CC BY) license (<https://creativecommons.org/licenses/by/4.0/>).

**Keywords:** cerium oxide nanoparticles; terrestrial ecosystem; wild plant species; plant growth

## 1. Introduction

Nanoscience and nanotechnology are rapidly developing in different applications, having the potential to considerably improve human life. Much progress has been made in applying the application of engineered nanomaterials (ENMs) and nano-enabled products in medicine, energy, electronics, innovative materials and many more fields [1]. On the other hand, the increase in the industrial production of ENMs inevitably leads to their release into the environment [2].

Once released in terrestrial ecosystems, ENMs enter watercourses and soils reaching the biota [3]. Since 2006, the Organization for Economic Cooperation and Development (OECD) has developed toxicity test guidelines for ENMs [4]. Currently, the end-points/targets of such tests are the green algae *Raphidocelis subcapitata*, the daphnid *Daphnia magna*, the fish *Danio rerio*, the sediment organism *Lumbriculus variegatus*, soil microflora and terrestrial invertebrates *Enchytraeus crypticus* and *Eisenia fetida* [5].

The global biomass on Earth is dominated by plants, which are the primary producers in terrestrial and water ecosystems and represent about 80% of the biota [6]. Their life cycle is strongly dependent on their relationships with air, soil, and water. However, for that very reason, they constitute the first biological target of ENMs, and are not considered among the environmental targets of ENMs by the OECD guidelines. It would be advisable to evaluate the impact of ENMs and consider the consequences concerning the ecosystem services that plants provide [7].

The literature lacks systematic knowledge regarding the effects of ENMs on vascular plants. In part, this is due to the very high pace of research and development on nanomaterials.

rials. However, the most important reason concerns the fact that the discussion regarding the most appropriate experimental strategies is still open [8,9]. The studies carried out on crops [10–12] have been far more numerous compared to those on spontaneous plant species, and between the latter the papers on aquatic species largely prevail over those on terrestrial plants. According to the last “State of the World’s Plants and Fungi” release [13], the number of vascular plants species currently known is about 391,000. Only about 150 species have a significant commercial value, and 20% of them account for more than half of the plants eaten by humans [14,15]. Therefore, we optimistically assume that the relationships between ENMs and vascular plants have been studied much less than 0.05% of higher plant species, so far. Practical gap-filling actions are expected on this issue in the next future.

Cerium oxide nanoparticles ( $n\text{CeO}_2$ ) are a rare earth nanomaterial with several engineering and biological applications due to their catalytic, electrochemical, and optical properties [16]. With an estimated annual global production of 100–1000 tons per year,  $n\text{CeO}_2$  is among the most widely utilized metal oxide nanoparticle in Europe [17]. The Organization for Economic Cooperation and Development included  $n\text{CeO}_2$  in the list of ENMs for immediate priority testing [18].

As previously mentioned, the existing body of literature regarding the relationships between ENMs and plants is mostly focused on agricultural plant species. While this is justified concerning the potential risks of human exposure to nanomaterials through food consumption, in a broader ecological context, the impacts of ENMs on the whole primary producers should not be underrated in a broader ecological context. From this perspective, more aquatic [19–21] and wetland species [22–24] have been studied than terrestrial varieties. Concerning terrestrial ecosystems, to the best of our knowledge, *Pinus sylvestris* L. and *Quercus robur* L. are the only non-food terrestrial plant species to have been investigated for the exposure to ENMs [25].

The fate and effects of ENMs in the soil-plant system are always studied by supplying plants with ENMs at different concentrations, sizes, and shapes, and structured with several capping molecules in a single dose and at given time [26]. What remains is whether and how ENMs affect plant metabolism and plant growth under realistic conditions. Regardless of the ENMs source, plants are likely exposed to ENMs over a much longer time, at relatively lower concentrations but repeated pulses of ENMs; it is this last aspect about which we developed our experiment. The main goal of this study was to evaluate and compare the effects of a single dose and two and three repeated applications of  $n\text{CeO}_2$  at different concentrations on the growth of *Silene flos-cuculi* (L.).

## 2. Materials and Methods

### 2.1. $n\text{CeO}_2$ Characterization

Nanoparticle characterization was carried out at the laboratories of the National Research Council—Institute of Science and Technology for Ceramics (Faenza, Italy). The cerium oxide nanopowders with an average particle size of 25 nm were purchased from Sigma-Aldrich (St. Louis, MO, USA). The  $n\text{CeO}_2$  had a mass weight of  $172.11 \text{ g mol}^{-1}$ , density of  $7.13 \text{ g mL}^{-1}$  at  $25^\circ\text{C}$ , and 99.95% purity. The size and average shape were measured with a transmission electron microscope (TEM, FEI Tecnai F20, FEI Company, Eindhoven, The Netherlands). The  $n\text{CeO}_2$  was suspended in deionized water and sonicated in a water bath for 30 min with a sonication intensity of 180 watts. The suspensions were characterized for Z—average size at pH 7 and hydrodynamic diameter (Hd), whose distributions were measured by dynamic light scattering (DLS) on a Zetasizer Nano ZS (Malvern Ltd., Worcestershire, UK).

### 2.2. Plant Material

*Silene flos-cuculi* L. (synonym *Lychnis flos-cuculi*) is a diploid polycarpic herbaceous perennial wetland plant, belonging to the *Caryophyllaceae* family. This species is native and distributed throughout Europe, where it is found in moist open habitats, along roads and

flood plain, in wet meadows and pastures, but it also grows in the northern United States and eastern Canada [27]. In arable landscapes, it has become scarce because of the loss of habitats, but is still found in secondary habitats such as ditches and stream verges. The species is predominantly outcrossing, but capable of self-fertilization [28]. *S. flos-cuculi* forms vegetative rosettes with numerous flower stems that could be from 30 to 90 cm tall. The stems have barbed hairs that make the plant rough to the touch; stems grow over the foliage and end with pink flowers, which open between April and June, and many types of insects are attracted by the flower's nectar. Another characteristic of these flowers is that they have five narrow petals divided into four lobes. The leaves are paired: the lower ones are stalked and the upper leaves present pointed apices. The fruits consist of small capsules, containing many dark seeds, which can be dispersed mechanically [29].

### 2.3. Experimental Setup

Seeds of *S. flos-cuculi* were purchased from SemeNostrum (Udine, Italy). The soil used for this experiment was Compo Sana organic potting mix containing forest products, compost, perlite, and fertilizer (soil pH = 6.8–7.2). The potting substrate, having a Ce concentration of 17.3 mg kg<sup>-1</sup>, was amended with water suspensions of *n*CeO<sub>2</sub> of 25 nm in order to reach a final substrate concentration of 20 and 200 mg kg<sup>-1</sup> *n*CeO<sub>2</sub>. Tap water was used as the control. Before sowing, *n*CeO<sub>2</sub> suspensions were stirred and sonicated for 30 min to avoid the aggregation, and the first addition of *n*CeO<sub>2</sub> to the substrate occurred in one dose through irrigation. The amended substrate was carefully mixed in order to obtain the prearranged concentrations. The *n*CeO<sub>2</sub> amended substrates were stored in the dark at 15 °C for three days for conditioning before planting seeds. After soil equilibration, the pots were filled with 500 g soil. Repeated applications of *n*CeO<sub>2</sub> were performed after 20 and 40 days from seedling emergence (DSE) in separate sets of pots. The experimental setup is showed in Figure 1. More precisely, D1 refers to the pots that received only the *n*CeO<sub>2</sub> dose before sowing; D2 refers to the pots that received a second adjustment 20 DSE; and D3 refers to the pots that underwent three applications (the last one occurred 40 DSE). The additional treatments were carried out via irrigation with the solutions containing the same initial *n*CeO<sub>2</sub> concentration (20 or 200 mg L<sup>-1</sup>). This was to attempt to recreate a situation of chronic "contamination". The experiment was carried out in a semi-controlled greenhouse facility at the experimental farm of the University of Udine (Italy).

The trial was set up in a randomized experimental design, focusing the attention in particular on repeated treatments. Each treatment was replicated four times. Seeds were put about 2.5 cm deep in the soil and pots were placed in full sunlight, at 18–27 °C (night/day) with a relative humidity of around 60%. Two weeks after seed planting, the seedlings were thinned to two seedlings per pot. During the trial, pots were irrigated every three days and randomly reallocated every week. After 60 days, control and treated plants were harvested. Fresh plant biomass was separated into roots, stems, and leaves, and then weighed. Then, the plant fractions were thoroughly washed in tap water and rinsed three times with distilled water. In addition, roots were washed in 400 mL of 0.01 M of nitric acid in a shaker bath at 300 rpm for 5 min to remove metal ions adsorbed at the surface. Leaf area was measured using an LI-3100C Area Meter (Li-Cor Corporation, Lincoln, NE, USA). After that, the plant fractions were oven dried at 60 °C for three days, and weighed.

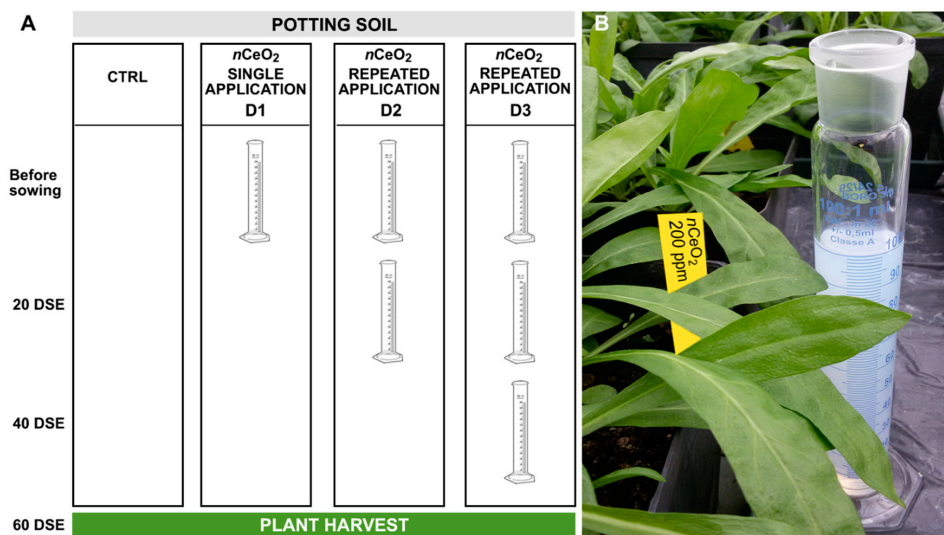


**Figure 1.** (A) Experimental setup showing the combination of treatments: control, single-, double-, and triple-dosed plants (Ctrl, D1, D2, and D3, respectively); (B) *S. flos-cuculi* plants at 40 DSE.

#### 2.4. *nCeO<sub>2</sub>* Extraction from Plant Tissues

In our study, plants grew for the entire life cycle in a solid substrate enriched with *nCeO<sub>2</sub>* at the beginning and with additional treatments during the experiment. From a subset of pots prepared for this purpose, 20 days after the appearance of the cotyledon leaves of *S. flos-cuculi*, the plants were harvested in order to verify the entry of *nCeO<sub>2</sub>* in their tissues by enzymatic digestion and single particle inductively coupled plasma mass spectrometry (spICP-MS) analysis. The plant fractions (roots, stems and leaves) were separated and in turn sent for preparation. The digesting enzyme used was Macerozyme R-10 Pectinase from *Rhizopus* sp. (Sigma-Aldrich). Small sections (0.03 g) of fresh roots, stems, and leaves were harvested, rinsed three times with deionized water, and homogenized with 8 mL of 2 mM citrate buffer at pH 4.5, using an ultrasonic bath for 5 min. After the homogenization, for every sample 2 mL of the enzyme solution (0.05 g of enzyme dissolved in 2 mL of MilliQ water) were added [30]. The final supernatants were analyzed via spICP-MS (NexION 350 ICP-MS PerkinElmer, Waltham, MA, USA) to obtain the size distribution of *nCeO<sub>2</sub>* present in roots and leaves.

#### 2.5. *Ce* Concentration in Plant Fractions

Plant fractions were carefully washed with deionized water. The material was then oven-dried for three days at 60 °C. Subsequently, 0.3 g of dry plant fraction tissues were acid-digested on a CEM microwave oven (MARS Xpress, CEM, Matthews, NC, USA), using 9 mL of HNO<sub>3</sub> (65%) and 1 mL of hydrogen peroxide (H<sub>2</sub>O<sub>2</sub>) in Teflon cylinders at 180 °C, according to the USEPA 3052 method [31]. After mineralization, plant extracts were filtered at room temperature under a fume hood with Whatman 0.45 μm PTFE membrane filters, and finally diluted and analyzed. Determinations of the total content of cerium were carried out using the NexION 350 ICP-MS. The accuracy of the analytical procedure adopted for ICP-MS analysis was checked by running standard solutions every 20 samples.

#### 2.6. Data Analysis

Statistical analysis was carried out with one- and two-way ANOVA. A posteriori comparison of individual means was performed using Tukey's test ( $p < 0.05$ ). Before ANOVA, arcsine and logarithmic transformations were used to determine seed germination percent-

age and Ce concentration data, respectively. spICP-MS data on  $n\text{CeO}_2$  size distribution were processed using Syngistix Nano Application Module software and interpolated with Gaussian curves.

### 3. Results

#### 3.1. Characterization of $n\text{CeO}_2$

$n\text{CeO}_2$  characterization data are showed in Table S1, Supplementary Materials. The Hd distribution of both the materials is in agreement with the value provided by the supplier. The  $n\text{CeO}_2$  exhibited a monodisperse size particle distribution with relatively low PDI. The highest particle size was 62.0 nm (Figure 2A). The relative Z-averages were much larger than that value due to particle aggregation (Figure 2B).

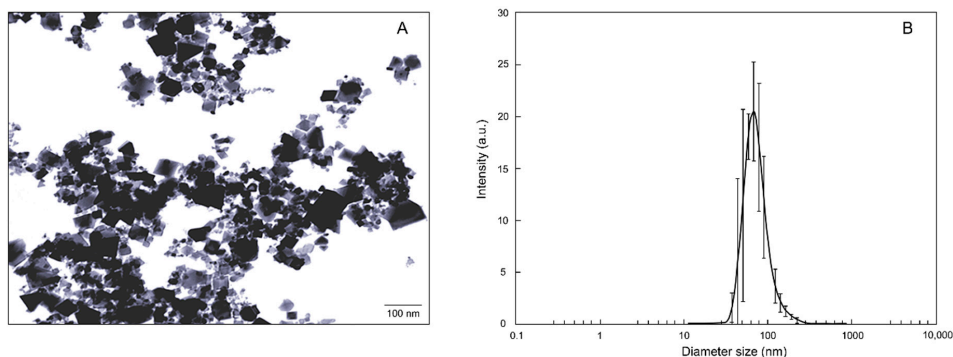


**Figure 2.** (A) Particle size distribution obtained by dynamic light scattering (DLS). (B) Transmission electron microscopy (TEM) image of  $n\text{CeO}_2$  25 nm suspension.

#### 3.2. $n\text{CeO}_2$ in Plant Fractions

Before setting up the experiment on the entire vegetative cycle of *S. flos-cuculi*, some preliminary observations were carried out to demonstrate that  $n\text{CeO}_2$  was assimilated by the roots of plants and subsequently translocated to the upper plant parts. They were evidently necessary to set up the subsequent experiment illustrated in this paper. At first, a test was carried out to demonstrate the entry of  $n\text{CeO}_2$  within germinating seeds of *S. flos-cuculi* seeds [32]. Subsequently, under the same conditions as the main experiment, we wanted to verify that even in the presence of a complex matrix (that is, the potting soil compared to the very simple conditions of the germination test) the roots of *S. flos-cuculi* were able to take up the  $n\text{CeO}_2$ .

The results reported in Figure 3A,B clearly show that the  $n\text{CeO}_2$  was absorbed by the roots of *S. flos-cuculi*, and then moved upwards to reach the leaf tissues. The magnitude of pulses quantitatively represents the presence of  $n\text{CeO}_2$  in plant tissue; after the  $n\text{CeO}_2$  root absorption, only about 25% of nanoparticles moved to the plant leaves (Figure 3B). The mean size of  $n\text{CeO}_2$  was  $33 \pm 2$  nm and  $31 \pm 1.5$  nm in the roots and leaves, respectively (Table S2, Supplementary Materials), meaning that after being assimilated,  $n\text{CeO}_2$  did not undergo relevant aggregation. In the plant extract sample, the spICP-MS analysis also provided the concentration of the ionic form of an element dissolved from a nanostructure. In our case, the dissolved ionic Ce was very low, and equal to  $4.86 \pm 0.4 \mu\text{g kg}^{-1}$  in the roots and  $0.08 \pm 0.03 \mu\text{g kg}^{-1}$  in the leaves of *S. flos-cuculi*, respectively (Table S2, Supplementary Materials).

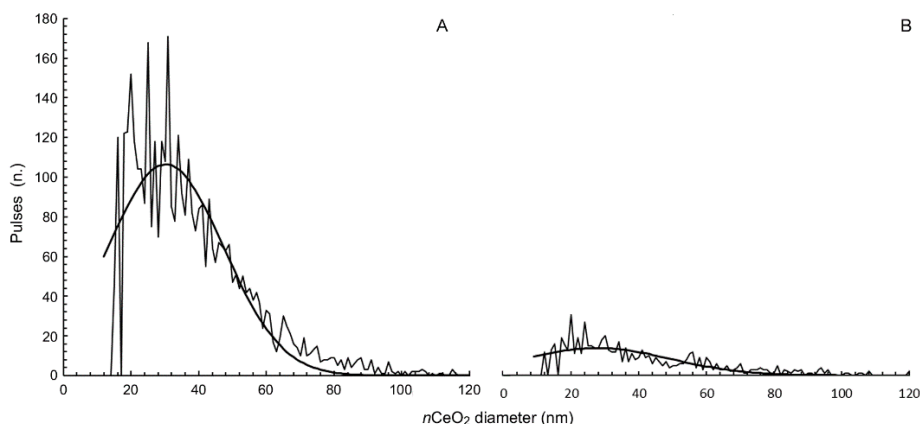


**Figure 3.** Particle size distribution of  $n\text{CeO}_2$  extracted after enzymatic digestion procedure from (A) roots and (B) leaves of *S. flos-cuculi*.

### 3.3. Plant Growth

An overall view of the experimental data relating to plant growth is showed in Table S3, Supplementary Materials, containing the results of a two-way ANOVA. In particular, the table reports the  $p$ -values testing the statistically significant effects of the  $n\text{CeO}_2$  dose (D1, D2 and D3),  $n\text{CeO}_2$  concentration (20 and 200  $\text{mg kg}^{-1}$ ), and their interaction on biometric variables of *S. flos-cuculi*.

In broad terms, only the root dry weight ( $p = 0.0009$  \*\*\*) responded in a statistically significant way to the dose of  $n\text{CeO}_2$ , while this did not happen in the case of the other plant fractions and the leaf area. The factor “concentration” determined statistically significant effects in the case of root dry matter ( $p = 0.0281$  \*), stem dry matter ( $p = 0.0000$  \*\*\*), and total plant dry weight ( $p = 0.0000$  \*\*\*), as well. Finally, because the root apparatus was directly exposed to the soil matrix, as expected we recorded a statistically significant interaction of “dose X concentration” for root dry matter ( $p = 0.0018$  \*) (Table S3, Supplementary Materials).

Carefully observing the effects of treatments on the vegetative development of *S. flos-cuculi*, some aspects of particular interest can be highlighted. As already mentioned, the root biomass dry weight, being the plant fraction directly exposed to the treatments, showed to be particularly sensitive to the experimental conditions. The development of the root apparatus responded positively to D1 (single dose of  $n\text{CeO}_2$  provided to pot soil before seed germination). At both concentrations of  $n\text{CeO}_2$ , an increase of 29% (at 20  $\text{mg kg}^{-1}$ ) and 9% (at 200  $\text{mg kg}^{-1}$ ) in root biomass compared to the control was observed (Figure 4).

At the lowest concentration, the higher doses of  $n\text{CeO}_2$  (D2 and D3) did not promote the same effect detected for D1. The weight of the root biomass returned to a level very close to that of the control plants. This also occurred for D2 at the highest concentration (200  $\text{mg kg}^{-1}$ ), while the response to D3 was a reduction of about 27% in root development compared to the control (Figure 4). Additionally, a statistical analysis was performed by isolating the concentration factor, i.e., testing the effect of single and repeated administration of  $n\text{CeO}_2$  to plants within the same concentration level. In this case, considering D1 as the reference within each concentration, we evaluated the effect of the additional doses of  $n\text{CeO}_2$  on the plant root biomass (Figure 4). Whether the single  $n\text{CeO}_2$  dose stimulated the production of root biomass, the second additional dose (D3), even though supplied to the plants at a late vegetative stage, resulted in a reduction in the root biomass. Compared to D1, we recorded a reduction in root dry matter of *S. flos-cuculi* by approximately 21% and 33%, for  $n\text{CeO}_2$  20  $\text{mg kg}^{-1}$  and 200  $\text{mg kg}^{-1}$ , respectively (Figure 4).

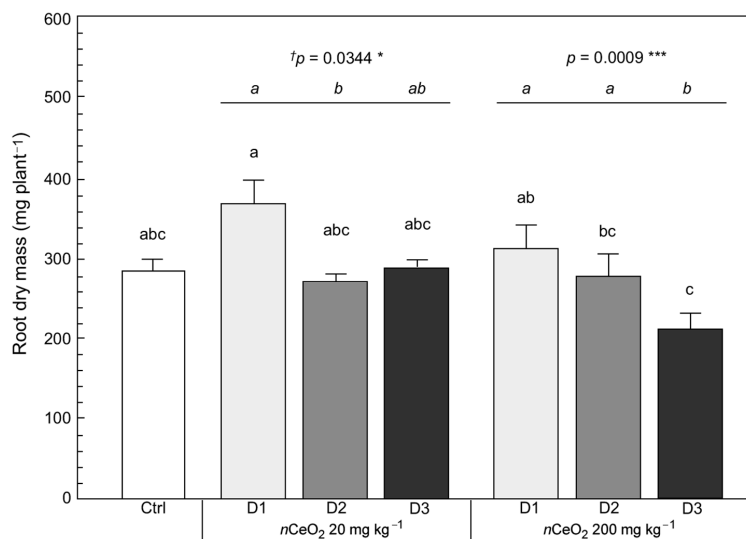


**Figure 4.** Root dry mass of *S. flos cuculi*. Comparison of effects based on single (D1) and repeated (D2, D3) applications of 20 and 200 mg kg<sup>-1</sup> nCeO<sub>2</sub>, respectively. Letters indicate statistically significant difference between treatments ( $p \leq 0.05$ ) using one-way ANOVA followed by Tukey's test. † One-way ANOVA  $p$ -value within each concentration: asterisks indicate the statistically significant difference of dose factor at \*  $0.05 \geq p \geq 0.01$ ; \*\*\* $p \geq 0.001$ , respectively.

As reported in Table S3 Supplementary Materials, some other biometric variables were observed in plants. In particular, on the aboveground plant biomass, the number of stems and leaves for each plant were counted. The total leaf area per plant and the leaf dry matter were recorded as well. For these variables, the statistical analysis did not reveal significant effects of the treatments, whereas there was a very evident negative effect of nCeO<sub>2</sub> on dry matter accumulation in the stems of *S. flos-cuculi* (Figure 5). Regardless of the concentration and dose of nCeO<sub>2</sub>, the negative effect of the treatment determined an average reduction of 75.5% in dry matter accumulation in the stems compared to the control.

As reported in Supplementary Materials (Figures S1–S4), the response to treatments of other biometric variables did not confirm either the stimulating effect highlighted on the case of root biomass or the negative effect on the dry matter accumulation on the stems *S. flos-cuculi*. Indeed, although the biomass of the stems was reduced, the architecture of the plants was not affected; the number of stems in the treated plants was no different from that of the control plants (Figure S1, Supplementary Materials). Even the number of leaves per plant, the leaf area per plant and the accumulation of dry matter in the leaves themselves were not affected by the treatments (Figures S2–S4, Supplementary Materials).

Figure 6 reports the plants' total dry matter. Aggregating the different effects observed on the plant fractions could hide the impact of nCeO<sub>2</sub> treatments. However, in our case this did not happen. Albeit to a lesser extent than that observed for the weight of the stems, the effect of nCeO<sub>2</sub> on plant development is also visible on total biomass production. The negative effect of the treatments on the growth of *S. flos-cuculi* is statistically significant ( $p = 0.00000$  \*\*\*), regardless of the nCeO<sub>2</sub> dose and even at the lower concentration of nanoparticles (Figure 6).

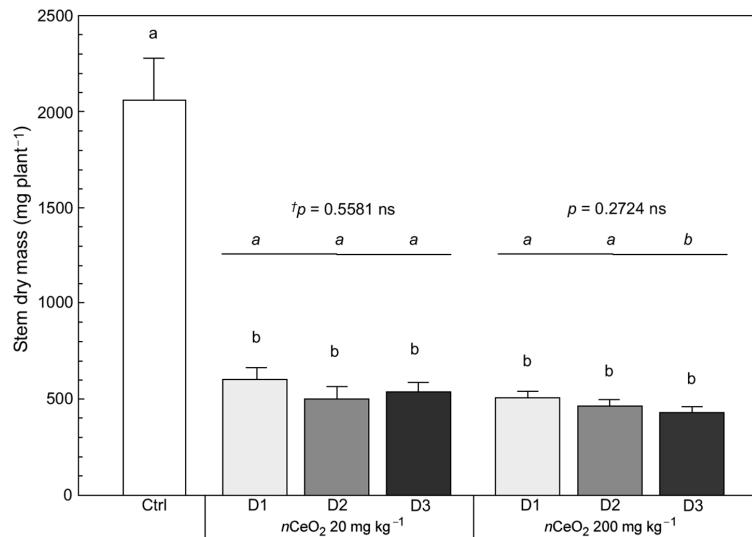


**Figure 5.** Stem dry mass of *S. flos cuculi*. Comparison of effects based on single (D1) and repeated applications (D2, D3) of 20 and 200 mg kg<sup>-1</sup> nCeO<sub>2</sub>, respectively. Letters indicate statistically significant difference between treatments ( $p \leq 0.05$ ) using one-way ANOVA followed by Tukey’s test. † One-way ANOVA  $p$ -value within each concentration.

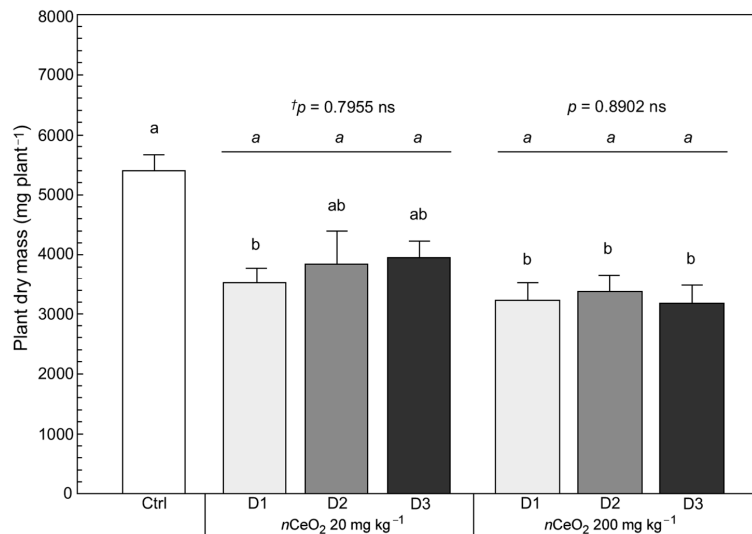


**Figure 6.** Plant dry mass of *S. flos cuculi*. Comparison of effects based on single (D1) and repeated applications (D2, D3) of 20 and 200 mg kg<sup>-1</sup> nCeO<sub>2</sub>, respectively. Letters indicate statistically significant difference between treatments ( $p \leq 0.05$ ) using one-way ANOVA followed by Tukey’s test. † One-way ANOVA  $p$ -value within each concentration.

After C fixation, the plant biomass was allocated according to species-specific patterns that are also influenced by environmental conditions as well as biotic and abiotic stress. Data regarding the dry weight of the plant fractions and the leaf area per plant were used to calculate new parameters (see Table S4, Supplementary Materials) that allowed us to evaluate the effects of nCeO<sub>2</sub> treatments with a more accurate perspective. Additionally, in

this case we can appreciate an overview of the effects of the experimental factors through the results of the two-way ANOVA (Table S5, Supplementary Materials). The effect of the “dose” factor was statistically significant only in the case of the root mass fraction (RMF) and the S/R ratio, while the response to the “concentration” factor was much more evident: only for specific leaf area (SLA) was the effect not statistically significant in the ANOVA. The interaction between the experimental factors was statistically significant for the RMF and the SLA (Table S5, Supplementary Materials). One-way ANOVA was used to evaluate the effects of treatments compared to the control and within the same concentration of  $n\text{CeO}_2$ .

Compared to the control and regardless of the  $n\text{CeO}_2$  concentration, the RMF was enhanced by D1, whereas D2 and D3 determined a subsequent drop of RMF. At the lowest concentration of  $n\text{CeO}_2$  concerning D1, we observed an almost-equal reduction in RMF in response to D2 and D3 (−33%). Additionally, at the highest concentration of  $n\text{CeO}_2$ , the response to D2 and D3 was negative, although in this case it was gradual, with the reduction in RMF concerning D1 equal to −17% and −33%, for D2 and D3, respectively. However, the RMF of D2 and D3 treated plants was always higher than the control plants (Table 1).

**Table 1.** Root mass fraction (RMF), shoot to root ratio (S/R ratio), and specific leaf area (SLA) ± standard deviation of *S. flos-cuculi* grown in presence of different inputs of 20–200 mg  $\text{kg}^{-1}$   $n\text{CeO}_2$ . Statistically significant differences ( $p \leq 0.05$ ) are indicated by the letters using one-way ANOVA followed by Tukey’s test. Dashed box indicate ANOVA  $p$ -values ( $p \leq 0.05$ ) within the  $n\text{CeO}_2$  concentration. ns: not significant at  $p \leq 0.05$ ; \* and \*\* significant at  $p \leq 0.05$  and  $p \leq 0.01$ .

Treatment	Dose	RMF	SLA
		( $\text{g g}^{-1}$ )	( $\text{m}^2 \text{kg}^{-1}$ )
Ctrl	D0	0.054 ± 0.003 c	25.3 ± 0.70 ab
	D1	0.117 ± 0.009 a	25.7 ± 1.21 ab
	D2	0.078 ± 0.008 bc	27.3 ± 1.32 ab
	D3	0.077 ± 0.007 bc	24.4 ± 1.42 b
$n\text{CeO}_2$ 20 mg $\text{kg}^{-1}$		$p = 0.0028^{**}$	$p = 0.2801$ ns
	D1	0.105 ± 0.009 ab	24.1 ± 1.31 b
	D2	0.087 ± 0.01 abc	28 ± 1.63 ab
	D3	0.070 ± 0.006 c	30 ± 1.36 a
		$p = 0.0271^*$	$p = 0.0243^*$
$n\text{CeO}_2$ 200 mg $\text{kg}^{-1}$	D1	0.105 ± 0.009 ab	24.1 ± 1.31 b
	D2	0.087 ± 0.01 abc	28 ± 1.63 ab
	D3	0.070 ± 0.006 c	30 ± 1.36 a
		$p = 0.0271^*$	$p = 0.0243^*$

SLA did not respond to the single experimental factors; however, ANOVA revealed a statistically significant effect for the interaction “dose X concentration” ( $p = 0.0243^*$ ). Regarding the effects of the treatments, we observed a possible SLA stimulating effect of  $n\text{CeO}_2$  20 mg  $\text{kg}^{-1}$  D1 and D2. At the same time, a certain variability prevented this empirical evidence from being statistically verified, whereas we observed a significant reduction in SLA in plants that received D3 compared to the controls (Table 1). In plants of *S. flos-cuculi* treated with  $n\text{CeO}_2$  200 mg  $\text{kg}^{-1}$ , SLA responded differently ( $p = 0.0243^*$ ). Indeed, a slight reduction in SLA compared to the control due to treatment D1 (−4.7%) is associated with an evident increase in this parameter in response to treatments D2 and D3 (+10.7% and +18.6% greater than the control, respectively) (Table 1). Further ratios calculated from biometric variables (Stem mass fraction SMF, Leaf mass fraction LMF, Shoot to root ratio Shoot/Root and Leaf area ratio LAR) are reported in Supplementary Materials (Figures S5–S8).

### 3.4. Cerium Concentration in Plant Fractions

A general view of the Ce uptake and accumulation in plant tissues as affected by experimental factors is given in Table S6, Supplementary Materials. The factor “dose” result was statistically significant only for Ce concentration in plant stems ( $p = 0.0000^{***}$ ), while the Ce accumulation in each plant tissue, as expected, increased responding to the

factor “concentration”. A statistically significant interaction “dose x concentration” was observed in the roots ( $p = 0.0313^*$ ) and stems ( $p = 0.0021^{**}$ ).

Table 2 reports data regarding the Ce concentrations in plant fractions. At first glance, the data indicate that plant Ce uptake was not very high compared to the treatments. Concerning the plant fractions, as expected, Ce in the roots was higher than the others.

**Table 2.** Ce concentration in plant fraction and Ce translocation factor in *S. flos cuculi* grown in the presence of different inputs of  $n\text{CeO}_2$  (20 and 200  $\text{mg kg}^{-1}$ .) Data are mean  $\pm$  standard deviation. Statistically significant differences ( $p \leq 0.05$ ) are indicated by the letters using one-way ANOVA followed by Tukey’s test. Dashed boxes indicate ANOVA  $p$ -values ( $p \leq 0.05$ ) within  $n\text{CeO}_2$  concentration. ns: not significant at  $p \leq 0.05$ ; \*\* significant at  $p \leq 0.01$ .

Treatment	Dose	Ce roots ( $\mu\text{g kg}^{-1}$ )	Ce stems ( $\mu\text{g kg}^{-1}$ )	Ce leaves ( $\mu\text{g kg}^{-1}$ )	
Ctrl	D0	546 $\pm$ 390 b	154 $\pm$ 125 b	254 $\pm$ 198 b	
	$n\text{CeO}_2$ 20 $\text{mg kg}^{-1}$	D1	1300 $\pm$ 112 b	333 $\pm$ 281 b	1083 $\pm$ 70 ab
		D2	2407 $\pm$ 793 b	477 $\pm$ 172 ab	1240 $\pm$ 170 ab
		D3	2670 $\pm$ 1130 b	1450 $\pm$ 918 a	1770 $\pm$ 96.7 a
		$p = 0.1653$ ns	$p = 0.0988$ ns	$p = 0.3638$ ns	
$n\text{CeO}_2$ 200 $\text{mg kg}^{-1}$	D1	3023 $\pm$ 700 ab	573 $\pm$ 87 ab	1580 $\pm$ 60.7 ab	
	D2	3130 $\pm$ 2210 ab	816 $\pm$ 91 ab	2063 $\pm$ 41.8 a	
	D3	5910 $\pm$ 1140 a	1023 $\pm$ 61 ab	1827 $\pm$ 24 a	
			$p = 0.0941$ ns	$p = 0.0015^{**}$	$p = 0.4643$ ns

On average, the treatment concentration of Ce in the root tissues (3074  $\mu\text{g kg}^{-1}$ ) was four times higher than that of the stems (779  $\mu\text{g kg}^{-1}$ ) and two times higher than that found in the leaves (1594  $\mu\text{g kg}^{-1}$ ), respectively. However, we do not observe a clear and statistically significant response to the  $n\text{CeO}_2$  doses regardless of the treatment concentration. However, the statistically significant interaction “dose X concentration” is explained by the different response in terms of Ce accumulation in roots after dose D3  $n\text{CeO}_2$  200  $\text{mg kg}^{-1}$  that was about 49% higher than the average D1–D2. (Table 2).

After being taken up by the roots, a fraction of Ce moved towards the aerial plant fractions to be allocated in the stems. A statistically significant effect of the dose factor and of the interaction is visible by observing the concentration of Ce in the stems (Table 2). Here, although the highest Ce concentration was detected at D3  $n\text{CeO}_2$  20  $\text{mg kg}^{-1}$ , the most evident effect of the “dose” factor can be appreciated for plants exposed to  $n\text{CeO}_2$  200  $\text{mg kg}^{-1}$  ( $p = 0.0015^{**}$ ; Table 2). Finally, the leaves represent the final allocation of Ce in plant aerial biomass. Here, Ce accumulation was higher in than in stems; however, due to a certain variability, it was not possible to statistically verify a significant effect of the experimental treatments (Table 2)

#### 4. Discussion

Only in 2012 were the effects of ENMs over the whole plant cycle studied [33]. In soybeans (*Glycine max* L.), it was demonstrated that Ce concentrations in the roots and the concentration of  $n\text{CeO}_2$  in soil were correlated. Nanoceria negatively influenced the yield of soybean and  $\text{N}_2$ -fixation by affecting the efficiency of the symbiotic system established with *Bradyrhizobium*: a dramatic example of the influence on cultivated plants and wild species’ ecological services, as well.

A large body of literature reports negative responses observed at different plant growth stages. When germinating seeds are exposed to  $n\text{CeO}_2$ , other effects could be verified, basically depending on particle size and concentration. Additionally, statistically significant species-specific responses were reported, regarding root elongation being more sensitive to  $n\text{CeO}_2$  than germination [34–36]. Other studies explored the physiological implications of the  $n\text{CeO}_2$  plant uptake, concluding that plants responded to the treatments

increasing the antioxidant enzyme activities. However, the oxidative stress induced by high concentrations of  $n\text{CeO}_2$  cannot be attenuated by the antioxidant system [37–40].

The growth of *S. flos-cuculi* was negatively affected by  $n\text{CeO}_2$ . Suppose the root apparatus development in plants treated at the lowest  $n\text{CeO}_2$  concentration has not undergone apparent alterations at the highest concentration; in this case, the effect is evident and progressively increases as the  $n\text{CeO}_2$  dose increases. The impact of  $n\text{CeO}_2$  on plant growth was much more apparent in the biomass of plant stems. We observed a slowdown in plant growth. The number of plant stems did not change, but they were shorter than the controls'. No statistically significant evidence was found regarding the effects of treatments on leaf biomass (evaluated by counting the number of leaves per plant, the leaf area, and the leaf dry weight). However, likely the relevant data variability detected in the treated plants compared to that of the control plants was an early signal of plant stress.

SLA is a very informative parameter in plant ecology. The total leaf area ratio to total leaf dry mass correlates with whole-plant growth linking C gain and water loss [41]. Even though we calculated the SLA using data from a single biomass sampling at the end of the growth cycle of *S. flos-cuculi*, the response of SLA to the  $n\text{CeO}_2$  treatments allowed us to interpret the experimental data more effectively. In particular, the increase in SLA responded to the dose of  $n\text{CeO}_2$  received by the plant. Moreover, this could be a consequence of the slowing of the vegetative growth rate and could lead us to conclude that the  $n\text{CeO}_2$  negatively affects the C accumulation by leaf tissues. Our data do not allow us to identify the specific cause precisely. However, this observation corroborates the literature evidence regarding the slowing of the plant growth cycle [42] and photosynthesis, both in terrestrials and aquatic plants [43,44].

The growing number of nanotechnology applications in various fields inevitably results in the release of nanomaterials into the environment. Models demonstrated that wastewater and sewage sludge are the primary vectors by which ENMs end up in the environment [45]. Apart from the quantitative aspect, nanomaterials' flows can occur differently concerning the position of the target to the source (e.g., a single massive event or events repeated over time). Literature papers concerning the effects of ENMs on plants always report experiments where the nanomaterials were applied in a single concentration, whereas a more realistic exposure scenario involves repeated pulses.

In our study, plants of *S. flos-cuculi* were grown in soil amended with  $n\text{CeO}_2$ . The experimental design was conceived assuming that the soil could receive different  $n\text{CeO}_2$  pulses over time, thereby obtaining three different doses of  $n\text{CeO}_2$  supplied at different growth stages of *S. flos-cuculi*. At the moment, we cannot compare our data with other works having the same experimental approach. We have already cited a paper reporting Ag and Cu nanoparticles' effects on seedlings of *Pinus sylvestris* and *Quercus robur*. A single dose of nanomaterials was administered to plants by three subsequent foliar applications in that study, whereas in our experiment were provided three amounts of  $n\text{CeO}_2$ . However, in both experiments, the experimental factor "dose" or merely the phenological stage at which plants received the treatments showed some influence on the consequences of the treatment. Therefore, this early indication suggests that this type of study should be further developed. Other studies of soil ecology have used the same approach. In particular, it was demonstrated that soil enzyme activity is differently affected by repeated ENM doses, indicating that additive effects occur [46,47]. It will be necessary to compile these different works to achieve a complete evaluation of the effects of ENMs on the soil–plant system.

**Supplementary Materials:** The following are available online at <https://www.mdpi.com/2079-4991/11/229/s1>: Figure S1. Number of stems per plant in specimens of *S. flos-cuculi*. Comparison of effects based on single (D1) and repeated applications (D2, D3) of 20 and 200 mg kg<sup>-1</sup>  $n\text{CeO}_2$ , respectively. Letters indicate statistically significant difference between treatments ( $p \leq 0.05$ ) using one-way ANOVA followed by Tukey's test. † One-way ANOVA  $p$ -value within each concentration. Figure S2. Number of leaves per plant in specimens of *S. flos-cuculi*. Comparison of effects based on single (D1) and repeated applications (D2, D3) of 20 and 200 mg kg<sup>-1</sup>  $n\text{CeO}_2$ , respectively. Letters indicate statistically significant difference between treatments ( $p \leq 0.05$ ) using one-way

ANOVA followed by Tukey's test. † One-way ANOVA  $p$ -value within each concentration. Figure S3. Total leaf area in plants of *S. flos-cuculi*. Comparison of effects based on single (D1) and repeated applications (D2, D3) of 20 and 200 mg kg<sup>-1</sup> nCeO<sub>2</sub>, respectively. Letters indicate statistically significant difference between treatments ( $p \leq 0.05$ ) using one-way ANOVA followed by Tukey's test. † One-way ANOVA  $p$ -value within each concentration. Figure S4. Leaf dry matter in plants of *S. flos-cuculi*. Comparison of effects based on single (D1) and repeated applications (D2, D3) of 20 and 200 mg kg<sup>-1</sup> nCeO<sub>2</sub>, respectively. Letters indicate statistically significant difference between treatments ( $p \leq 0.05$ ) using one-way ANOVA followed by Tukey's test. † One-way ANOVA  $p$ -value within each concentration. Figure S5. Stem mass fraction of *S. flos-cuculi*. Comparison of effects based on single (D1) and repeated applications (D2, D3) of 20 and 200 mg kg<sup>-1</sup> nCeO<sub>2</sub>, respectively. Letters indicate statistically significant difference between treatments ( $p \leq 0.05$ ) using one-way ANOVA followed by Tukey's test. † One-way ANOVA  $p$ -value within each concentration. Figure S6. Leaf mass fraction of *S. flos-cuculi*. Comparison of effects based on single (D1) and repeated applications (D2, D3) of 20 and 200 mg kg<sup>-1</sup> nCeO<sub>2</sub>, respectively. Letters indicate statistically significant difference between treatments ( $p \leq 0.05$ ) using one-way ANOVA followed by Tukey's test. † One-way ANOVA  $p$ -value within each concentration. Figure S7. Shoot to root ratio in *S. flos-cuculi*. Comparison of effects based on single (D1) and repeated applications (D2, D3) of 20 and 200 mg kg<sup>-1</sup> nCeO<sub>2</sub>, respectively. Letters indicate statistically significant difference between treatments ( $p \leq 0.05$ ) using one-way ANOVA followed by Tukey's test. † One-way ANOVA  $p$ -value within each concentration. Figure S8. Leaf area ratio of *S. flos-cuculi*. Comparison of effects based on single (D1) and repeated applications (D2, D3) of 20 and 200 mg kg<sup>-1</sup> nCeO<sub>2</sub>, respectively. Letters indicate statistically significant difference between treatments ( $p \leq 0.05$ ) using one-way ANOVA followed by Tukey's test. † One-way ANOVA  $p$ -value within each concentration. Table S1. Average, PDI and  $\zeta$ -potentials of nCeO<sub>2</sub> 25 nm. Table S2. Most frequent particle size, mean particle size, number of pulses and concentration of dissolved Ce determined by sp-ICP-MS analysis after enzymatic extraction from roots and leaves of *Silene flos-cuculi*. Table S3. Two-way ANOVA  $p$ -values testing the statistically significant effects of dose and concentration and their interaction of nCeO<sub>2</sub> on biometric variables of *S. flos-cuculi*. Table S4. Biomass allocation variables calculated from plant measurements (Poorter et al., 2011). Table S5. Two-way ANOVA  $p$ -values testing the statistically significant effects of dose and concentration and their interaction of nCeO<sub>2</sub> on growth indices of *S. flos-cuculi*. Table S6. Two-way ANOVA  $p$ -values testing the statistically significant effects of dose and concentration and their interaction on Ce concentrations in fractions of *S. flos-cuculi* and Ce translocation factor.

**Author Contributions:** Conceptualization, D.L. and L.M.; formal analysis, D.L. and L.M.; funding acquisition, L.M.; investigation, D.L.; methodology, A.M., B.P. and E.G.; supervision, L.M.; Writing—Original draft, L.M.; Writing—Review and editing, G.F. All authors have read and agreed to the published version of the manuscript.

**Funding:** This research was funded by the Regione Friuli Venezia Giulia, General Directorate of Environment, project "Nanomateriali 2017–2020".

**Data Availability Statement:** The data presented in this study are available on request from the corresponding author.

**Acknowledgments:** The authors are grateful to PhD course in "Environmental Life Sciences" jointly offered by the Universities of Trieste (Italy) and University of Udine (Italy). L.M. is grateful to Regione Friuli Venezia Giulia, General Directorate of Environment, for the financial support.

**Conflicts of Interest:** The authors declare no conflict of interest.

## References

1. Hull, M.S.; Bowman, D.M. Nanotechnology Environmental Health and Safety. In *Risks, Regulation, and Management*, 3rd ed.; Elsevier: Amsterdam, The Netherlands, 2019.
2. Meesters, J.A.J.; Quik, J.T.K.; Koelmans, A.A.; Hendriks, A.J.; van de Meent, D. Multimedia environmental fate and speciation of engineered nanoparticles: A probabilistic modeling approach. *Environ. Sci. Nano* **2016**, *3*, 715. [[CrossRef](#)]
3. Holden, P.A.; Gardea-Torresdey, J.L.; Klaessig, F.; Turco, R.F.; Mortimer, M.; Hund-Rinke, K.; Cohen Hubal, E.A.; Avery, D.; Barceló, D.; Behra, R.; et al. Considerations of environmentally relevant test conditions for improved evaluation of ecological hazards of engineered nanomaterials. *Environ. Sci. Technol.* **2016**, *50*, 6124–6145. [[CrossRef](#)]

4. Hund-Rinke, K.; Baun, A.; Cupi, D.; Fernandes, T.F.; Handy, R.; Kinross, J.H.; Navas, J.M.; Peijnenburg, W.; Schlich, K.; Shaw, B.J.; et al. Regulatory ecotoxicity testing of nanomaterials—Proposed modifications of OECD test guidelines based on laboratory experience with silver and titanium dioxide nanoparticles. *Nanotoxicology* **2016**, *10*, 1442–1447. [[CrossRef](#)]
5. Rasmussen, K.; Rauscher, H.; Kearns, P.; González, M.; Riego Sintes, J. Developing OECD test guidelines for regulatory testing of nanomaterials to ensure mutual acceptance of test data. *Reg. Toxicol. Pharmacol.* **2019**, *104*, 74–83. [[CrossRef](#)]
6. Bar-On, Y.M.; Phillips, R.; Milo, R. The biomass distribution on Earth. *Proc. Natl. Acad. Sci. USA* **2018**, *115*, 16506–16511. [[CrossRef](#)]
7. Isbell, F.; Calcagno, V.; Hector, A.; Connolly, J.; Stanley Harpole, W.; Reich, P.B.; Scherer-Lorenzen, M.; Schmid, B.; Tilman, D.; van Ruijven, J.; et al. High plant diversity is needed to maintain ecosystem services. *Nature* **2011**, *477*, 199–202. [[CrossRef](#)]
8. Kah, M.; Kookana, R.S.; Gogos, A.; Bucheli, T.D. A critical evaluation of nanopesticides and nanofertilizers against their conventional analogues. *Nat. Nanotechnol.* **2018**, *13*, 677–684. [[CrossRef](#)]
9. Petersen, E.J.; Mortimer, M.; Burgess, R.M.; Handy, R.; Hanna, S.; Ho, K.T.; Johnson, M.; Loureiro, S.; Henriette Selck, H.; Scott-Fordsmand, J.J.; et al. Strategies for robust and accurate experimental approaches to quantify nanomaterial bioaccumulation across a broad range of organisms. *Environ. Sci. Nano* **2019**, *6*, 1619–1656. [[CrossRef](#)]
10. Zuverza-Mena, N.; Martínez-Fernández, D.; Du, W.; Hernandez-Viezas, J.A.; Bonilla-Bird, N.; López-Moreno, M.L.; Komárek, M.; Peralta-Videa, J.R.; Gardea-Torresdey, J.L. Exposure of engineered nanomaterials to plants: Insights into the physiological and biochemical responses—A review. *Plant Physiol. Biochem.* **2017**, *110*, 236–264. [[CrossRef](#)]
11. Ma, X.; Yan, J. Plant uptake and accumulation of engineered metallic nanoparticles from lab to field conditions. *Curr. Opin. Environ. Sci. Health* **2018**, *6*, 16–20. [[CrossRef](#)]
12. Sun, T.Y.; Gottschalk, F.; Hungerbühler, K.; Nowack, B. Comprehensive probabilistic modelling of environmental emissions of engineered nanomaterials. *Environ. Pollut.* **2014**, *185*, 69–76. [[CrossRef](#)] [[PubMed](#)]
13. Antonelli, A.; Fry, C.; Smith, R.J.; Simmonds, M.S.J.; Kersey, P.J.; Pritchard, H.W.; Sofu, A.; Haelewaters, D.; Gâteblé, G. *State of the World's Plants and Fungi 2020*; Royal Botanic Gardens: Kew, UK, 2020.
14. Wiersma, J.H.; Léon, B. *World Economic Plants: A Standard Reference*; CRC Press: Boca Raton, FL, USA, 1999.
15. Janick, J. New crops and the search for new food resources. In *Perspectives on New Crops and New Uses*; Janick, J., Ed.; ASHS Press: Alexandria, VA, USA, 1999; pp. 281–304.
16. Singh, K.R.B.; Nayak, V.; Sarkar, T.; Singh, R.P. Cerium oxide nanoparticles: Properties, biosynthesis and biomedical application. *RSC Adv.* **2020**, *10*, 27194. [[CrossRef](#)]
17. Piccinno, F.; Gottschalk, F.; Seeger, S.; Nowack, B. Industrial production quantities and uses of ten engineered nanomaterials in Europe and the world. *J. Nanopart. Res.* **2012**, *14*, 1109. [[CrossRef](#)]
18. OECD. *ENV/JM/MONO(2010)46-List of Manufactured Nanomaterials and List of Endpoints for Phase One of the Sponsorship Programme for the Testing of Manufactured Nanomaterials: Revision*; OECD: Paris, France, 2010.
19. Ding, Y.; Bai, X.; Ye, Z.; Ma, L.; Liang, L. Toxicological responses of Fe<sub>3</sub>O<sub>4</sub> nanoparticles on *Eichhornia crassipes* and associated plant transportation. *Sci. Total Environ.* **2019**, *671*, 558–567. [[CrossRef](#)] [[PubMed](#)]
20. Ekperusia, A.O.; Sikokic, F.D.; Nwachukwu, E.O. Application of common duckweed (*Lemna minor*) in phytoremediation of chemicals in the environment: State and future perspective. *Chemosphere* **2019**, *223*, 285–309. [[CrossRef](#)]
21. Geitner, N.K.; Cooper, J.L.; Avellan, A.; Castellon, B.T.; Perrotta, B.G.; Bossa, N.; Simonin, M.; Anderson, S.M.; Inoue, S.; Hochella, M.F.; et al. Size-based differential transport, uptake, and mass distribution of ceria (CeO<sub>2</sub>) nanoparticles in wetland mesocosms. *Environ. Sci. Technol.* **2018**, *52*, 9768–9776. [[CrossRef](#)]
22. Yin, L.; Colman, B.P.; McGill, B.M.; Wright, J.P.; Bernhardt, E.S. Effects of silver nanoparticle exposure on germination and early growth of eleven wetland plants. *PLoS ONE* **2012**, *7*, e47674. [[CrossRef](#)]
23. Jacob, D.L.; Borchardt, J.D.; Navaratnam, L.; Otte, M.L.; Bezbaruah, A.N. Uptake and translocation of Ti nanoparticles in crops and wetland plants. *Int. J. Phytorem.* **2013**, *15*, 142–153. [[CrossRef](#)]
24. Song, U.; Lee, S. Phytotoxicity and accumulation of zinc oxide nanoparticles on the aquatic plants *Hydrilla verticillata* and *Phragmites australis*: Leaf-type-dependent responses. *Environ. Sci. Pollut. Res.* **2016**, *23*, 8539–8545. [[CrossRef](#)]
25. Aleksandrowicz-Trzczińska, M.; Bederska-Błaszczak, M.; Szaniawski, A.; Olchowik, J.; Studnicki, M. The effects of copper and silver nanoparticles on container-grown Scots Pine (*Pinus sylvestris* L.) and Pedunculate Oak (*Quercus robur* L.) seedlings. *Forests* **2019**, *10*, 269. [[CrossRef](#)]
26. Servin, A.D.; White, J.C. Nanotechnology in agriculture: Next steps for understanding engineered nanoparticle exposure and risk. *NanoImpact* **2016**, *1*, 9–12. [[CrossRef](#)]
27. Jalas, J.; Suominen, J. *Atlas Florae Europaeae (AFE)—Distribution of Vascular Plants in Europe 7 (Caryophyllaceae (Silenoideae))*; Committee for Mapping the Flora of Europe and Societas Biologica Fennica Vanamo: Vanamo, Helsinki, 1986.
28. Aavik, T.; Holderegger, R.; Bolliger, J. The structural and functional connectivity of the grassland plant *Lychnis flos-cuculi*. *Heredity* **2014**, *112*, 471–478. [[CrossRef](#)] [[PubMed](#)]
29. Biere, A. Parental effects in *Lychnis flos-cuculi* L.: Seed size, germination and seedling performance in a controlled environment. *J. Evol. Biol.* **1999**, *4*, 447–465. [[CrossRef](#)]
30. Jiménez-Lamana, J.; Wojcieszek, J.; Jakubiak, M.; Asztemborska, M.; Szpunar, J. Single particle ICP-MS characterization of platinum nanoparticles uptake and bioaccumulation by *Lepidium sativum* and *Sinapis alba* plants. *J. Anal. At. Spectrom.* **2016**, *31*, 2321–2329. [[CrossRef](#)]

31. US EPA. EPA Method 3052. Microwave assisted acid digestion of siliceous and organically based matrices in US Environmental Protection Agency. In *Test Methods for Evaluating Solid Waste*; US EPA: Washington, DC, USA, 1995.
32. Lizzi, D.; Mattiello, A.; Piani, B.; Fellet, G.; Adamiano, A.; Marchiol, L. Germination and early development of three spontaneous plant species to nanoceria ( $n\text{CeO}_2$ ) with different concentrations and particle sizes. *Nanomaterials* **2020**, *10*, 2534. [[CrossRef](#)] [[PubMed](#)]
33. Priester, J.H.; Ge, Y.; Mielke, R.E.; Horst, A.M.; Moritz, S.C.; Espinosa, K.; Gelb, J.; Walker, S.L.; Nisbet, R.M.; An, Y.J.; et al. Soybean susceptibility to manufactured nanomaterials with evidence for food quality and soil fertility interruption. *Proc. Natl. Acad. Sci. USA* **2012**, *109*, 2451–2456. [[CrossRef](#)]
34. López-Moreno, M.L.; De La Rosa, G.; Hernandez-Viezcas, J.A.; Peralta-Videa, J.R.; Gardea-Torresdey, J.L. X-ray absorption spectroscopy (XAS) corroboration of the uptake and storage of  $\text{CeO}_2$  nanoparticles and assessment of their differential toxicity in four edible plant species. *J. Agric. Food Chem.* **2010**, *58*, 3689–3693. [[CrossRef](#)]
35. Mattiello, A.; Pošćić, F.; Musetti, R.; Giordano, C.; Vischi, M.; Filippi, A.; Bertolini, A.; Marchiol, L. Evidences of genotoxicity and phytotoxicity in *Hordeum vulgare* exposed to  $\text{CeO}_2$  and  $\text{TiO}_2$  nanoparticles. *Front. Plant Sci.* **2015**, *6*, 1043. [[CrossRef](#)]
36. Andersen, C.P.; King, G.; Plocher, M.; Storm, M.; Pokhrel, L.R.; Johnson, M.G.; Rygielwicz, P.T. Germination and early plant development of ten plant species exposed to titanium dioxide and cerium oxide nanoparticles. *Environ. Toxicol. Chem.* **2016**, *35*, 2223–2229. [[CrossRef](#)]
37. Rico, C.M.; Morales, M.I.; Barrios, A.C.; McCreary, R.; Hong, J.; Lee, W.Y.; Nunez, J.; Peralta-Videa, J.R.; Gardea-Torresdey, J.L. Effect of cerium oxide nanoparticles on the quality of rice (*Oryza sativa* L.) grains. *J. Agric. Food Chem.* **2013**, *61*, 11278–11285. [[CrossRef](#)]
38. Barrios, A.C.; Medina-Velo, I.A.; Zuverza-Mena, N.; Dominguez, O.D.; Peralta-Videa, J.R.; Gardea-Torresdey, J.L. Nutritional quality assessment of tomato fruits after exposure to uncoated and citric acid coated cerium oxide nanoparticles, bulk cerium oxide, cerium acetate and citric acid. *Plant Physiol. Biochem.* **2017**, *110*, 100–107. [[CrossRef](#)] [[PubMed](#)]
39. Zhang, P.; Ma, Y.; Liu, S.; Wang, G.; Zhang, J.; He, X.; Zhang, J.; Rui, Y.; Zhang, Z. Phytotoxicity, uptake and transformation of nano- $\text{CeO}_2$  in sand cultured romaine lettuce. *Environ. Pollut.* **2017**, *220*, 1400–1408. [[CrossRef](#)] [[PubMed](#)]
40. Servin, A.D.; De La Torre-Roche, R.; Castillo-Michel, H.; Pagano, L.; Hawthorne, J.; Musante, C.; Pignatello, J.; Uchimiya, M.; White, J.C. Exposure of agricultural crops to nanoparticle  $\text{CeO}_2$  in biochar-amended soil. *Plant Physiol. Biochem.* **2017**, *110*, 147–157. [[CrossRef](#)] [[PubMed](#)]
41. Gunn, S.; Farrar, J.F.; Collis, B.E.; Nason, M. Specific leaf area in barley: Individual leaves versus whole plants. *New Phytol.* **1999**, *143*, 45–51. [[CrossRef](#)]
42. Marchiol, L.; Mattiello, A.; Pošćić, F.; Fellet, G.; Zavalloni, C.; Carlino, E.; Musetti, R. Changes in physiological and agronomical parameters of barley (*Hordeum vulgare*) exposed to cerium and titanium dioxide nanoparticles. *Int. J. Environ. Res. Public Health* **2016**, *13*, 332. [[CrossRef](#)]
43. Cao, Z.; Stowers, C.; Rossi, L.; Zhang, W.; Lombardini, L.; Ma, X. Physiological effects of cerium oxide nanoparticles on the photosynthesis and water use efficiency of soybean (*Glycine max* (L.) Merr.). *Environ. Sci. Nano* **2017**, *4*, 1086–1094. [[CrossRef](#)]
44. Rodea-Palomares, I.; Gonzalo, S.; Santiago-Morales, X.; Leganés, F.; García-Calvo, E.; Rosal, R.; Fernández-Piñas, F. An insight into the mechanisms of nanoceria toxicity in aquatic photosynthetic organisms. *Aquatic Toxicol.* **2012**, *122–123*, 133–143. [[CrossRef](#)]
45. Giese, B.; Klaessig, F.; Park, P.; Kaegi, R.; Steinfeldt, M.; Wigger, H.; von Gleich, A.; Gottschalk, F. Risks, release and concentrations of engineered nanomaterial in the environment. *Sci. Rep.* **2018**, *8*, 1565. [[CrossRef](#)]
46. Schlich, K.; Beule, L.; Hund-Rinke, K. Single versus repeated applications of  $\text{CuO}$  and  $\text{Ag}$  nanomaterials and their effect on soil microflora. *Environ. Pollut.* **2016**, *215*, 322–330. [[CrossRef](#)]
47. Mishra, P.; Xue, L.; Eivazi, F.; Afrasiabi, Z. Size, concentration, coating, and exposure time effects of silver nanoparticles on the activities of selected soil enzymes. *Geoderma* **2021**, *381*, 114682. [[CrossRef](#)]

Review

# Nanomaterials Induced Genotoxicity in Plant: Methods and Strategies

Marta Marmiroli <sup>1,\*</sup>, Nelson Marmiroli <sup>2</sup> and Luca Pagano <sup>1,\*</sup>

<sup>1</sup> Department of Chemistry, Life Sciences and Environmental Sustainability, University of Parma, Parco Area delle Scienze 11/A, 43124 Parma, Italy

<sup>2</sup> Consorzio Interuniversitario Nazionale per le Scienze Ambientali (CINSA), Parco Area delle Scienze 11/A, 43124 Parma, Italy; nelson.marmiroli@unipr.it

\* Correspondence: marta.marmiroli@unipr.it (M.M.); luca.pagano@unipr.it (L.P.)

**Abstract:** In recent years, plant-nanomaterial interactions have been studied, highlighting their effects at physiological and molecular levels. Transcriptomics and proteomics studies have shown pathways and targets of nanomaterial exposure and plant response, with particular regard to abiotic stress and oxidative stress. Only little information has been reported on engineered nanomaterial (ENMs) interactions with plant genetic material, both at a genomic and organellar DNAs level. Plants can be useful experimental material, considering they both contain chloroplast and mitochondrial DNAs and several plant genomes have been completely sequenced (e.g., *Arabidopsis thaliana*, *Solanum lycopersicum*, *Allium cepa*, *Zea mays*, etc.). In this mini review, the methods and the evidence reported in the present literature concerning the level of genotoxicity induced by ENMs exposure have been considered. Consolidated and potential strategies, which can be applied to assess the nanomaterial genotoxicity in plants, are reviewed.

**Keywords:** nanomaterials; plant genotoxicity; methods; biomarkers; organelles

**Citation:** Marmiroli, M.; Marmiroli, N.; Pagano, L.

Nanomaterials Induced Genotoxicity in Plant: Methods and Strategies.

*Nanomaterials* **2022**, *12*, 1658.

<https://doi.org/10.3390/nano12101658>

nano12101658

Academic Editor: Olivier Joubert

Received: 11 April 2022

Accepted: 11 May 2022

Published: 12 May 2022

**Publisher's Note:** MDPI stays neutral with regard to jurisdictional claims in published maps and institutional affiliations.



**Copyright:** © 2022 by the authors. Licensee MDPI, Basel, Switzerland. This article is an open access article distributed under the terms and conditions of the Creative Commons Attribution (CC BY) license (<https://creativecommons.org/licenses/by/4.0/>).

## 1. ENM Genotoxicity in Plant: The Current State

The global market for nanotechnology might grow from USD 5.2 bln in 2021 to USD 23.6 bln by 2026, with annual growth rate (CAGR) of 35.5%, respectively for the years 2021–2026. The North American market for nanotechnology is estimated to grow from USD 1.6 bln in 2021 to USD 7.2 bln by 2026, at a CAGR of 34.5% for the period 2021–2026, while the Asia–Pacific market for nanotechnology is estimated to grow from USD 1.2 to USD 6.0 bln, at a CAGR of 37.6%, respectively, for the same time period, as reported by Nanotechnology Services Global Market Report 2022.

Nanotechnology has captured the attention of a wide range of industries in many sectors, gaining in a short period large attraction and significant public investments in research and development, in addition to increasing private-sector investments. Many governments are implementing the application of nanotechnology notwithstanding the associated risks and uncertainties [1]. Nanotechnology allows the development and improvement of completely new products, processes, and services [2].

However, engineered nanomaterials (ENMs) are in the process of being dispersed into the environment, coming into contact with non-mammal organisms and plants [3,4]. So far, scientists have just started to investigate the impact of nanomaterials on plants, which has contrasting outcomes depending on the type of nanomaterial and on the plant species [5]. The field of nanotoxicology has been extended from microorganisms to plants and animals, even if the idea of ENM genotoxicology for plants is not so widespread. In fact, a search in Scopus [6] for publications with the word “Nanotoxicology” since 2013 produced 625 results. Research in the same timeframe, from 2013 to 2022, using the word “nanomaterial genotoxicology” produced only four outcomes. A more extensive database research has been conducted by Ghosh et al. [7], who found that there are few papers dealing with

the genotoxicity of the nanoparticles in respect to other effects that nanoparticles exert on plants.

In the field of toxicology, the term genotoxicity generally refers to any kind of damage to the genetic material, the genome, as cytotoxicity indicates injury to the cell instead. Toxic effects to the genetic material have attracted great attention for many reasons, including in particular that the genome of germ cells, the reproductive cells, determine all heritable characteristics of organisms [8]. Investigation of injury to the genome has led to the definition of a specific kind of toxicity, genotoxicity, and to the development of the subspecialty of genetic toxicology [9].

Several plant species have the intrinsic capability of being used as multiple genetic assay systems. These plant genetic systems have played important roles in detecting new mutagens and developing techniques later used in other systems for advancing mutagenesis knowledge. Some of the mainly used higher plant species are: *Allium cepa* L. (2n = 16), *Arabidopsis thaliana* L. (2n = 10), *Crepis capsularis* (L.) Wallr (2n = 6), *Glycine max* L. (2n = 40), *Hordeum vulgare* L. (2n = 14), *Solanum lycopersicum* L. (2n = 16), *Nicotiana tabacum* L. (2n = 48), *Pisum sativum* L. (2n = 14), *Tradescantia Ruppianus* ex L. (2n = 24), *Vicia faba* L. (2n = 12) and *Zea mays* L. (2n = 20) [10].

## 2. Mechanisms of ENM-Induced Genotoxicity

In vitro and in vivo characterization of the response to ENM exposure in both growth media and biological matrices have been extensively discussed in recent years [11]: uptake, pathways, biotransformation, and the mechanisms of ENM genotoxicity. In vitro and in vivo characterization of the response to ENM exposure in both growth media and biological matrices have been extensively discussed in recent years [11]: uptake, pathways, biotransformation, and the mechanisms of ENM genotoxicity. Different mechanisms can be exploited depending on the different ENM physico-chemical properties: (i) ENMs simply able to pass through the cellular membrane lipid bilayer, depending on several factors such as size, charge, hydrophobicity, composition and shape; (ii) endocytosis processes by which ENMs are taken up and accumulated in plant tissues, as well as Trojan horse mechanism and possible biotransformation processes (including corona protein interactions), lead to ENMs accumulation in plant cells; (iii) the utilization of membrane transporters which can mediate the translocation of ENMs into the plant cell, due to their affinity to the transporter itself [12,13]. As a result, ENMs response can be explicated by two different mechanisms: effects directly ascribed to the ENMs interaction with the cellular components, or its biotransformed physico-chemical forms (including ions released, depending on the ENM stability) [14] and indirectly, due to ROS production, increase mediated by mitochondrion and chloroplast functionality alteration, leading to a general cellular oxidative stress increase by triggering ENM-induced cytotoxicity and genotoxicity mechanisms [12]. The response observed is an effect of the activation defense mechanisms, including antioxidant defense mechanisms, apoptosis and secondary metabolite (e.g., phytohormone) production and antioxidant enzymes [11].

As a key metabolite, ROS are necessary in plants for many important signaling reactions, however they also constitute by-products in aerobic metabolism that can induce oxidative damage in plants [15]. It has been demonstrated that nanoparticles and ROS can directly enter the nucleus of the plant cell and, by binding chromatin and/or interacting with DNA, induce damages [16], showing potential mutagenic effect.

For nanoparticles (NPs) such as Ag NPs (coated and uncoated), carbon nanotubes, ZnO NPs, Al<sub>2</sub>O<sub>3</sub> NPs, Fe<sub>2</sub>O<sub>3</sub> NPs, Co<sub>3</sub>O<sub>4</sub> NPs, and NiO NPs, the main features that determine genotoxicity have been found to be ions release, dimension, and zeta potentials [7]. As a fact, these features contribute to the penetration of the nanoparticle into the cell nucleus and the consequent damage to DNA [17]. Several assays have been developed that use higher plants to measure the mutagenic effects of chemicals in general as indicators of carcinogenicity. These assays using plants require less complex equipment and materials than many other genotoxicity tests, which is a potential advantage, particularly when

research resources are limited [18]. Standard genotoxicity tests have been reviewed by the Gene-Tox program of the U.S. Environmental Protection Agency (EPA) concerning gene mutation, chromosomal effects and DNA damage repair on the following plants: *A. thaliana*, *G. max*, *H. vulgare*, *Tradescantia*, *Z. mays* [18,19]. Early studies on plants progressed to more sophisticated and complex assays on many other plants, and to many more materials including ENMs [7,17].

In this minireview, the most important genotoxicity assays applied on plants are explained, with a focus on how they can be utilized to determine the genotoxic effects for nanoparticles, which include standard techniques available and new tools and instruments. DNA damage may cause epigenetic changes, through covalent DNA modification, histones modification, and regulation of non-coding RNAs (miRNAs, lncRNAs, piRNAs). Modifications at the level of DNA methylation (global or gene-specific) may have a profound impact on chromatin remodeling and on locus-specific gene expression, respectively [20].

### 3. Current Methods and Functional Applied Strategies

#### 3.1. Standard Techniques

From an operational point of view, different approaches can be utilized to pinpoint the genotoxic effects of ENMs on plant DNA [7]. All these approaches are able to assess ENM genotoxicity from different points of view, showing potential advantages and disadvantages in terms of sensitivity and resolution, respectively. Methods described and relevant examples are schematized in Figure 1.

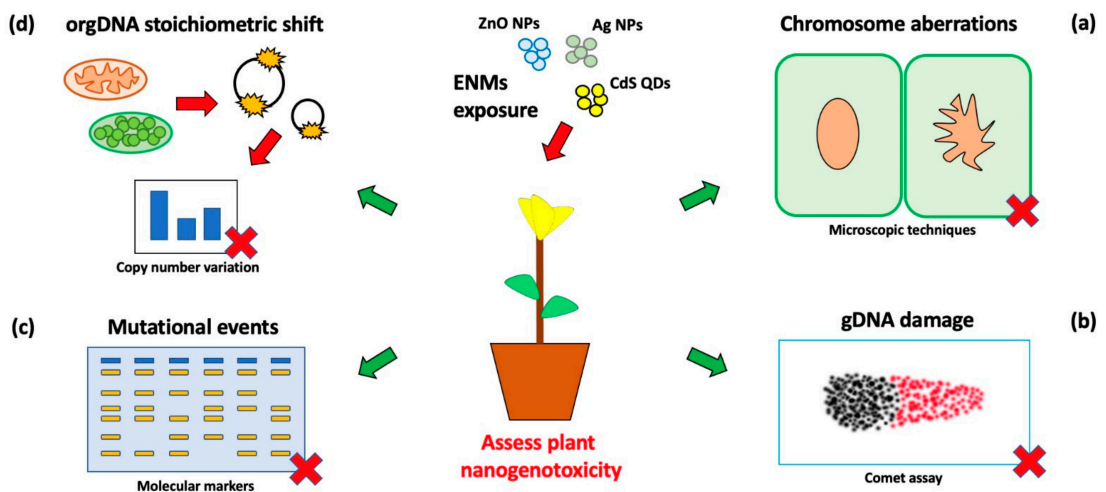


**Figure 1.** Schematic representation of the methodologies utilized to highlight plant ENM genotoxicity: (a) microscopic techniques to highlight chromosomal aberrations, (b) electrophoresis-based methods (e.g., comet assay) to highlight genomic DNA (gDNA) damage, (c) molecular markers (e.g., RAPD) to show mutational events and (d) Real time PCR based methods to highlight copy number variation (stoichiometric or sub-stoichiometric shift) in plastid (ptDNA) or mitochondrial (mtDNA) genomes. These techniques can be utilized as Alternative Testing Strategies (ATS), in assessing and/or characterizing the risk associated with ENMs exposure/effects, not only in experimental controlled conditions, but also in monitoring of realistic scenarios, at early exposure stages.

Among the major effects observed from the exogenous genotoxic effects on plant genomes, the chromosomal aberrations, which are the result of structural and numerical chromosome changes, preferentially within heterochromatic regions, are composed mainly of repetitive DNA sequences [21]. Optical, fluorescence and confocal laser scanning microscopy techniques are able to highlight aberrations at the level of the chromosome

structure, including chromosomal breaks, sticky, multipolar, and laggard chromosomes, as well as micronucleus formation [22–24].

Chromosomal aberrations have been observed by Pakrashi et al. [25], studying the effect of titania nanoparticles (TiO<sub>2</sub> NPs) on *Allium cepa* L. root tips, in the range 0–100 mg L<sup>-1</sup>. Optical and fluorescence microscopic analyses showed a dose-dependent frequency of the aberration appearance, which includes chromosomal breaks, chromosome stickiness during metaphase, multiple micronucleus formation, as well as the occurrence of binucleate cells. Confocal microscopic images highlighted the formation of chromosomal bridges, in addition to a distorted and notched nucleus.

Similarly, Panda et al. [26] observed micronucleus mitotic aberrations formations in *Allium cepa* L. cells exposed to 0–80 mg L<sup>-1</sup> of different forms of silver ionic colloidal nanoparticles (Ag NPs). Additionally, in this case, the percentage of increase in aberrations was concentration dependent.

Silva and Monteiro [27] investigated the genotoxic and phytotoxic impacts of silica-based nanomaterials (SiO<sub>2</sub> NPs, in a range between 0.54–1.82 g L<sup>-1</sup>) using root tip cells of *Allium cepa* L., highlighting chromosomal aberrations and delays in mitosis due to disturbed metaphase. Sun et al. [28] studied the cytotoxic and genotoxic effects of ZnO NPs (5–50 mg L<sup>-1</sup>) in root meristems of *Allium cepa* L. cells by cell membrane integrity, metabolic activity, reactive oxygen species (ROS) accumulation, DNA damage and chromosomal aberration, highlighting how ZnO NP accumulation within cell nuclei affected cell mitosis, inducing chromosome breaks, bridges, stickiness, and micronuclei formation. As often reported, the utilization of *Allium cepa* L. is considered an efficient bioindicator in genotoxicity testing, due to its reduced number of chromosomes and rapid root growth rate [29]. Abdelsalam et al. [30] investigated the effects of foliar application of (nitrogen-phosphorus-potassium) NPK nanoparticles (2.5 to 5 kg ha<sup>-1</sup>) for two harvest seasons on *Triticum aestivum* L. as an alternative to conventional fertilizers, assessing yield and genotoxic effects. Although fertilization with NPK nanoparticles produced an increase in yield, root-tip cells showed various types of chromosomal aberrations such as multinuclei, micronuclei, chromosome deletion, lagging chromosome and cell membrane damage, and the NPK nanoparticles treatment at 5 kg ha<sup>-1</sup> produced 35.7–38.9% of abnormal cells. With a similar approach, Abdelsalam et al. [31] tested on *Triticum aestivum* L. seeds the utilization of (amino-zinc) AZ nanoparticles (50–150 mg L<sup>-1</sup>) in vitro medium for 8, 16, or 24 h. Genotoxicity was evaluated in root meristems, revealing mitotic activity variations, chromosomal aberrations, and micronuclei formation and a growth inhibit of the normal cellular function.

### 3.2. Gel Electrophoresis-Based Methods

DNA damage in individual plant cells can be highlighted by gel electrophoresis-based methods [32]: cells embedded in agarose on a microscope slide are lysed with detergent and high salt concentrations to form nucleoids containing supercoiled loops of DNA linked to the nuclear matrix; subsequent electrophoresis conducted at high pH produces structures resembling comets, which can be observed by fluorescence microscopy. The intensity of the “comet tail” reflects the breaks in DNA sequences. Comet assay is able to detect DNA single-strand breaks, DNA double-strand breaks, and the formation of apoptotic nuclei [33]. This assay is often utilized as a confirmation method for microscopic evidence [26,34,35].

Several examples can be found in recent literature related to ENM genotoxicity in plants: Panda et al. [26], through comet assay, observed a significant DNA damage rate determined by dose-dependent Ag NPs exposure and correlated to ROS formation. Faisal et al. [36] utilized the comet assay to assess the genotoxic effects in *Solanum lycopersicum* L. seedlings exposed to NiO NPs (0–2 g L<sup>-1</sup>). Analyses showed a significant increase in genomic DNA damage, and an increase in the number of apoptotic (21.8%) and necrotic (24.0%) cells. Cıgerci et al. [34] studied Indium tin oxide (ITO, In<sub>2</sub>O<sub>3</sub>/SnO<sub>2</sub>, ratiion 90/10%) particles (1–100 mg L<sup>-1</sup>), observing a significant increase in DNA damages in *A. cepa* root meristematic cells, highlighting potential alterations in the cell cycle, as demonstrated

by the higher number of cells able to enter into mitosis, as compared with the untreated controls. Thiruvengadam et al. [37] studied physiological, metabolic, and transcriptional effects of Ag NPs ( $1\text{--}10\text{ mg L}^{-1}$ ) *Brassica rapa* spp. observing a dose dependent DNA damage effects in turnip cells. Sun et al. [28] confirmed by comet assay the chromosomal aberration generated in *A. cepa*, highlighting a significant increase in DNA fragmentation after ZnO NPs exposure.

### 3.3. Molecular Markers and Biomarker Assays

Not only electrophoresis-based methods and chromosomal aberration analyses are utilized to detect potential genotoxic effects. Molecular markers can be also implemented as tools to detect the ENMs effect on genetic materials [38]. Molecular markers are defined as fragments or amplicons of DNA associated with a certain location within the genome. Molecular markers can be used as a biotechnological tool to identify and characterize a particular sequence of DNA when there is a limited knowledge of the sequence itself. This is the case, for example, of Random Amplified Polymorphic DNA (RAPD), markers based on PCR amplification of DNA fragments from random segments of genomic DNA, with a single primer of an arbitrary nucleotide sequence [39]. RAPDs do not require specific knowledge of the DNA sequence of the target organism. The occurrence of mutation at the level of DNA, particularly at the site that was previously complementary to the primer, will not allow amplicon production, resulting in a different pattern of amplified DNA fragments, which results in a molecular marker that is mainly dominant [40]. Since the early 1990s, several molecular marker tools have been developed in order to increase the detail of the physical genomic mapping and QTL analysis, with pros and cons related to the intrinsic properties of each molecular marker, respectively [41].

Molecular markers can be also utilized as tools to determine potential mutations at the level of the DNA sequence [42], which can support or validate data previously obtained, but also to isolate potential targets functional to biomarker characterization and development [43,44].

Hosseinpour et al. [45] studied the effects of the application of ZnO NPs ( $0\text{--}40\text{ mg L}^{-1}$ ) and plant growth promoting bacteria on *S. lycopersicum* L. under salt stress, with particular regard to DNA damage and cytosine methylation changes. RAPD analysis has been performed to determine the effects of co-exposure to bacteria and ZnO NPs on tomato genomic DNA. The rate of polymorphism observed in case of salinity stress treatment (42.2%) was a decrease in case of exposure to ZnO NPs and/or plant growth promoting bacteria from 32.4% to 25.3%, respectively. The results obtained through the application of different bacteria and ZnO NPs concentrations suggest the inverse relationship between the level of cytosine methylation and salinity stress tolerance. Mosa et al. [46] studied the genotoxic effects and genomic alterations in *Cucumis sativus* L. of copper-based nanoparticles (Cu NPs) using the RAPD technique. Cu NPs ( $0\text{--}200\text{ mg L}^{-1}$ ) showed a concentration-dependent increase rate of polymorphism occurrence, highlighting the Cu NPs genotoxic effect. Kokina et al. [47] studied the impact of iron oxide nanoparticles ( $\text{Fe}_3\text{O}_4$  NPs,  $0\text{--}4\text{ mg L}^{-1}$ ) on *Medicago falcata* L. The utilization, in this case, of the RAPD technique highlighted the genotoxic effect of  $\text{Fe}_3\text{O}_4$  NPs, which induced genomic DNA modifications. This type of PCR-based molecular marker for its randomic amplification nature may be subject to experimental or technical variability, and thus requires procedures of validation [38,39]. Several other type of molecular markers and biomarkers can be utilized as more reliable tools to assess genomic variations, either at the level of genomic DNA (gDNA) and plastid and mitochondrial DNA (ptDNA, mtDNA). Pagano et al. [44] highlighted a modulation of the organellar functionality in *Arabidopsis thaliana* L. Heynh in direct comparison to a modulated organelle genome replication level, upon exposure to  $\text{CeO}_2$  NPs, FeOx NPs, ZnS QDs, CdS QDs ( $80\text{--}500\text{ mg L}^{-1}$ ). In this case, multiple target genes at the level of ptDNA and mtDNA were utilized as structural markers to assess the potential variations at the level of DNA replication by real time qPCR. In particular, CdS QD exposure triggered potential variations at the sub-stoichiometric level of the two organellar genomes, while

nanoscale FeOx NPs and ZnS QDs exposure triggered an increase in organellar DNA copy numbers. These findings suggested how modification in organellar genomes stoichiometry may result from a potential morpho-functional adaptive response to ENM exposure, which led to decreased rates of photosynthesis and cellular respiration.

### 3.4. Other Approaches

Other approaches, which included *A. thaliana* transgenic lines for homologous recombination and transcriptional gene silencing, were adopted to assess the genotoxicity of ZnO NPs [48]. The results showed, at the level of roots, how exposure to ZnO NPs (0–20 mg L<sup>-1</sup>) resulted in an increase in homologous recombination (in particular the gene *atRad54-GFP-GUS* expression) and a reduction in transcriptional gene silencing in leaves (which contained the multicopy construct *P35S::GUS*), which can be ascribed to genotoxic effects triggered by ZnO NPs dissolution to free Zn ions. Methods described and relevant examples are reported in Table 1.

**Table 1.** Reference list of relevant experiments performed with different tools to identify ENM genotoxic effects in plants.

ENM	Treatment (*)	Plant	Analyses	Reference
TiO <sub>2</sub> NPs	Conc.: 0–100 mg L <sup>-1</sup> (hydroponic), 4 h treatment	<i>Allium cepa</i> L.	Chromosome aberration	Pakrashi et al. [25]
Ag NPs	Conc.: 0–80 mg L <sup>-1</sup> (hydroponic), 1 h treatment	<i>Allium cepa</i> L.	Chromosome aberration, Comet assay	Panda et al. [26]
SiO <sub>2</sub> NPs	Conc.: 0.54–1.82 g L <sup>-1</sup> (hydroponic), 24 h treatment	<i>Allium cepa</i> L.	Chromosome aberration	Silva and Monteiro [27]
ZnO NPs	Conc.: 5–50 mg L <sup>-1</sup> (hydroponic), 36 h treatment	<i>Allium cepa</i> L.	Chromosome aberration, Comet assay	Sun et al. [28]
NPK particles	Conc.: 2.5–5.0 kg ha <sup>-1</sup> (in soil, foliar spray), two harvest seasons	<i>Triticum aestivum</i> L.	Chromosome aberration	Abdelsalam et al. [30]
AZ particles	Conc.: 50–150 mg L <sup>-1</sup> (in vitro), 8, 16, 24 h treatment	<i>Triticum aestivum</i> L.	Chromosome aberration	Abdelsalam et al. [31]
NiO NPs	Conc.: 0–2 g L <sup>-1</sup> (in vitro), 12 d treatment	<i>Solanum lycopersicum</i> L.	Comet assay	Faisal et al. [36]
In <sub>2</sub> O <sub>3</sub> /SnO <sub>2</sub> particles	Conc.: 1–100 mg L <sup>-1</sup> (hydroponic), 4 h treatment	<i>Allium cepa</i> L.	Comet assay	Cigerci et al. [34]
Ag NPs	Conc.: 1–10 mg L <sup>-1</sup> (in vitro), 14 d treatment	<i>Brassica rapa</i> spp.	Comet assay	Thiruvengadam et al. [37]
ZnO NPs	Conc.: 0–40 mg L <sup>-1</sup> (in vitro), 14 d treatment	<i>Solanum lycopersicum</i> L.	RAPD	Hosseinpour et al. [45]
Cu NPs	Conc.: 0–200 mg L <sup>-1</sup> (in vitro), 21 d treatment	<i>Cucumis sativus</i> L.	RAPD	Mosa et al. [46]
Fe <sub>3</sub> O <sub>4</sub> NPs	Conc.: 0–4 mg L <sup>-1</sup> (hydroponic), 35 d treatment	<i>Medicago falcata</i> L.	RAPD	Kokina et al. [47]
CeO <sub>2</sub> NPs, FeOx NPs, ZnS QDs, CdS QDs	Conc.: 80 mg L <sup>-1</sup> (CdS QDs), 500 mg L <sup>-1</sup> (CeO <sub>2</sub> NPs, FeOx NPs, ZnS QDs), (in vitro) 21 d treatment	<i>Arabidopsis thaliana</i> L.	mtDNA, ptDNA copy number variation	Pagano et al. [44]
ZnO NPs	Conc.: 0–20 mg L <sup>-1</sup> (hydroponic), 20 d treatment	<i>Arabidopsis thaliana</i> L.	Gene silencing	Yang et al. [48]

\*, treatment conditions information includes concentration, experimental setup, and time of exposure utilized. Reference list order in the table reflects the order of appearance in the text, depending on the type of analyses performed.

## 4. Conclusions

In conclusion, in recent years, different techniques, previously exploited for animal cells, have been developed and applied to plants to assess the genotoxic effects related to ENM exposure. These approaches, considering their properties, and the relative pros and cons, which include high/low resolution vs. high/low target specificity, may be implemented for cross-validation of the results obtained. This may also include potential applications related to the utilization of novel methods of mutagenesis (e.g., CRISPR-Cas9) [49].

In this context, plants and microorganisms can be utilized as model organisms instead of animal models for Alternative Testing Strategies (ATS) to assess and characterize the risk, with particular regard to genotoxicity, related to ENMs exposure/effects [44,50]. Adoption of ATS for new organisms, endpoints, and span of variations in experimental scale and complexity have been increasingly functional in nanotoxicological literature through iterative processes able to combine results from physiological and molecular approaches [51]. Moreover, the monitoring of ENMs dispersal in the environment, especially at very early exposure stages and in realistic scenarios, can be further implemented [52] in accordance with the recently published EFSA guidance on risk assessment of the application of nanoscience and nanotechnologies in the food and feed chain, human and animal health, which considers in vitro/in vivo toxicological testing (e.g., in vitro degradation, toxicokinetics, genotoxicity,

local and systemic toxicity), and the European Registration, Evaluation Authorization and Restriction of Chemicals (REACH) protocols for chemical safety assessment [1,53].

**Author Contributions:** Conceptualization, M.M., N.M. and L.P.; writing—original draft preparation, M.M., N.M. and L.P.; writing—review and editing, M.M., N.M. and L.P. All authors have read and agreed to the published version of the manuscript.

**Funding:** This research received no external funding.

**Institutional Review Board Statement:** Not applicable.

**Informed Consent Statement:** Not applicable.

**Data Availability Statement:** The data presented in this study are available on request from the corresponding authors.

**Acknowledgments:** All authors acknowledge the support of FIL (“Fondi Locali per la Ricerca”).

**Conflicts of Interest:** Authors declare no competing financial interest.

## References

- Nielsen, M.B.; Baun, A.; Mackevica, A.; Thit, A.; Odnevall Wallinder, I.; Gallego, J.A.; Westergaard Clausen, L.P.; Rissler, J.; Skjolding, L.; Nilsson, A.; et al. Nanomaterials in the European chemicals legislation—Methodological challenges for registration and environmental safety assessment. *Environ. Sci. Nano* **2021**, *8*, 731–747. [CrossRef]
- Aithal, P.S.; Aithal, S. Business Strategy for Nanotechnology Based Products and Services. *Int. J. Bus. Manag. Sci.* **2016**, *5*, 139–149.
- Keller, A.A.; McFerran, S.; Lazareva, A.; Suh, S. Global life cycle releases of engineered nanomaterials. *J. Nanopart. Res.* **2013**, *169*, 6. [CrossRef]
- Marmiroli, N.; White, J.C.; Song, J. (Eds.) *Exposure to Engineered Nanomaterials in the Environment*; Micro&Nano Technologies Series; Elsevier: Amsterdam, The Netherlands, 2019.
- Holden, P.A.; Gardea-Torresdey, J.L.; Klaessig, F.; Turco, R.F.; Mortimer, M.; Hund-Rinke, K.; Cohen Hubal, E.A.; Avery, D.; Barceló, D.; Behra, R.; et al. Considerations of Environmentally Relevant Test Conditions for Improved Evaluation of Ecological Hazards of Engineered Nanomaterials. *Environ. Sci. Technol.* **2015**, *50*, 6124–6145. [CrossRef]
- Scopus Search for “Nanotoxicology” by Title, Abstract and Keywords. Available online: <https://www.scopus.com/search/form.uri?display=basic&zone=TopNavBar&origin=sbrowse#basic> (accessed on 10 April 2022).
- Ghosh, M.; Ghosh, I.; Godderis, L.; Hoet, P.; Mukherjee, A. Genotoxicity of engineered nanoparticles in higher plants. *Mutat. Res. Genet. Toxicol. Environ. Mutagenesis* **2019**, *842*, 132–145. [CrossRef]
- Sugden, K.D.; Campo, C.K.; Martin, D.D. Direct Oxidation of Guanine and 7,8-Dihydro-8-oxoguanine in DNA by a High-Valent Chromium Complex: A Possible Mechanism for Chromate Genotoxicity. *Chem. Res. Toxicol.* **2001**, *14*, 1315–1322. [CrossRef]
- Williams, G.M. Methods for evaluating chemical genotoxicity. *Annu. Rev. Pharmacol. Toxicol.* **1989**, *29*, 189–211. [CrossRef]
- Grant, W.F. The present status of higher plant bioassays for the detection of environmental mutagens. *Mut. Res.* **1994**, *310*, 175–185.
- Ma, C.; White, J.C.; Zhao, J.; Zhao, Q.; Xing, B. Uptake of Engineered Nanoparticles by Food Crops: Characterization, Mechanisms, and Implications. *Annu. Rev. Food Sci. Technol.* **2018**, *9*, 129–153. [CrossRef]
- Mehrian, S.K.; De Lima, R. Nanoparticles cyto and genotoxicity in plants: Mechanisms and abnormalities. *Environ. Nanotechnol. Monit. Manag.* **2016**, *6*, 184–193. [CrossRef]
- Pagano, L.; Maestri, E.; Caldara, M.; White, J.C.; Marmiroli, N.; Marmiroli, M. Engineered Nanomaterial Activity at the Organelle Level: Impacts on the Chloroplasts and Mitochondria. *ACS Sustain. Chem. Eng.* **2018**, *6*, 12562–12579. [CrossRef]
- Marmiroli, M.; Lepore, G.O.; Pagano, L.; d’Acapito, F.; Gianoncelli, A.; Villani, M.; Lazzarini, L.; White, J.C.; Marmiroli, N. The fate of CdS Quantum Dots in plants as revealed by Extended X-ray Absorption Fine Structure (EXAFS) analysis. *Environ. Sci. Nano* **2020**, *7*, 1150–1162. [CrossRef]
- Mittler, R. ROS Are Good. *Trends Plant Sci.* **2017**, *22*, 11–19. [CrossRef] [PubMed]
- Degtyareva, N.P.; Heyburn, L.; Sterling, J.; Resnick, M.A.; Gordenin, D.A.; Doetsch, P.W. Oxidative stress-induced mutagenesis in single-strand DNA occurs primarily at cytosines and is DNA polymerase zeta-dependent only for adenines and guanines. *Nucleic Acids Res.* **2013**, *41*, 8995–9005. [CrossRef] [PubMed]
- Wang, H.; Wu, F.; Wei Meng, W.; White, J.C.; Holden, P.; Xing, B. Engineered Nanoparticles May Induce Genotoxicity. *Environ. Sci. Technol.* **2013**, *47*, 13212–13214. [CrossRef]
- Ennever, F.K.; Andreano, G.; Rosenkranz, H.S. The ability of plant genotoxicity assays to predict carcinogenicity. *Mut. Res.* **1988**, *205*, 99–105. [CrossRef]
- Auletta, A.E.; Brown, M.; Wassom JSCimino, M.C. Current Status of the Gene-Tox Program. *Environ. Health Perspec.* **1991**, *96*, 33–36. [CrossRef]
- Gedda, M.R.; Babele, P.K.; Zahra, K.; Madhukar, P. Epigenetic Aspects of Engineered Nanomaterials: Is the Collateral Damage Inevitable? *Front. Bioeng. Biotechnol.* **2019**, *7*, 228. [CrossRef]

21. Schubert, I.; Pecinka, A.; Meister, A.; Schubert, V.; Klätte, M.; Jovtchev, G. DNA damage processing and aberration formation in plants. *Cytogenet. Genome Res.* **2004**, *104*, 104–108. [[CrossRef](#)]
22. Janicke, M.A.; Lasko, L.; Oldenbourg, R.; LaFountain, J.R. Chromosome malorientations after meiosis II arrest cause nondisjunction. *Mol. Biol. Cell.* **2007**, *18*, 1645–1656. [[CrossRef](#)]
23. Pessim, C.; Pagliarini, M.S.; Silva, N.; Jank, L. Chromosome stickiness impairs meiosis and influences reproductive success in *Panicum maximum* (Poaceae) hybrid plants. *Genet. Mol. Res. GMR* **2015**, *14*, 4195. [[CrossRef](#)] [[PubMed](#)]
24. Kwasniewska, J.; Bara, A.W. Plant Cytogenetics in the Micronuclei Investigation—The Past, Current Status, and Perspectives. *Int. J. Mol. Sci.* **2022**, *23*, 1306. [[CrossRef](#)] [[PubMed](#)]
25. Pakrashi, S.; Jain, N.; Dalai, S.; Jayakumar, J.; Chandrasekaran, P.T.; Raichur, A.M.; Chandrasekaran, N.; Mukherjee, A. In Vivo Genotoxicity Assessment of Titanium Dioxide Nanoparticles by *Allium cepa* Root Tip Assay at High Exposure Concentrations. *PLoS ONE* **2014**, *9*, e87789. [[CrossRef](#)]
26. Panda, K.K.; Achary, V.M.; Krishnaveni, R.; Padhi, B.K.; Sarangi, S.N.; Sahu, S.N.; Panda, B.B. In vitro biosynthesis and genotoxicity bioassay of silver nanoparticles using plants. *Toxicol. Vitro.* **2011**, *25*, 1097–1105. [[CrossRef](#)] [[PubMed](#)]
27. Silva, G.H.; Monteiro, R.T.R. Toxicity assessment of silica nanoparticles on *Allium cepa*. *Ecotoxicol. Environ. Contam.* **2017**, *12*, 25–31. [[CrossRef](#)]
28. Sun, Z.; Xiong, T.; Zhang, T.; Wang, N.; Chen, D.; Li, S. Influences of zinc oxide nanoparticles on *Allium cepa* root cells and the primary cause of phytotoxicity. *Ecotoxicology* **2019**, *28*, 178–195. [[CrossRef](#)]
29. Leme, D.M.; Marin-Morales, M.A. *Allium cepa* test in environmental monitoring: A review on its application. *Mut. Res.* **2009**, *682*, 71–81. [[CrossRef](#)]
30. Abdelsalam, N.R.; Kandil, E.E.; Al-Msari, M.A.F.; Al-Jaddafi, M.A.M.; Ali, H.M.; Salem, M.Z.M.; Elshikh, M.S. Effect of foliar application of NPK nanoparticle fertilization on yield and genotoxicity in wheat (*Triticum aestivum* L.). *Sci. Total Environ.* **2019**, *653*, 1128–1139. [[CrossRef](#)]
31. Abdelsalam, N.R.; Abdel-Megeed, A.; Ghareeb, R.Y.; Ali, H.M.; Salem, M.Z.M.; Akrami, M.; Al-Hayalif, M.F.A.; Desoky, E.M. Genotoxicity assessment of amino zinc nanoparticles in wheat (*Triticum aestivum* L.) as cytogenetical perspective. *Saudi J. Biol. Sci.* **2022**, *29*, 2306–2313. [[CrossRef](#)]
32. Collins, A.R. The comet assay for DNA damage and repair: Principles, applications, and limitations. *Mol. Biotechnol.* **2004**, *26*, 249–261. [[CrossRef](#)]
33. Olive, P.; Banáth, J. The comet assay: A method to measure DNA damage in individual cells. *Nat. Protoc.* **2006**, *1*, 23–29. [[CrossRef](#)] [[PubMed](#)]
34. Cigerci, I.; Liman, R.; Ozgüül, E.; Konuk, M. Genotoxicity of indium tin oxide by *Allium* and Comet tests. *Cytotechnology* **2015**, *67*, 157–163. [[CrossRef](#)] [[PubMed](#)]
35. Santos, C.L.V.; Pourrut, B.; Ferreira de Oliveira, J.M.P. The use of comet assay in plant toxicology: Recent advances. *Front. Genet.* **2015**, *6*, 216. [[CrossRef](#)] [[PubMed](#)]
36. Faisal, M.; Saquib, Q.; Alatar, A.A.; Al-Khedhairi, A.A.; Hegazy, A.K.; Musarrat, J. Phytotoxic hazards of NiO-nanoparticles in tomato: A study on mechanism of cell death. *J. Hazard. Mater.* **2013**, *250–251*, 318–332. [[CrossRef](#)]
37. Thiruvengadam, M.; Gurunathan, S.; Chung, I.M. Physiological, metabolic, and transcriptional effects of biologically-synthesized silver nanoparticles in turnip (*Brassica rapa* ssp. *rapa* L.). *Protoplasma* **2015**, *252*, 1031–1046. [[CrossRef](#)]
38. Hasan, N.; Choudhary, S.; Naaz, N.; Sharma, N.; Laskar, R.A. Recent advancements in molecular marker-assisted selection and applications in plant breeding programmes. *J. Genet. Eng. Biotechnol.* **2021**, *19*, 128. [[CrossRef](#)]
39. Conte, C.; Mutti, I.; Puglisi, P.; Ferrarini, A.; Regina, G.; Maestri, E.; Marmiroli, N. DNA fingerprinting analysis by a PCR based method for monitoring the genotoxic effects of heavy metals pollution. *Chemosphere* **1998**, *37*, 2739–2749. [[CrossRef](#)]
40. Mbwana, J.; Bölin, I.; Lyamuya, E.; Mhalu, F.; Lagergård, T. Molecular characterization of *Haemophilus ducreyi* isolates from different geographical locations. *J. Clin. Microbiol.* **2006**, *44*, 132–137. [[CrossRef](#)]
41. Dhingani, R.M.; Umrانيا, V.V.; Tomar, R.S.; Parakhia, M.V.; Golakiya, B.A. Introduction to QTL mapping in plants. *Ann. Plant Sci.* **2015**, *4*, 1072–1079.
42. Monteiro, M.; Santos, C.; Mann, R.M.; Soares, A.M.V.M.; Lopes, T. Evaluation of cadmium genotoxicity in *Lactuca sativa* L. using nuclear microsatellites. *Environ. Exp. Bot.* **2007**, *60*, 421–427. [[CrossRef](#)]
43. Li, C.; Zheng, Y.; Huang, P. Molecular markers from the chloroplast genome of rose provide a complementary tool for variety discrimination and profiling. *Sci. Rep.* **2020**, *10*, 12188. [[CrossRef](#)] [[PubMed](#)]
44. Pagano, L.; Marmiroli, M.; Villani, M.; Magnani, J.; Rossi, R.; Zappettini, A.; White, J.C.; Marmiroli, N. Engineered nanomaterial exposure affects organelle genetic material replication in *Arabidopsis thaliana*. *ACS Nano* **2022**, *16*, 2249–2260. [[CrossRef](#)] [[PubMed](#)]
45. Hosseinpour, A.; Haliloglu, K.; Tolga Cinişli, K.; Ozkan, G.; Oztürk, H.L.; Pour-Aboughadareh, A.; Poczai, P. Application of Zinc Oxide Nanoparticles and Plant Growth Promoting Bacteria Reduces Genetic Impairment under Salt Stress in Tomato (*Solanum lycopersicum* L. ‘Linda’). *Agriculture* **2020**, *10*, 521. [[CrossRef](#)]
46. Mosa, K.A.; El-Naggar, M.; Ramamoorthy, K.; Alawadhi, H.; Elnaggar, A.; Wartanian, S.; Ibrahim, E.; Hani, H. Copper Nanoparticles Induced Genotoxicity, Oxidative Stress, and Changes in Superoxide Dismutase (SOD) Gene Expression in Cucumber (*Cucumis sativus*) Plants. *Front. Plant Sci.* **2018**, *9*, 872. [[CrossRef](#)]
47. Kokina, I.; Plaksenkova, I.; Jermalonoka, M.; Petrova, A. Impact of iron oxide nanoparticles on yellow medick (*Medicago falcata* L.) plants. *J. Plant. Inter.* **2020**, *15*, e1708489. [[CrossRef](#)]

48. Yang, A.; Wu, J.; Deng, C.; Wang, T.; Bian, P. Genotoxicity of Zinc Oxide Nanoparticles in Plants Demonstrated Using Transgenic *Arabidopsis thaliana*. *Bull. Environ. Contam. Toxicol.* **2018**, *101*, 514–520. [[CrossRef](#)] [[PubMed](#)]
49. Demirel, G.S.; Silva, T.N.; Jackson, C.T.; Thomas, J.B.; Ehrhardt, S.W.; Rhee, S.Y.; Mortimer, J.C.; Landry, M.P. Nanotechnology to advance CRISPR—Cas genetic engineering of plants. *Nat. Nanotechnol.* **2021**, *16*, 243–250. [[CrossRef](#)] [[PubMed](#)]
50. Boldrin, A.; Hansen, S.F.; Baun, A.; Hartmann, N.I.B.; Astrup, T.F. Environmental Exposure Assessment Framework for Nanoparticles in Solid Waste. *J. Nanopart. Res.* **2014**, *16*, 2394. [[CrossRef](#)]
51. Hjorth, R.; Holden, P.A.; Hansen, S.F.; Colman, B.P.; Griegerf, K.; Hendrene, C.O. The role of alternative testing strategies in environmental risk assessment of engineered nanomaterials. *Environ. Sci. Nano* **2017**, *4*, 292–301. [[CrossRef](#)]
52. Marmioli, M.; Pagano, L.; Rossi, R.; De La Torre-Roche, R.; Lepore, G.O.; Ruotolo, R.; Gariani, G.; Bonanni, V.; Pollastri, S.; Puri, A.; et al. Copper Oxide Nanomaterial Fate In Plant Tissue: Nanoscale Impacts On Reproductive Tissues. *Environ. Sci. Technol.* **2021**, *55*, 10769–10783. [[CrossRef](#)]
53. EFSA Scientific Committee. Guidance on risk assessment of nanomaterials to be applied in the food and feed chain: Human and animal health. *EFSA J.* **2021**, *19*, e06768. [[CrossRef](#)]





Review

# Direct and Indirect Genotoxicity of Graphene Family Nanomaterials on DNA—A Review

Kangying Wu <sup>1,2</sup>, Qixing Zhou <sup>1,2,\*</sup> and Shaohu Ouyang <sup>1,2,\*</sup>

<sup>1</sup> Key Laboratory of Pollution Processes and Environmental Criteria (Ministry of Education)/Tianjin Key Laboratory of Environmental Remediation and Pollution Control, Nankai University, Tianjin 300350, China; wukangyingcool@163.com

<sup>2</sup> College of Environmental Science and Engineering, Nankai University, Tianjin 300350, China

\* Correspondence: zhouqx@nankai.edu.cn (Q.Z.); ouyangshaohu@nankai.edu.cn (S.O.)

**Abstract:** Graphene family nanomaterials (GFNs), including graphene, graphene oxide (GO), reduced graphene oxide (rGO), and graphene quantum dots (GQDs), have manifold potential applications, leading to the possibility of their release into environments and the exposure to humans and other organisms. However, the genotoxicity of GFNs on DNA remains largely unknown. In this review, we highlight the interactions between DNA and GFNs and summarize the mechanisms of genotoxicity induced by GFNs. Generally, the genotoxicity can be sub-classified into direct genotoxicity and indirect genotoxicity. The direct genotoxicity (e.g., direct physical nucleus and DNA damage) and indirect genotoxicity mechanisms (e.g., physical destruction, oxidative stress, epigenetic toxicity, and DNA replication) of GFNs were summarized in the manuscript, respectively. Moreover, the influences factors, such as physicochemical properties, exposure dose, and time, on the genotoxicity of GFNs are also briefly discussed. Given the important role of genotoxicity in GFNs exposure risk assessment, future research should be conducted on the following: (1) developing reliable testing methods; (2) elucidating the response mechanisms associated with genotoxicity in depth; and (3) enriching the evaluation database regarding the type of GFNs, applied dosages, and exposure times.

**Citation:** Wu, K.; Zhou, Q.; Ouyang, S. Direct and Indirect Genotoxicity of Graphene Family Nanomaterials on DNA—A Review. *Nanomaterials* **2021**, *11*, 2889. <https://doi.org/10.3390/nano11112889>

**Keywords:** graphene family nanomaterials; genotoxicity; DNA damage; safety; toxicity

Academic Editor: Marta Marmiroli

Received: 21 September 2021

Accepted: 21 October 2021

Published: 28 October 2021

**Publisher's Note:** MDPI stays neutral with regard to jurisdictional claims in published maps and institutional affiliations.



**Copyright:** © 2021 by the authors. Licensee MDPI, Basel, Switzerland. This article is an open access article distributed under the terms and conditions of the Creative Commons Attribution (CC BY) license (<https://creativecommons.org/licenses/by/4.0/>).

## 1. Introduction

Graphene, a two-dimensional crystal repeatedly peeled from graphite, is a single layer of carbon atoms with a  $sp^2$ -hybridized structure (Figure 1a) [1,2]. Graphene and its derivatives, including graphene oxide (GO), reduced graphene oxide (rGO), and graphene quantum dots (GQDs), exhibit various excellent physical, electrochemical, and optical advantages [3–5]. GO is an amphiphilic sheet-like graphenic carbon and contains fewer oxygen functional groups (Figure 1b) [6,7]. rGO is prepared by oxidative exfoliation of graphite and has lower C/O ratios than GO (Figure 1c) [8]. GQDs are similar to graphene but have unique zero-dimensional structures due to their nanoscale sized lateral dimensions (Figure 1d) [9].

Currently, GFNs, as promising nanomaterials, have attracted increasing attention in the scientific community and are in commercial production for many applications, such as energy storage [10–17], medicine [18–25], environmental protection [26–31], and industrial manufacturing [32–34]. For example, the market for graphene-based products is forecast to reach \$675 million by 2020 [35]. With rapid developments in application and production of GFNs, their potential for release into the environment and the environmental risks of GFNs have become emerging issues [36–38]. Consequently, many studies have shown that adverse effects can be induced by GFNs in vivo and in vitro, such as organ (e.g., lung, liver, and spleen) toxicity, cytotoxicity, immunotoxicity, neurotoxicity, and reproductive and developmental toxicity [3,39]. Moreover, the toxicity mechanisms of GFNs to organisms, including physical destruction, oxidative stress, inflammatory response, apoptosis,

autophagy, and necrosis, are summarized in Table 1. However, the genotoxicity of GFNs on DNA (e.g., DNA damage) remains largely unknown.

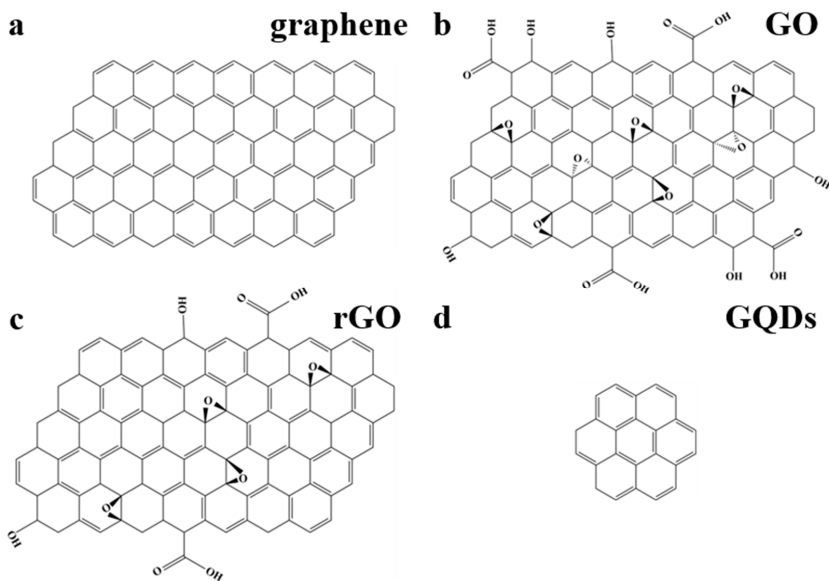


**Figure 1.** Structural models of single-layer graphene (a), graphene oxide (b), reduced graphene oxide (c), and graphene quantum dots (d).

Genotoxicity is broadly defined as ‘damage to the genome’ and also a distinct and important type of toxicity, as specific genotoxic events are considered hallmarks of cancer [40]. Generally, the genotoxicity can be sub-classified into direct genotoxicity and indirect genotoxicity in cells or the nucleus [41–43]. Nanoparticles (NPs) can be uptaken by the nucleus and induce DNA damage, leading to direct genotoxicity on organisms [42]. While many studies have shown that most NPs cannot enter the nucleus, they still indirectly affect genotoxicity by oxidative stress, epigenetic changes, inflammation, and autophagy [42]. Moreover, genotoxicity plays a key role in assessing the safety of NPs on human health and the environment [44–47]. Although there has been many researches about the genotoxicity of NPs in recent years, it is mainly focused on traditional artificial nanomaterials, such as TiO<sub>2</sub>, carbon nanotubes, and silver and gold NPs [48–50]. However, the existing literature on genotoxicity of GFNs remains limited and conflicting. A few studies showed that GFNs had no adverse effects on genotoxicity [51]. In contrast, many researchers have reported that the small size and sharp edges of GFNs (e.g., GO and GQDs) can induce genotoxicity on aquatic organisms (e.g., fish and algae) [52–54]. However, the direct and indirect genotoxicity mechanisms of GFNs remain unclear, despite genotoxic phenomena being widely reported.

The purpose of this article is to critically review the existing literatures on the genotoxicity of GFNs. This review will focus mainly on the genotoxicity mechanisms of GFNs in order to (1) expand our understanding of possible mechanisms underlying the promotion of DNA damage by GFNs; (2) highlight the direct and indirect genotoxicity of different subsets of GFNs; and (3) explore the factors that influence the genotoxicity of GFNs. This review will provide new insights into the genotoxicity and environmental risks of engineered nanoparticles (ENPs).

**Table 1.** The toxicity of GFNs in vivo and in vitro.

Products	Supplier or Synthesis Methods	Dose	Animal or Cell Models	Toxicological Mechanisms	Adverse Effects	Ref.
graphene nanoplatelets	cheaptubes.com (Brattleboro, VT, USA)	0.3, 1 mg/rat	rat	oxidative stress, inflammation	lung inflammation	[55]
commercial GO and rGO	Nanjing XFNANO Materials Tech Co., Ltd., (China)	2.0 mg/kg body weight	rat	transcriptional and epigenetic	liver zoned accumulation	[56]
amination QDs	Nanjing XFNANO Materials Tech Co., Ltd., (China)	100, 200 µg/mL	A549 cells	autophagy	cytotoxicity	[57]
carboxylated QDs						
hydroxylated QDs						
GO and rGO oxidated from carbon nanofibers	Grupo Antolin (Spain)	0.1, 1.0, 10, 50 mg/L	erythrocyte cell	oxidative stress	genotoxicity	[58]
GO nanosheets	Sigma-Aldrich (St. Louis, MO, USA)	40, 60, 80 mg/L	Human SH-SY5Y neuroblastoma cell	oxidative stress, autophagy-lysosomal network dysfunction	cytotoxicity	[59]
pristine rGO	Chengdu Organic Chemicals Co., Ltd., the Chinese Academy of Sciences	1–100 mg/L	Earthworm coelomocytes	oxidative stress	immunotoxicity	[60]
single layer GO (product no. GNOP10A5)	ACS Materials LLC (Medford, MA, USA)	1, 10, 50, 150, 250, 500 mg/L	<i>Escherichia coli</i>	physical destruction	toxicity against bacteria	[61]
GO	modified Hummers method	25 mg/L	THP-1 and BEAS-2B cells	lipid peroxidation, membrane adsorption, membrane damage	cytotoxicity	[62]
GO	modified Hummers method	2 mg/kg	rat	lipid peroxidation, membrane adsorption, membrane damage	acute lung inflammation	[62]
GO	Nanjing XFNANO Materials Tech Co., Ltd., (China)	0–100 mg/L	zebrafish embryos	oxidative stress	developmental toxicity	[63]
GO	modified Hummers method	10 mg/L	<i>Caenorhabditis elegans</i>	oxidative stress	toxicity	[64]
graphene, GO	modified Hummers method	3.125–200 mg/L	human erythrocytes and skin fibroblasts	oxidative stress	cytotoxicity	[65]
graphene exfoliated form graphite, GO oxidated from carbon fibers	Grupo Antolin Ingenieria (Burgos, Spain)	1, 10 mg/L	primary neurons	inhibition of synaptic transmission, altered calcium homeostasis	neurotoxicity	[66]

## 2. Direct Genotoxicity of GFNs

Adsorption on DNA is a critical physiochemical process at the DNA–GFNs interface due to large surface area and surface-active properties of the GFNs. This process can (1) induce the direct genotoxicity of GFNs (e.g., DNA damage); and (2) alter the function of DNA through coating and modification by GFNs. In reviewing the current literature, the adsorption of GFNs on DNA and molecular interactions were investigated.

### 2.1. Direct Physical Nucleus Damage by GFNs

After GFNs exposure, monolayer or a few-layer GFNs (GO and rGO) sheets are able to cut and penetrate cell membranes and the cell wall (if present), resulting in direct physical membrane damage [67,68]. Moreover, small pieces of GFNs will enter the nucleus, interacting directly with DNA [69]. Generally, nuclear DNA is the main target of gene toxicity [42]. Prokaryotes (e.g., bacteria) only have naked DNA without a nuclear envelope. GFNs can directly contact bacteria RNA/DNA hydrogen groups, interrupting the replicative stage after internalization [70]. During mitosis, GFNs are likely to interact with DNA, leading to DNA aberration when the nuclear membrane ruptures [3]. As shown in Figure 2, the nuclear uptake and nuclear response related to contact with QGDs have been systematically reported by using atomic force microscopy (Figure 2a,b), confocal microscopy (Figure 2c,d), transmission electron microscopy (Figure 2e,f), and high content screening (Figure 2g,h) [69]. QGDs are mainly uptaken into cells via energy-dependent endocytosis, phagocytosis, and caveolae-mediated endocytosis. More than half of QGDs are exposed and accumulated in the nucleus by microscopy investigation. The accumulated QGDs may direct contact with DNA strand, thereby causing physical damage. After 1 h exposure, the rGO nanoplatelet can pierce the nucleus of the human mesenchymal stem cells (hMSCs), leading to DNA fragmentation and chromosomal aberrations at 0.1 and 1.0 mg/L. Notably, rGO sheets with the same size or larger size showed no genotoxicity in the hMSCs after 24 h exposure at 100 mg/L [71]. The single-layer rGO nanoribbons can penetrate into the hMSCs nucleus at 100 mg/L detected by confocal fluorescence imaging, and cells showed a high degree of DNA fragmentation. The above DNA damage is mainly related to oxidative stress caused by DNA released, rather than DNA damage within the nucleus. Interestingly, rGO nanoribbons showed no significant cytotoxicity at 1.0 mg/L but can induce genotoxicity through DNA fragmentation and chromosomal aberrations in the hMSCs [72]. In a word, GFNs can interact directly with chromatin and DNA, causing DNA damage and thus exhibiting genotoxicity.

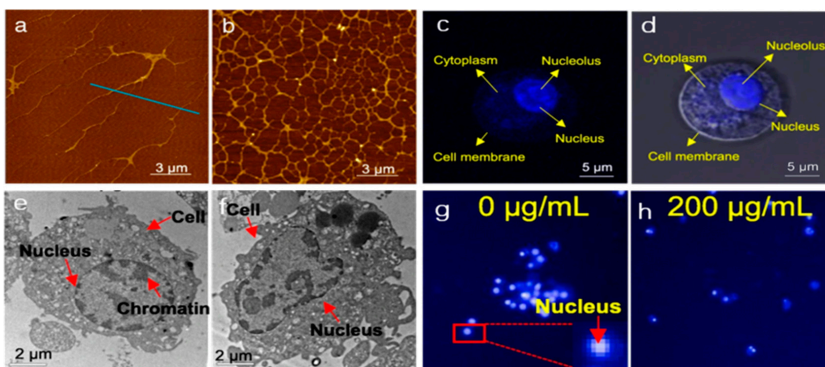


**Figure 2.** Effects of QGDs on the nucleus and DNA in the nucleus. (a,b) DNA chain damage caused by QGDs; (c,d) accumulation of QGDs; (e,f) nuclear damage by QGDs; (g,h) effect of QGDs on nuclear viability and area; (a,c,e,g) are the blank control groups, and (b,d,f,h) are the exposed groups of 200 mg/L QGDs for 24 h, reproduced from [69], from BioMed Central, 2018.

## 2.2. Interaction Mechanisms between DNA and GFNs

Interaction between GFNs and DNA is critical for understanding and assessing direct genotoxicity. DNA is a biological macromolecule with a repetitive nucleotide structure that controls biological functions. The backbone of DNA is a regular sequence of deoxyribose sugar and phosphate groups. DNA is always negatively charged at most pH values [73]. The oxidized domains of GO are rich in oxygen-containing groups (e.g., epoxides, hydroxyl, carboxyl, and carbonyl groups). The negatively charged carboxyl groups would electrostatically repel negatively charged DNA and use hydrogen bonding as the main attraction force [47]. The GFNs mainly interact with DNA via H-bonding and  $\pi$ - $\pi$  stacking, causing the DNA distortion and even DNA cleavage. The DNA damaging mechanism of GQDs depends on their size. The small GQDs easily enter the DNA molecule leading to DNA base mismatch. Large GQDs tend to stick to the ends of the DNA molecule, causing the DNA to unfold [74]. The zipper-like unfolding of double-stranded DNA caused by graphene wrinkles has been investigated by using molecular dynamics simulations. The results show that the zipper pattern brings more DNA bases into contact with the wrinkled region, resulting in accelerated deformation of double-stranded DNA [75]. The GO combining with copper ions can intercalate into DNA molecules and cleave DNA fragments, and the system of this DNA cleavage is oxidative and hydrolytic [76]. Unlike AuNPs, which rely on stronger DNA base coordination, the adsorption of GO is weak, owing to the weak binding affinity [77]. Furthermore, the GO surface shows great heterogeneity for DNA adsorption and hydrophobic regions for exclusion of DNA. Thus, both the external environment and the physicochemical property (e.g., oxidized degree and size) have a strong influence on the adsorption capacity of GO [47,76–78]. Further research into the direct effects of GFNs on DNA or genetic material is important to explain GFN-mediated targeted genotoxicity.

## 3. Indirect Genotoxicity of GFNs

Although GFNs can induce direct genotoxicity, most of the current studies focus on GFNs' indirect genotoxicity on the indirect effect on gene normal tissue expression. Indirect genotoxicity covers different aspects. Here, we describe the indirect genotoxicity of GFNs in the following aspects: oxidative stress, epigenetic toxicity, DNA replication, repair and transcription affected by GFNs, and inflammation and autophagy.

### 3.1. Oxidative Stress

The internalization NPs by organism can induce intracellular reactive oxygen species (ROS) generation and antioxidant defense. ROS generation can lead to typical oxidative DNA damage (e.g., single- and double-stranded DNA breaks, DNA cross-links, and base modifications) [78–80]. Indirect genotoxicity of GFNs mediated by oxidative stress has been explored *in vivo* and *in vitro*. For instance, ROS generation and ROS-dependent DNA damage and genotoxicity were observed in human retinal pigment epithelium (ARPE-19) cells after 24 h exposure to GO and rGO [81]. Similarly, GO and rGO can also trigger genotoxicity of female C57BL/6 mice by induction of oxidative stress [82]. Exposed to few-layer graphene (FLG), the indirect DNA damage in THP-1 macrophages and human-transformed type-I alveolar epithelial cells was also driven by oxidative stress [43]. The specific induced mechanisms of indirect DNA damage are identified by baseline levels of micronuclei induction. Moreover, the indirect genotoxicity induced by FLG also correlates with an increase of inflammatory mediator (IL-8), decreased antioxidant (rGSH), and a depletion in mitochondrial ATP production [83]. Zhao et al. reported that GO can induce oxidative stress and genotoxicity in earthworms and the excessive accumulation of ROS, leading to lipid peroxidation, lysosomal membrane damage, and DNA damage [84]. Organisms possess a well-developed inhibition of antioxidant defense, including ROS-scavenging enzymes (e.g., superoxide dismutase (SOD), peroxidase, and catalase) and regulatory mechanisms to protect organisms from the negative effects of ROS [46,84]. The ROS generation benefitted from inhibition of fatty acid, carbohydrate, and amino acid metabolism [85]. ROS induced by GO seemed to be the main mechanism leading to human

lung fibroblast (HLF) cells of genotoxicity [86]. Natural nanocolloids (Ncs) can mediate the phytotoxicity of GO such that GO–Ncs induced stronger ROS production and DNA damage compared with GO alone [87]. The mitochondrial oxidative stress induced by GQDs in microglia can cause ferroptosis.

### 3.2. Epigenetic Toxicity

Epigenetic regulatory mechanisms can be observed after exposure to NPs, including DNA methylation, histone modification, non-coding RNA (ncRNA) gene expression regulation, and dynamic chromatin organization [88,89]. As a response to internal and external stimuli, these above epigenetic regulations and complex, time-specific, and tissue-specific control of gene expression were allowed during development and differentiation [90]. DNA methylation, a covalent modification of cytosine residues in DNA, plays a supreme role in the stabilization and regulation of gene expression during development or differentiation [91,92]. Ting et al. [91] firstly proved that GQDs can inhibit the DNA methylation of transcription factor Sox2 and regulated DNA methyltransferase and demethyltransferase expressions. Global DNA hypomethylation of caprine fetal fibroblast cells, which are exposed to GO–AgNPs, might result from oxidative stress [93]. Histone modifications containing phosphorylation, methylation, and acetylation also are major components of epigenetic regulatory mechanisms [92]. The role of epigenetic regulation about toxicity of GFNs has been described in human embryonic kidney 293T cells [89]. The results showed that the GO triggered the formation of new intra-chromosomal looping (A1–A3) and enhanced and promoted cyclo-oxygenase-2 (Cox2) expression and activation. The epigenetic mechanisms of GO on transgenerational reproductive toxicity were determined using a house crickets generational experiment [94].

GO can activate microRNA (miRNA) protection regulation and inhibit the reproductive toxicity of *Caenorhabditis elegans*, which was also an epigenetic signal encoded protection mechanism [95]. Moreover, miRNAs can activate death receptor pathways by altering the expression of caspase-3 and tumor necrosis factor  $\alpha$  receptor in GO-exposed pulmonary adenocarcinoma (GLC-82) cells [96]. Therefore, the epigenetic process induced by GFNs are complex and multi-layered. Currently, the existing studies are mainly limited to the reactions of epigenetic toxicity induced indirect genotoxicity of GFNs. How to explain the causal epigenetic mechanisms induced by GFNs remains challenging. Future experimental studies should be carefully designed for better understanding the genotoxic effects of GFNs induced epigenetic modifications that directly or indirectly cause DNA damage.

### 3.3. The DNA Replication, Repair, and Transcription Affected by GFNs

GFNs have the ability to alter gene expression by interacting with signal transduction cascades or replication/repair/transcription mechanisms [97,98]. GO exposure activates a variety of signaling pathways, triggering the expression of many kinds of genes related to autophagy, apoptosis, and necrosis [89,99]. Cell apoptosis and the upregulation of the tumor protein p53 gene in the cell cycle induced by both nano- and micro-sized GO was detected [99]. In the work, both nano- and micro-sized GO block the cell cycle in the S phase, a critical period in the cell cycle. The GQDs (100 mg/L) can induce genotoxicity through ROS generation and inhibition of gene regulation in the cell cycle of rat alveolar macrophage cells [100]. The key genes (such as RAD51, BRCA2, ATM, and PARP1) regulate some key biological processes (e.g., nucleosome assembly, stress response, protein folding, and DNA damage) in FLG-exposed human primary endothelial cells [97]. Moreover, related study have shown that GFNs may cause genotoxicity by affecting the nucleotide excision repair and the repair system of non-homologous end connections [101].

### 3.4. Inflammation

Inflammation, including acute and chronic inflammation, is a complex biological response to harmful stimuli such as pathogens, poisons, or dead cells [102]. GO induced

high expression of Cox2, a hallmark of inflammation and which is involved in acute and chronic diseases [103]. Inflammation is also one of the reactions of ROS induced indirect genotoxicity [104]. Chronic inflammation can induce secondary genotoxicity, which is manifested in the accumulation of reactive oxygen species, after GFNs exposed to cells [43,105]. Interestingly, there was no oxidative damage and a weak anti-inflammatory response for assessing the potential genotoxicity of GO and graphene nanoplatelets in the human intestinal barrier in vitro model simulation [106]. However, both GO and GNPs can induce DNA breaks, and GO can activate the nuclear factor kappa-B signaling pathway, which may lead to macrophage inflammation [107]. Excess inflammatory cytokines can cause DNA damage [108]. There are complex causal interactions between inflammation and ROS, and they may have independent induction mechanisms. In summary, the genotoxicity of GFNs mediated by inflammation can be attributed to the direct stimulation, secondary effect of cytokine release or ROS accumulation.

### 3.5. Autophagy

Autophagy, a cell survival mechanism, is described as a highly regulated intracellular catabolic pathway involving degradation of unnecessary or dysfunctional components to maintain cell homeostasis [109,110]. Autophagy controls transformation of nuclear components (e.g., nuclear lamina, chromatin, and DNA), which is important for maintaining genomic stability [111]. Inhibition of autophagy obstructs normal DNA damage repair and induces cell death in response to genotoxic stress. GFNs can induced ROS generation in mitochondria, which begin to exert autophagy to avoid oxidative damage and to reduce mutation of mitochondrial DNA [112]. GO was able to result in accumulation of autophagosomes, reduction in autophagic degradation, and lysosomal impairment [113]. Autophagy and epigenetic changes jointly regulate cell survival, and autophagy may be a downstream mechanism of epigenetic changes, one of the manifestations of secondary genotoxicity [114]. Graphene oxide quantum dot exposure induced autophagy in a ROS-dependent manner [115]. The relationship between autophagy and DNA damage is complex, while autophagy can regulate the levels of various proteins participating in the repair and detection of damaged DNA [116]. The relationship between autophagy and other toxicity mechanisms (e.g., oxidative stress, epigenetic changes, apoptosis, and inflammation) of other GFNs is still unclear [114]. Understanding GFNs-mediated autophagy is of great significance to explain the genotoxicity of GFNs.

## 4. Factors Influencing Genotoxicity of GFNs

As is known to all, there is a strong correlation between cytotoxicity and the physicochemical properties of NPs, such as particle size and shape, surface characteristics, and surface functionalization. Similarly, the genotoxicity of GFNs can be affected by these factors [117]. The genotoxicity of GFNs is greatly varied in the literature, which can be attributed to numerous factors including physicochemical properties (morphology, surface chemistry, size, shape, and purity), dose, test species, exposure time, and exposure assay [80,118].

### 4.1. Surface Properties

The oxygen-containing functional groups play a key role in the genotoxicity of GFNs [58,81–83,119]. For example, the rGO with lower oxygen content can induce stronger genotoxicity on ARPE-19 cells than these GO with higher oxygen content, suggesting that GO has a better biocompatibility owing to more saturated C–O bonds [81]. The remove of epoxy groups from the GO surface mitigates GO in vivo genotoxicity toward *Xenopus laevis* tadpoles [58]. Compared with GO, graphene, rGO, and graphite all induce higher levels of genotoxicity in glioblastoma multiforme cells, and the difference was attributed to the hydrophilic and hydrophobic surface and edge structure of GFNs [119]. GO has hydrophilic properties and smooth and regular edges, while rGO and graphene have hydrophobic properties and sharp and irregular edges, which can damage the integrity of cell membranes

greatly. The carboxyl groups in the surface of carboxyl-FLG may scavenge oxidative radical on bronchial epithelial cells to alleviate the genotoxicity of FLG [83]. Moreover, different immunological mechanisms triggered by GFNs can be attributed to the proportion of hydroxyl groups [82]. Cells produce a stronger inflammatory response after being exposed to GO than rGO by detecting transcriptomic changes, and the reason is attributed to the large number of hydroxyl groups on the surface of GO [82]. The surface functionalization also can significantly modulate the toxicity of GFNs [53,85,86,120]. For example, amino functionalized GQDs induced lower ferroptosis effects than nitrogen-doped GQDs [85]. Similarly, the DNA methylation of various tissues induced by GQDs was depend on their different surface chemical modifications [53]. Increased cytotoxicity and genotoxicity of the aminated GO were detected by following 24 h exposure on Colon 26 cells [120]. A study on the genotoxicity reduced by GO and rGO showed that the GTPs-rGO reduced by green tea polyphenols (GTPs) yielded more biocompatible and reduced sheets with lower genotoxic effects, as compared to the  $N_2H_4$ -rGO, which were reduced by hydrazine ( $N_2H_4$ ) [121]. The acid-polyethylene glycol (LA-PEG) and PEG modified GO induced gentle DNA damage and decreased the genotoxicity of GO to HLF cells [86]. Surface charge also influences significantly the genotoxicity of GFNs [86,122]. The genotoxic effect of GO on cells is proportional to the amount of positive charge on the surface [86]. The surface charge density of graphene in aqueous solution can transform to chemically-converted graphene, leading to the capture of large amounts of DNA [122]. The different hydrophilic and hydrophobic properties of GO/rGO regulated by differential surface chemistry (especially the O/C ratio) determine the potential of graphene to interact with organisms [123–125]. Despite hydrophilic and hydrophobic rGO exhibiting similar toxic responses (e.g., cytotoxicity, DNA damage, and oxidative stress) to cells, their biological and molecular mechanisms are different [123]. The hydrophilic GO and hydrophobic rGO induce both kinds of DNA damage, namely single stranded and double stranded breaks, but the dose dependency was very significant and evident in GO exposure in DNA damage but not in rGO exposure [123]. Hydrophilicity, also an important factor in determining the biocompatibility and colloidal stability of GFNs, leads to different interactions with cells and bio-distribution of GFNs [124,125]. For example, simple accumulation of hydrophobic pristine graphene on the surface of monkey kidney cells without any cellular internalization led to severe metabolic toxicity, whereas hydrophilic GO was internalized by the cells and concentrated near the perinuclear region without causing any toxicity under lower concentrations [124]. Therefore, the surface properties play an important role in understanding the genotoxicity manifestations and biological and molecular mechanisms of GFNs.

#### 4.2. Size and Structure

The genotoxicity of GFNs within organisms is size-dependent. Compared with large GFNs, small GFNs have bigger surface areas and provide more sites to interact with cells, leading to greater cellular uptake of GFNs [126]. The size effect plays a key role in the genotoxicity of GFNs. For example, small rGO (average lateral dimensions 114 nm) induce higher genotoxicity in the hMSCs than large rGO ( $3.8 \pm 0.4 \mu\text{m}$ ) at 0.1 and 1.0  $\mu\text{g}/\text{mL}$  after 1 h exposure. The lateral size and extremely sharp edged structure of GFNs can result in higher permeability to the cell and nucleus, resulting in greater genotoxicity. Similarly, the size of GFNs is an important determinant of subcellular penetration [126]. Li et al. [127] suggested that the larger the lateral size of GO, the more severe is the pyroptosis induced by GO in Kupffer cells. Moreover, there is a strong correlation between the size of GO and the structural change in small-interfering RNAs [128]. The large GO merely reduces the A-helical pitch, while small GO inserted into the double strands can wreak havoc on the RNA conformation [129]. In addition, Kong et al. [74] proved that the DNA damage mechanism of GQDs was limited by the size of GQDs through molecular dynamics simulations. Briefly, the relatively large GQDs (61 benzene rings) tend to stick to the ends of the DNA molecule, causing the DNA to unfold, while the small GQDs (seven benzene rings) are easily embedded in DNA molecules, leading to DNA base mismatches.

The planar structure of GFNs may also have an effect on DNA damage. The dsDNA bases have a stronger binding affinity with wrinkled GFNs and even cause more DNA damage than with planar GFNs [75]. Given these discordant results, it is necessary to clarify the size- and structure-related genotoxicity of GFNs.

#### 4.3. Exposure Dose and Time

The dose–response relationship is an important principle in nanotoxicology [42]. The modified GQDs may induce DNA hypermethylation in a time and dose dependent manner [53]. The high-dose (50 mg/L) GO induces more serious DNA methylation (hypermethylation) than low-dose (10 mg/L) treatment [101]. The effective accumulation of GFNs in the nucleus is regulated by two nuclear pore complex genes (Kap $\beta$ 2 and Nup98), and their cellular internalization and absorption are related to exposure time [69]. Notably, the rGO sheets with the same size or larger size, higher concentration (100  $\mu$ g/mL), and longer exposure time (24 h) showed no obvious genotoxicity in the hMSCs [71]. Overall, there are few studies on the genotoxicity of GFNs doses, and especially the combination of GFNs type and dose exposure is rare.

#### 4.4. The Resistance of Cell Structures and Biological Barriers

From an organism's perspective, the responses of various types of cells, organs, and tissues with different structures and functions to GFNs exposure were highly diverse. Internalization and direct contact membrane stress with extremely sharp edges of GFNs are considered as important mechanisms of toxicity [130,131]. For different bacterial models to graphene toxicity, the outer membranes can better "protect" bacteria from graphene [132]. The biological barrier is crucial for mammals against the damage from GFNs [3,117]. Both GO and graphene were able to induce DNA breaks in an in vitro model simulating the human intestinal barrier [106]. Moreover, GO nanosheets could break through the first line of host defense by disrupting the ultrastructure and biophysical properties of lung surfactant membranes [133]. Combined with the routes and doses of human exposure, relevant biological barriers toxicity can be considered as an aspect of assessing GFNs genotoxicity.

### 5. Genotoxicity Testing of GFNs

#### 5.1. Detection of GFNs in Cells and Organism Tissues

The detection of GFNs internalization (distribution and behavior) in model organisms and cells is a key step for a better understanding of their genotoxicity and underlying mechanisms. The most commonly used detection technique includes direct observation of localization of GFNs in organisms and cells by transmission electron microscopy (TEM) [88]. The hyperspectral imaging is also used to visualize cellular interactions with NPs [134], such as cellular uptake and binding of GFNs [87]. The label-based approaches to image GFNs exist in cells by confocal and fluorescence microscopy, reflection-based imaging, and flow cytometry. Additionally, scanning electron microscopy (SEM) can be used to detect the attachment of GFNs in the surface zone of cells [52,87]. Raman spectroscopy and atomic force microscopy (AFM) were used to evaluate nuclear area changes and the disruption of DNA chains impacted by GQDs, respectively [69]. However, these traditional techniques are limited by low observation efficiency and large errors of quantitative results, with are disadvantages in the detection of GFNs [88]. Few studies focus on GFNs nuclear detecting techniques. In the biological imaging field, most research pays attention to safe application of fluorescent GFNs nuclear images rather than assessing genotoxicity of GFNs from an environmental toxicology point of view [135–137]. It is necessary to further optimize and develop detection techniques of GFNs in cells and organism tissues for a better understanding of genotoxicity. For example, Chen et al. [138] used laser desorption/ionization mass spectrometry imaging to map and quantify precisely the sub-organ distribution of the carbon nanotubes, GO, and carbon nanodots in mice. The SEM–Raman spectroscopy co-located system provide both SEM and Raman data from the

same area on the cell sample, which avoids sample registration issues and makes observed results more accurate [139].

### 5.2. Genotoxicity Assay of GFNs

There are several assays available to access the genotoxicity of GFNs, measuring various endpoints [98]. The Ames test (bacterial reverse mutation), the comet assay (single cell gel electrophoresis), the chromosomal aberration (CHA), and micronuclei (MN) are the most common tests for genotoxicity. The Ames test (bacterial reverse mutation) can provide initial testing for genotoxicity. The comet assay can detect DNA damage, while the CHA and MN can test large chromosomal abnormalities. The hypoxanthine phosphoribosyl transferase (HPRT) gene is suitable for assessing mutations induced by suspect genotoxic agents, such as NPs [98]. Oxidative DNA damage should be considered one of the causes of genotoxicity. Superoxide radicals can lead to the activation of oxidation of the guanine bases present in the DNA strands, causing rupture to these strands. The most commonly used detection techniques include 8-hydroxydeoxyguanosine and 7, 8-dihydro-oxodeoxyguanine by HPLC with electrochemical detection [140].

## 6. Conclusions, Challenges, and Perspectives

On the basis of the existing literatures, we propose several genotoxic effects for GFNs in Figure 3. To date, there are few studies on genotoxicity mediated by direct interactions with DNA for GFNs (only GO and QGDs). That oxidative stress induced by GFNs causes DNA damage has been well established and studied. Regarding other indirect genotoxicity (e.g., epigenetic toxicity, inflammation, and autophagy), the studies largely focus on genotoxic effects induced by GFNs, and there is a lack of studies on the mechanisms underlying the observed effects. The genotoxicity of GFNs will depend on both inherent physicochemical properties (e.g., surface functionalization and coatings), exposure dose and times, and their fate in organisms or the environment. Although this review paper provides preliminary information on the genotoxicity of GFNs, the data is still very limited, especially with regard to the type of GFNs and exposure dose. The traditional techniques are limited by low observation efficiency and large errors of quantitative results, which are disadvantages in the detection of GFNs.

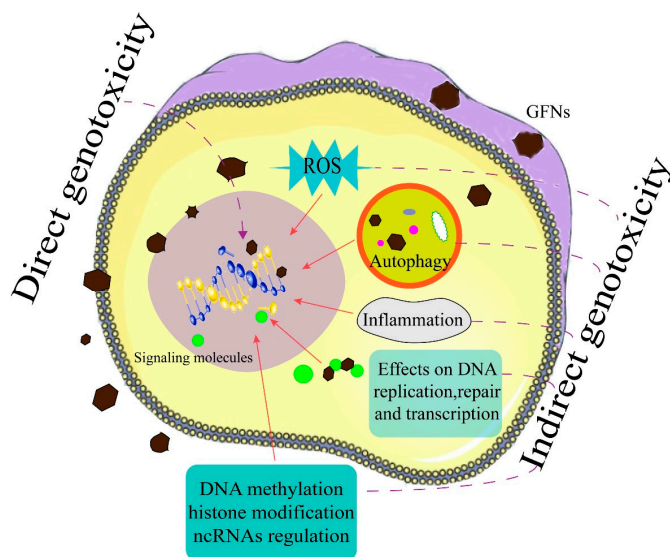


**Figure 3.** Direct and indirect effects of GFNs on DNA.

A number of issues remain in this area: (1) a lack of nuclear detecting and tracking techniques for GFNs to investigate the direct interactions of GFNs with DNA; (2) a challenge to reveal mechanisms underlying the indirect genotoxicity of GFNs, such as causal epigenetic mechanisms; and (3) an incomplete evaluation database regarding the type of GFNs, applied dosages, and exposure times, etc. These limitations are expected since genotoxicity research of NPs, especially GFNs, is still in their infancy when compared to other areas of toxicity (e.g., cytotoxicity, immunotoxicity, neurotoxicity, reproductive and developmental toxicity). Overall, further studies should address the questions mentioned above to clarify the genotoxic mechanisms of GFNs.

**Author Contributions:** Conceptualization, K.W. and S.O.; methodology, K.W.; software, K.W.; validation, K.W., Q.Z. and S.O.; formal analysis, K.W.; investigation, S.O.; resources, Q.Z.; data curation, K.W.; writing—original draft preparation, K.W.; writing—review and editing, S.O.; visualization, K.W.; supervision, Q.Z.; project administration, S.O.; funding acquisition, S.O. All authors have read and agreed to the published version of the manuscript.

**Funding:** This work was financially supported by the National Natural Science Foundation of China for grant number No. U1906222, the National Key Research and Development Project for grant number No. 2019YFC1804104, the Fellowship of China Postdoctoral Science Foundation for grant number No. 2020M680867, and the Ministry of Education, People's Republic of China as a 111 program for grant number No. T2017002.

**Data Availability Statement:** Not applicable.

**Acknowledgments:** The authors thank Jing Sun and Zhicheng Bi for their assistance in paper discussion. We thank all the reviewers for their constructive comments.

**Conflicts of Interest:** The authors declare no conflict of interest.

## References

- Novoselov, K.S.; Geim, A.K.; Morozov, S.V.; Jiang, D.; Zhang, Y.; Dubonos, S.V.; Grigorieva, I.V.; Firsov, A.A. Electric field effect in atomically thin carbon films. *Science* **2004**, *306*, 666–669. [[CrossRef](#)]
- Castro Neto, A.H.; Guinea, F.; Peres, N.M.R. Drawing conclusions from graphene. *Phys. World* **2006**, *19*, 33–37. [[CrossRef](#)]
- Ou, L.; Song, B.; Liang, H.; Liu, J.; Feng, X.; Deng, B.; Sun, T.; Shao, L. Toxicity of graphene-family nanoparticles: A general review of the origins and mechanisms. *Part. Fibre Toxicol.* **2016**, *13*, 57. [[CrossRef](#)] [[PubMed](#)]
- Liang, L.; Kong, Z.; Kang, Z.; Wang, H.; Zhang, L.; Shen, J.-W. Theoretical evaluation on potential cytotoxicity of graphene quantum dots. *ACS Biomater. Sci. Eng.* **2016**, *2*, 1983–1991. [[CrossRef](#)] [[PubMed](#)]
- Huang, X.; Qi, X.Y.; Boey, F.; Zhang, H. Graphene-based composites. *Chem. Soc. Rev.* **2012**, *41*, 666–686. [[CrossRef](#)] [[PubMed](#)]
- Lerf, A.; He, H.Y.; Forster, M.; Klinowski, J. Structure of graphite oxide revisited. *J. Phys. Chem. B* **1998**, *102*, 4477–4482. [[CrossRef](#)]
- Mattevi, C.; Eda, G.; Agnoli, S.; Miller, S.; Mkhoyan, K.A.; Celik, O.; Mastrogianni, D.; Granozzi, G.; Garfunkel, E.; Chhowalla, M. Evolution of electrical, chemical, and structural properties of transparent and conducting chemically derived graphene thin films. *Adv. Funct. Mater.* **2009**, *19*, 2577–2583. [[CrossRef](#)]
- Singh, V.; Joung, D.; Zhai, L.; Das, S.; Khondaker, S.I.; Seal, S. Graphene based materials: Past, present and future. *Prog. Mater. Sci.* **2011**, *56*, 1178–1271. [[CrossRef](#)]
- Yan, Y.; Gong, J.; Chen, J.; Zeng, Z.; Huang, W.; Pu, K.; Liu, J.; Chen, P. Recent advances on graphene quantum dots: From chemistry and physics to applications. *Adv. Mater.* **2019**, *31*, 1808283. [[CrossRef](#)] [[PubMed](#)]
- Chen, T.-T.; Song, W.-L.; Fan, L.-Z. Engineering graphene aerogels with porous carbon of large surface area for flexible all-solid-state supercapacitors. *Electrochim. Acta* **2015**, *165*, 92–97. [[CrossRef](#)]
- Kumar, R.; Sahoo, S.; Joanni, E.; Singh, R.K.; Tan, W.K.; Kar, K.K.; Matsuda, A. Recent progress in the synthesis of graphene and derived materials for next generation electrodes of high performance lithium ion batteries. *Prog. Energy Combust. Sci.* **2019**, *75*, 100786. [[CrossRef](#)]
- Li, G.; Huang, B.; Pan, Z.; Su, X.; Shao, Z.; An, L. Advances in three-dimensional graphene-based materials: Configurations, preparation and application in secondary metal (Li, Na, K, Mg, Al)-ion batteries. *Energy Environ. Sci.* **2019**, *12*, 2030–2053. [[CrossRef](#)]
- Li, Z.; Liu, X.; Wang, L.; Bu, F.; Wei, J.; Pan, D.; Wu, M. Hierarchical 3D all-carbon composite structure modified with N-doped graphene quantum dots for high-performance flexible supercapacitors. *Small* **2018**, *14*, 1801498. [[CrossRef](#)]
- Tsai, M.L.; Wei, W.-R.; Tang, L.; Chang, H.-C.; Tai, S.-H.; Yang, P.-K.; Lau, S.P.; Chen, L.-J.; He, J.-H. Si Hybrid Solar Cells with 13% Efficiency via concurrent improvement in optical and electrical properties by employing graphene quantum dots. *ACS Nano* **2016**, *10*, 815–821. [[CrossRef](#)] [[PubMed](#)]

15. Young, C.; Park, T.; Yi, J.W.; Kim, J.; Hossain, M.S.A.; Kaneti, Y.V.; Yamauchi, Y. Advanced functional carbons and their hybrid nanoarchitectures towards supercapacitor applications. *ChemSuschem* **2018**, *11*, 3546–3558. [[CrossRef](#)] [[PubMed](#)]
16. Zhao, Y.-Q.; Zhao, D.-D.; Tang, P.-Y.; Wang, Y.-M.; Xu, C.-L.; Li, H.-L. MnO<sub>2</sub>/graphene/nickel foam composite as high performance supercapacitor electrode via a facile electrochemical deposition strategy. *Mater. Lett.* **2012**, *76*, 127–130. [[CrossRef](#)]
17. Zhou, S.; Lin, M.; Zhuang, Z.; Liu, P.; Chen, Z. Biosynthetic graphene enhanced extracellular electron transfer for high performance anode in microbial fuel cell. *Chemosphere* **2019**, *232*, 396–402. [[CrossRef](#)] [[PubMed](#)]
18. Afsahi, S.; Lerner, M.B.; Goldstein, J.M.; Lee, J.; Tang, X.; Bagarozzi, D.A., Jr.; Pan, D.; Locascio, L.; Walker, A.; Barron, F.; et al. Novel graphene-based biosensor for early detection of Zika virus infection. *Biosens. Bioelectron.* **2018**, *100*, 85–88. [[CrossRef](#)]
19. Chen, H.; Wang, Z.; Zong, S.; Chen, P.; Zhu, D.; Wu, L.; Cui, Y. A graphene quantum dot-based FRET system for nuclear-targeted and real-time monitoring of drug delivery. *Nanoscale* **2015**, *7*, 15477–15486. [[CrossRef](#)] [[PubMed](#)]
20. Iannazzo, D.; Pistone, A.; Ferro, S.; De Luca, L.; Monforte, A.M.; Romeo, R.; Buemi, M.R.; Pannecouque, C. Graphene quantum dots based systems as HIV inhibitors. *Bioconjug. Chem.* **2018**, *29*, 3084–3093. [[CrossRef](#)]
21. Li, N.; Than, A.; Chen, J.; Xi, F.; Liu, J.; Chen, P. Graphene quantum dots based fluorescence turn-on nanoprobe for highly sensitive and selective imaging of hydrogen sulfide in living cells. *Biomater. Sci.* **2018**, *6*, 779–784. [[CrossRef](#)] [[PubMed](#)]
22. Li, N.; Than, A.; Sun, C.; Tian, J.; Chen, J.; Pu, K.; Dong, X.; Chen, P. Monitoring dynamic cellular redox homeostasis using fluorescence-switchable graphene quantum dots. *ACS Nano* **2016**, *10*, 11475–11482. [[CrossRef](#)]
23. Li, N.; Than, A.; Wang, X.; Xu, S.; Sun, L.; Duan, H.; Xu, C.; Chen, P. Ultrasensitive profiling of metabolites using tyramine-functionalized graphene quantum dots. *ACS Nano* **2016**, *10*, 3622–3629. [[CrossRef](#)]
24. Ma, N.; Liu, J.; He, W.; Li, Z.; Luan, Y.; Song, Y.; Garg, S. Folic acid-grafted bovine serum albumin decorated graphene oxide: An efficient drug carrier for targeted cancer therapy. *J. Colloid Interface Sci.* **2017**, *490*, 598–607. [[CrossRef](#)] [[PubMed](#)]
25. Marzo, A.M.L.; Mayorga-Martinez, C.C.; Pumera, M. 3D-printed graphene direct electron transfer enzyme biosensors. *Biosens. Bioelectron.* **2020**, *151*, 111980. [[CrossRef](#)]
26. Divyapriya, G.; Vijayakumar, K.K.; Nambi, I. Development of a novel graphene/Co<sub>3</sub>O<sub>4</sub> composite for hybrid capacitive deionization system. *Desalination* **2019**, *451*, 102–110. [[CrossRef](#)]
27. Gan, L.; Li, H.; Chen, L.; Xu, L.; Liu, J.; Geng, A.; Mei, C.; Shang, S. Graphene oxide incorporated alginate hydrogel beads for the removal of various organic dyes and bisphenol A in water. *Colloid Polym. Sci.* **2018**, *296*, 607–615. [[CrossRef](#)]
28. Liu, S.; Ge, H.; Wang, C.; Zou, Y.; Liu, J. Agricultural waste/graphene oxide 3D bio-adsorbent for highly efficient removal of methylene blue from water pollution. *Sci. Total Environ.* **2018**, *628–629*, 959–968. [[CrossRef](#)]
29. Miao, W.; Li, Z.-K.; Yan, X.; Guo, Y.-J.; Lang, W.-Z. Improved ultrafiltration performance and chlorine resistance of PVDF hollow fiber membranes via doping with sulfonated graphene oxide. *Chem. Eng. J.* **2017**, *317*, 901–912. [[CrossRef](#)]
30. Zhang, D.; Zhao, Y.; Chen, L. Fabrication and characterization of amino-grafted graphene oxide modified ZnO with high photocatalytic activity. *Appl. Surf. Sci.* **2018**, *458*, 638–647. [[CrossRef](#)]
31. Zhu, Z.; Jiang, J.; Wang, X.; Huo, X.; Xu, Y.; Li, Q.; Wang, L. Improving the hydrophilic and antifouling properties of polyvinylidene fluoride membrane by incorporation of novel nanohybrid GO@SiO<sub>2</sub> particles. *Chem. Eng. J.* **2017**, *314*, 266–276. [[CrossRef](#)]
32. Afroj, S.; Tan, S.; Abdelkader, A.M.; Novoselov, K.S.; Karim, N. Highly conductive, scalable, and machine washable graphene-based e-textiles for multifunctional wearable electronic applications. *Adv. Funct. Mater.* **2020**, *30*, 2000293. [[CrossRef](#)]
33. Kurra, N.; Jiang, Q.; Nayak, P.; Alshareef, H.N. Laser-derived graphene: A three-dimensional printed graphene electrode and its emerging applications. *Nano Today* **2019**, *24*, 81–102. [[CrossRef](#)]
34. Liu, C.; Qiu, S.; Du, P.; Zhao, H.; Wang, L. An ionic liquid-graphene oxide hybrid nanomaterial: Synthesis and anticorrosive applications. *Nanoscale* **2018**, *10*, 8115–8124. [[CrossRef](#)]
35. Ahmed, F.; Rodrigues, D.F. Investigation of acute effects of graphene oxide on wastewater microbial community: A case study. *J. Hazard. Mater.* **2013**, *256*, 33–39. [[CrossRef](#)] [[PubMed](#)]
36. Arvidsson, R.; Molander, S.; Sanden, B.A. Review of potential environmental and health risks of the nanomaterial graphene. *Hum. Ecol. Risk Assess.* **2013**, *19*, 873–887. [[CrossRef](#)]
37. Lee, J.H.; Han, J.H.; Kim, J.H.; Kim, B.; Bello, D.; Kim, J.K.; Lee, G.H.; Sohn, E.K.; Lee, K.; Ahn, K.; et al. Exposure monitoring of graphene nanoplatelets manufacturing workplaces. *Inhal. Toxicol.* **2016**, *28*, 281–291. [[CrossRef](#)]
38. Pelin, M.; Sosa, S.; Prato, M.; Tubaro, A. Occupational exposure to graphene based nanomaterials: Risk assessment. *Nanoscale* **2018**, *10*, 15894–15903. [[CrossRef](#)]
39. Seabra, A.B.; Paula, A.J.; De Lima, R.; Alves, O.L.; Duran, N. Nanotoxicity of graphene and graphene oxide. *Chem. Res. Toxicol.* **2014**, *27*, 159–168. [[CrossRef](#)]
40. Zhou, J.; Ouedraogo, M.; Qu, F.; Duez, P. Potential genotoxicity of traditional chinese medicinal plants and phytochemicals: An overview. *Phytother. Res.* **2013**, *27*, 1745–1755. [[CrossRef](#)]
41. Bohne, J.; Cathomen, T. Genotoxicity in gene therapy: An account of vector integration and designer nucleases. *Curr. Opin. Mol. Ther.* **2008**, *10*, 214–223.
42. Huang, R.; Zhou, Y.; Hu, S.; Zhou, P.-K. Targeting and non-targeting effects of nanomaterials on DNA: Challenges and perspectives. *Rev. Environ. Sci. Biotechnol.* **2019**, *18*, 617–634. [[CrossRef](#)]
43. Burgum, M.J.; Clift, M.J.D.; Evans, S.J.; Hondow, N.; Tarat, A.; Jenkins, G.J.; Doak, S.H. Few-layer graphene induces both primary and secondary genotoxicity in epithelial barrier models in vitro. *J. Nanobiotechnol.* **2021**, *19*, 24. [[CrossRef](#)]

44. De Souza, T.A.J.; Souza, L.R.R.; Franchi, L.P. Silver nanoparticles: An integrated view of green synthesis methods, transformation in the environment, and toxicity. *Ecotoxicol. Environ. Saf.* **2019**, *171*, 691–700. [[CrossRef](#)]
45. Mortezaee, K.; Najafi, M.; Samadian, H.; Barabadi, H.; Azarnezhad, A.; Ahmadi, A. Redox interactions and genotoxicity of metal-based nanoparticles: A comprehensive review. *Chem. Biol. Interact.* **2019**, *312*, 108814. [[CrossRef](#)]
46. Lam, P.L.; Wong, R.S.M.; Lam, K.H.; Hung, L.K.; Wong, M.M.; Yung, L.H.; Ho, Y.W.; Wong, W.Y.; Hau, D.K.P.; Gambari, R.; et al. The role of reactive oxygen species in the biological activity of antimicrobial agents: An updated mini review. *Chem. Biol. Interact.* **2020**, *320*, 109023. [[CrossRef](#)]
47. Liu, B.; Zhao, Y.; Jia, Y.; Liu, J. Heating Drives DNA to Hydrophobic regions while freezing drives DNA to hydrophilic regions of graphene oxide for highly robust biosensors. *J. Am. Chem. Soc.* **2020**, *142*, 14702–14709. [[CrossRef](#)] [[PubMed](#)]
48. Lan, J.; Gou, N.; Gao, C.; He, M.; Gu, A.Z. Comparative and mechanistic genotoxicity assessment of nanomaterials via a quantitative toxicogenomics approach across multiple species. *Environ. Sci. Technol.* **2014**, *48*, 12937–12945. [[CrossRef](#)] [[PubMed](#)]
49. Cavallo, D.; Fanizza, C.; Ursini, C.L.; Casciardi, S.; Paba, E.; Ciervo, A.; Fresegna, A.M.; Maiello, R.; Marcelloni, A.M.; Buresti, G.; et al. Multi-walled carbon nanotubes induce cytotoxicity and genotoxicity in human lung epithelial cells. *J. Appl. Toxicol.* **2012**, *32*, 454–464. [[CrossRef](#)]
50. Kim, Y.J.; Rahman, M.M.; Lee, S.M.; Kim, J.M.; Park, K.; Kang, J.-H.; Seo, Y.R. Assessment of in vivo genotoxicity of citrated-coated silver nanoparticles via transcriptomic analysis of rabbit liver tissue. *Int. J. Nanomed.* **2019**, *14*, 393–405. [[CrossRef](#)] [[PubMed](#)]
51. Jarosz, A.; Skoda, M.; Dudek, I.; Szukiewicz, D. Oxidative stress and mitochondrial activation as the main mechanisms underlying graphene toxicity against human cancer cells. *Oxid. Med. Cell. Longev.* **2016**, *2016*, 5851035. [[CrossRef](#)]
52. Ouyang, S.; Hu, X.; Zhou, Q. Envelopment-internalization synergistic effects and metabolic mechanisms of graphene oxide on single-cell *Chlorella vulgaris* are dependent on the nanomaterial particle size. *ACS Appl. Mater. Interfaces* **2015**, *7*, 18104–18112. [[CrossRef](#)] [[PubMed](#)]
53. Hu, J.; Lin, W.; Lin, B.; Wu, K.; Fan, H.; Yu, Y. Persistent DNA methylation changes in zebrafish following graphene quantum dots exposure in surface chemistry-dependent manner. *Ecotoxicol. Environ. Saf.* **2019**, *169*, 370–375. [[CrossRef](#)] [[PubMed](#)]
54. Zhao, J.; Wang, Z.; White, J.C.; Xing, B. Graphene in the aquatic environment: Adsorption, dispersion, toxicity and transformation. *Environ. Sci. Technol.* **2014**, *48*, 9995–10009. [[CrossRef](#)]
55. Lee, J.K.; Jeong, A.Y.; Bae, J.; Seok, J.H.; Yang, J.-Y.; Roh, H.S.; Jeong, J.; Han, Y.; Jeong, J.; Cho, W.-S. The role of surface functionalization on the pulmonary inflammogenicity and translocation into mediastinal lymph nodes of graphene nanoplatelets in rats. *Arch. Toxicol.* **2017**, *91*, 667–676. [[CrossRef](#)]
56. Wu, Y.; Feng, W.; Liu, R.; Xia, T.; Liu, S. Graphene oxide causes disordered zonation due to differential intralobular localization in the liver. *ACS Nano* **2020**, *14*, 877–890. [[CrossRef](#)]
57. Xie, Y.; Wan, B.; Yang, Y.; Cui, X.; Xin, Y.; Guo, L.-H. Cytotoxicity and autophagy induction by graphene quantum dots with different functional groups. *J. Environ. Sci.* **2019**, *77*, 198–209. [[CrossRef](#)] [[PubMed](#)]
58. Evariste, L.; Lagier, L.; Gonzalez, P.; Mottier, A.; Mouchet, F.; Cadarsi, S.; Lonchambon, P.; Daffe, G.; Chimowa, G.; Sarrieu, C.; et al. Thermal reduction of graphene oxide mitigates its in vivo genotoxicity toward xenopus laevis tadpoles. *Nanomaterials* **2019**, *9*, 584. [[CrossRef](#)]
59. Feng, X.L.; Zhang, Y.Q.; Luo, R.H.; Lai, X.; Chen, A.J.; Zhang, Y.L.; Hu, C.; Chen, L.L.; Shao, L.Q. Graphene oxide disrupted mitochondrial homeostasis through inducing intracellular redox deviation and autophagy-lysosomal network dysfunction in SH-SY5Y cells. *J. Hazard. Mater.* **2021**, *416*, 126158.
60. Xu, K.; Wang, X.; Lu, C.; Liu, Y.; Zhang, D.; Cheng, J. Toxicity of three carbon-based nanomaterials to earthworms: Effect of morphology on biomarkers, cytotoxicity, and metabolomics. *Sci. Total Environ.* **2021**, *777*, 146224. [[CrossRef](#)]
61. Barrios, A.C.; Wang, Y.; Gilbertson, L.M.; Perreault, F. Structure-property-toxicity relationships of graphene oxide: Role of surface chemistry on the mechanisms of interaction with bacteria. *Environ. Sci. Technol.* **2019**, *53*, 14679–14687. [[CrossRef](#)]
62. Li, R.; Guiney, L.M.; Chang, C.H.; Mansukhani, N.D.; Ji, Z.; Wang, X.; Liao, Y.-P.; Jiang, W.; Sun, B.; Hersam, M.C.; et al. Surface oxidation of graphene oxide determines membrane damage, lipid peroxidation, and cytotoxicity in macrophages in a pulmonary toxicity model. *ACS Nano* **2018**, *12*, 1390–1402. [[CrossRef](#)] [[PubMed](#)]
63. Chen, Y.; Ren, C.; Ouyang, S.; Hu, X.; Zhou, Q. Mitigation in multiple effects of graphene oxide toxicity in zebrafish embryogenesis driven by humic acid. *Environ. Sci. Technol.* **2015**, *49*, 10147–10154. [[CrossRef](#)]
64. Ding, X.; Rui, Q.; Zhao, Y.; Shao, H.; Yin, Y.; Wu, Q.; Wang, D. Toxicity of graphene oxide in nematodes with a deficit in the epidermal barrier caused by RNA interference knockdown of unc-52. *Environ. Sci. Technol. Lett.* **2018**, *5*, 622–628. [[CrossRef](#)]
65. Liao, K.-H.; Lin, Y.-S.; Mocosko, C.W.; Haynes, C.L. Cytotoxicity of graphene oxide and graphene in human erythrocytes and skin fibroblasts. *ACS Appl. Mater. Interfaces* **2011**, *3*, 2607–2615. [[CrossRef](#)] [[PubMed](#)]
66. Bramini, M.; Sacchetti, S.; Armirotti, A.; Rocchi, A.; Vazquez, E.; Leon Castellanos, V.; Bandiera, T.; Cesca, F.; Benfenati, F. Graphene oxide nanosheets disrupt lipid composition, Ca<sup>2+</sup> homeostasis, and synaptic transmission in primary cortical neurons. *ACS Nano* **2016**, *10*, 7154–7171. [[CrossRef](#)] [[PubMed](#)]
67. Tu, Y.; Lv, M.; Xiu, P.; Huynh, T.; Zhang, M.; Castelli, M.; Liu, Z.; Huang, Q.; Fan, C.; Fang, H.; et al. Destructive extraction of phospholipids from *Escherichia coli* membranes by graphene nanosheets. *Nat. Nanotechnol.* **2013**, *8*, 594–601. [[CrossRef](#)] [[PubMed](#)]

68. Lammel, T.; Boisseaux, P.; Fernandez-Cruz, M.-L.; Navas, J.M. Internalization and cytotoxicity of graphene oxide and carboxyl graphene nanoplatelets in the human hepatocellular carcinoma cell line Hep G2. *Part. Fibre Toxicol.* **2013**, *10*, 27. [[CrossRef](#)] [[PubMed](#)]
69. Xu, L.; Dai, Y.; Wang, Z.; Zhao, J.; Li, F.; White, J.C.; Xing, B. Graphene quantum dots in alveolar macrophage: Uptake-exocytosis, accumulation in nuclei, nuclear responses and DNA cleavage. *Part. Fibre Toxicol.* **2018**, *15*, 45. [[CrossRef](#)]
70. Mohammed, H.; Kumar, A.; Bekyarova, E.; Al-Hadeethi, Y.; Zhang, X.; Chen, M.; Ansari, M.S.; Cochis, A.; Rimondini, L. Antimicrobial mechanisms and effectiveness of graphene and graphene-functionalized biomaterials. A scope review. *Front. Bioeng. Biotechnol.* **2020**, *8*, 465. [[CrossRef](#)]
71. Akhavan, O.; Ghaderi, E.; Akhavan, A. Size-dependent genotoxicity of graphene nanoplatelets in human stem cells. *Biomaterials* **2012**, *33*, 8017–8025. [[CrossRef](#)] [[PubMed](#)]
72. Akhavan, O.; Ghaderi, E.; Emamy, H.; Akhavan, F. Genotoxicity of graphene nanoribbons in human mesenchymal stem cells. *Carbon* **2013**, *54*, 419–431. [[CrossRef](#)]
73. Liu, B.; Salgado, S.; Maheshwari, V.; Liu, J. DNA adsorbed on graphene and graphene oxide: Fundamental interactions, desorption and applications. *Curr. Opin. Colloid Interface Sci.* **2016**, *26*, 41–49. [[CrossRef](#)]
74. Kong, Z.; Hu, W.; Jiao, F.; Zhang, P.; Shen, J.; Cui, B.; Wang, H.; Liang, L. Theoretical evaluation of DNA genotoxicity of graphene quantum dots: A combination of density functional theory and molecular dynamics simulations. *J. Phys. Chem. B* **2020**, *124*, 9335–9342. [[CrossRef](#)]
75. Li, B.; Zhang, Y.; Meng, X.-Y.; Zhou, R. Zipper-Like unfolding of dsDNA caused by graphene wrinkles. *J. Phys. Chem. C* **2020**, *124*, 3332–3340. [[CrossRef](#)]
76. Ren, H.; Wang, C.; Zhang, J.; Zhou, X.; Xu, D.; Zheng, J.; Guo, S.; Zhang, J. DNA cleavage system of nanosized graphene oxide sheets and copper ions. *ACS Nano* **2010**, *4*, 7169–7174. [[CrossRef](#)]
77. Liu, J. Adsorption of DNA onto gold nanoparticles and graphene oxide: Surface science and applications. *Phys. Chem. Chem. Phys.* **2012**, *14*, 10485–10496. [[CrossRef](#)]
78. Flores-Lopez, L.Z.; Espinoza-Gomez, H.; Somanathan, R. Silver nanoparticles: Electron transfer, reactive oxygen species, oxidative stress, beneficial and toxicological effects. mini review. *J. Appl. Toxicol.* **2019**, *39*, 16–26. [[CrossRef](#)]
79. Toyokuni, S. Oxidative stress and cancer: The role of redox regulation. *Biotherapy* **1998**, *11*, 147–154. [[CrossRef](#)]
80. Singh, N.; Manshian, B.; Jenkins, G.J.S.; Griffiths, S.M.; Williams, P.M.; Maffei, T.G.G.; Wright, C.J.; Doak, S.H. NanoGenotoxicology: The DNA damaging potential of engineered nanomaterials. *Biomaterials* **2009**, *30*, 3891–3914. [[CrossRef](#)]
81. Ou, L.; Lv, X.; Wu, Z.; Xia, W.; Huang, Y.; Chen, L.; Sun, W.; Qi, Y.; Yang, M.; Qi, L. Oxygen content-related DNA damage of graphene oxide on human retinal pigment epithelium cells. *J. Mater. Sci. Mater. Med.* **2021**, *32*, 20. [[CrossRef](#)] [[PubMed](#)]
82. Poulsen, S.S.; Bengtson, S.; Williams, A.; Jacobsen, N.R.; Troelsen, J.T.; Halappanavar, S.; Vogel, U. A transcriptomic overview of lung and liver changes one day after pulmonary exposure to graphene and graphene oxide. *Toxicol. Appl. Pharmacol.* **2021**, *410*, 115343. [[CrossRef](#)] [[PubMed](#)]
83. Burgum, M.J.; Clift, M.J.D.; Evans, S.J.; Hondow, N.; Miller, M.; Lopez, S.B.; Williams, A.; Tarat, A.; Jenkins, G.J.; Doak, S.H. In vitro primary-indirect genotoxicity in bronchial epithelial cells promoted by industrially relevant few-layer graphene. *Small* **2021**, *17*, 2002551. [[CrossRef](#)] [[PubMed](#)]
84. Zhao, S.; Wang, Y.; Duo, L. Biochemical toxicity, lysosomal membrane stability and DNA damage induced by graphene oxide in earthworms. *Environ. Pollut.* **2021**, *269*, 116225. [[CrossRef](#)]
85. Wu, T.; Liang, X.; Liu, X.; Li, Y.; Wang, Y.; Kong, L.; Tang, M. Induction of ferroptosis in response to graphene quantum dots through mitochondrial oxidative stress in microglia. *Part. Fibre Toxicol.* **2020**, *17*, 30. [[CrossRef](#)]
86. Wang, A.; Pu, K.; Dong, B.; Liu, Y.; Zhang, L.; Zhang, Z.; Duan, W.; Zhu, Y. Role of surface charge and oxidative stress in cytotoxicity and genotoxicity of graphene oxide towards human lung fibroblast cells. *J. Appl. Toxicol.* **2013**, *33*, 1156–1164. [[CrossRef](#)]
87. Ouyang, S.; Zhou, Q.; Zeng, H.; Wang, Y.; Hu, X. Natural nanocolloids mediate the phytotoxicity of graphene oxide. *Environ. Sci. Technol.* **2020**, *54*, 4865–4875. [[CrossRef](#)]
88. Feng, X.; Chen, Q.; Guo, W.; Zhang, Y.; Hu, C.; Wu, J.; Shao, L. Toxicology data of graphene-family nanomaterials: An update. *Arch. Toxicol.* **2020**, *94*, 1915–1939.
89. Sun, Y.; Dai, H.; Chen, S.; Xu, M.; Wang, X.; Zhang, Y.; Xu, S.; Xu, A.; Weng, J.; Liu, S.; et al. Graphene oxide regulates Cox2 in human embryonic kidney 293T cells via epigenetic mechanisms: Dynamic chromosomal interactions. *Nanotoxicology* **2018**, *12*, 117–137. [[CrossRef](#)] [[PubMed](#)]
90. Dusinska, M.; Tulinska, J.; El Yamani, N.; Kuricova, M.; Liskova, A.; Rollerova, E.; Runden-Pran, E.; Smolkova, B. Immunotoxicity, genotoxicity and epigenetic toxicity of nanomaterials: New strategies for toxicity testing? *Food Chem. Toxicol.* **2017**, *109*, 797–811. [[CrossRef](#)] [[PubMed](#)]
91. Ku, T.; Hao, F.; Yang, X.; Rao, Z.; Liu, Q.S.; Sang, N.; Faiola, F.; Zhou, Q.; Jiang, G. Graphene quantum dots disrupt embryonic stem cell differentiation by interfering with the methylation level of Sox2. *Environ. Sci. Technol.* **2021**, *55*, 3144–3155. [[CrossRef](#)]
92. Pogribna, M.; Hammons, G. Epigenetic effects of nanomaterials and nanoparticles. *J. Nanobiotechnol.* **2021**, *19*, 2. [[CrossRef](#)]
93. Yuan, Y.-G.; Cai, H.-Q.; Wang, J.-L.; Mesalam, A.; Reza, A.M.M.T.; Li, L.; Chen, L.; Qian, C. Graphene oxide-silver nanoparticle nanocomposites induce oxidative stress and aberrant methylation in caprine fetal fibroblast cells. *Cells* **2021**, *10*, 682. [[CrossRef](#)]

94. Flasz, B.; Dziejwiecka, M.; Kedziorski, A.; Tarnawska, M.; Augustyniak, M. Multigenerational graphene oxide intoxication results in reproduction disorders at the molecular level of vitellogenin protein expression in *Acheta domestica*. *Chemosphere* **2021**, *280*, 130772. [[CrossRef](#)]
95. Zhao, Y.; Wu, Q.; Wang, D. An epigenetic signal encoded protection mechanism is activated by graphene oxide to inhibit its induced reproductive toxicity in *Caenorhabditis elegans*. *Biomaterials* **2016**, *79*, 15–24. [[CrossRef](#)]
96. Li, Y.; Wu, Q.; Zhao, Y.; Bai, Y.; Chen, P.; Xia, T.; Wang, D. Response of microRNAs to in vitro treatment with graphene oxide. *ACS Nano* **2014**, *8*, 2100–2110. [[CrossRef](#)] [[PubMed](#)]
97. Sasidharan, A.; Swaroop, S.; Chandran, P.; Nair, S.; Koyakutty, M. Cellular and molecular mechanistic insight into the DNA-damaging potential of few-layer graphene in human primary endothelial cells. *Nanomedicine* **2016**, *12*, 1347–1355. [[CrossRef](#)] [[PubMed](#)]
98. Magdolenova, Z.; Collins, A.; Kumar, A.; Dhawan, A.; Stone, V.; Dusinska, M. Mechanisms of genotoxicity. A review of in vitro and in vivo studies with engineered nanoparticles. *Nanotoxicology* **2014**, *8*, 233–278. [[CrossRef](#)]
99. Hashemi, E.; Akhavan, O.; Shamsara, M.; Majd, S.A.; Sanati, M.H.; Joupari, M.D.; Farmany, A. Graphene oxide negatively regulates cell cycle in embryonic fibroblast cells. *Int. J. Nanomed.* **2020**, *15*, 6201–6209. [[CrossRef](#)] [[PubMed](#)]
100. Xu, L.; Zhao, J.; Wang, Z. Genotoxic response and damage recovery of macrophages to graphene quantum dots. *Sci. Total Environ.* **2019**, *664*, 536–545. [[CrossRef](#)]
101. Chatterjee, N.; Yang, J.; Choi, J. Differential genotoxic and epigenotoxic effects of graphene family nanomaterials (GFNs) in human bronchial epithelial cells. *Mutat. Res. Genet. Toxicol. Environ. Mutagen.* **2016**, *798*, 1–10. [[CrossRef](#)]
102. Keshavan, S.; Calligari, P.; Stella, L.; Fusco, L.; Delogu, L.G.; Fadeel, B. Nano-bio interactions: A neutrophil-centric view. *Cell Death Dis.* **2019**, *10*, 569. [[CrossRef](#)]
103. Tomlinson, A.; Appleton, I.; Moore, A.R.; Gilroy, D.W.; Willis, D.; Mitchell, J.A.; Willoughby, D.A. Cyclo-oxygenase and nitric oxide synthase isoforms in rat carrageenin-induced pleurisy. *Br. J. Pharmacol.* **1994**, *113*, 693–698. [[CrossRef](#)]
104. Khanna, P.; Ong, C.; Bay, B.H.; Baeg, G.H. Nanotoxicity: An interplay of oxidative stress, inflammation and cell death. *Nanomaterials* **2015**, *5*, 1163–1180. [[CrossRef](#)] [[PubMed](#)]
105. Evans, S.J.; Clift, M.J.D.; Singh, N.; De Oliveira Mallia, J.; Burgum, M.; Wills, J.W.; Wilkinson, T.S.; Jenkins, G.J.S.; Doak, S.H. Critical review of the current and future challenges associated with advanced in vitro systems towards the study of nanoparticle (secondary) genotoxicity. *Mutagenesis* **2017**, *32*, 233–241. [[CrossRef](#)] [[PubMed](#)]
106. Domenech, J.; Hernandez, A.; Demir, E.; Marcos, R.; Cortes, C. Interactions of graphene oxide and graphene nanoplatelets with the in vitro Caco-2/HT29 model of intestinal barrier. *Sci. Rep.* **2020**, *10*, 2793. [[CrossRef](#)] [[PubMed](#)]
107. Zhou, H.; Zhao, K.; Li, W.; Yang, N.; Liu, Y.; Chen, C.; Wei, T. The interactions between pristine graphene and macrophages and the production of cytokines/chemokines via TLR- and NF-kappa B-related signaling pathways. *Biomaterials* **2012**, *33*, 6933–6942. [[CrossRef](#)]
108. Capasso, L.; Camatini, M.; Gualtieri, M. Nickel oxide nanoparticles induce inflammation and genotoxic effect in lung epithelial cells. *Toxicol. Lett.* **2014**, *226*, 28–34. [[CrossRef](#)]
109. Mohammadinejad, R.; Moosavi, M.A.; Tavakol, S.; Vardar, D.O.; Hosseini, A.; Rahmati, M.; Dini, L.; Hussain, S.; Mandegary, A.; Klionsky, D.J. Necrotic, apoptotic and autophagic cell fates triggered by nanoparticles. *Autophagy* **2019**, *15*, 4–33. [[CrossRef](#)]
110. Rabinowitz, J.D.; White, E. Autophagy and metabolism. *Science*. **2010**, *330*, 1344–1348. [[CrossRef](#)]
111. Hewitt, G.; Korolchuk, V.I. Repair, reuse, recycle: The expanding role of autophagy in genome maintenance. *Trends Cell Biol.* **2017**, *27*, 340–351. [[CrossRef](#)] [[PubMed](#)]
112. Kurihara, Y.; Kanki, T.; Aoki, Y.; Hirota, Y.; Saigusa, T.; Uchiyama, T.; Kang, D. Mitophagy plays an essential role in reducing mitochondrial production of reactive oxygen species and mutation of mitochondrial DNA by maintaining mitochondrial quantity and quality in yeast. *J. Biol. Chem.* **2012**, *287*, 3265–3272. [[CrossRef](#)]
113. Wan, B.; Wang, Z.-X.; Lv, Q.-Y.; Dong, P.-X.; Zhao, L.-X.; Yang, Y.; Guo, L.-H. Single-walled carbon nanotubes and graphene oxides induce autophagosome accumulation and lysosome impairment in primarily cultured murine peritoneal macrophages. *Toxicol. Lett.* **2013**, *221*, 118–127. [[CrossRef](#)]
114. Feng, X.; Zhang, Y.; Zhang, C.; Lai, X.; Zhang, Y.; Wu, J.; Hu, C.; Shao, L. Nanomaterial-mediated autophagy: Coexisting hazard and health benefits in biomedicine. *Part. Fibre Toxicol.* **2020**, *17*, 53. [[CrossRef](#)]
115. Li, X.; Liu, H.; Yu, Y.; Ma, L.; Liu, C.; Miao, L. Graphene oxide quantum dots-induced mineralization via the reactive oxygen species-dependent autophagy pathway in dental pulp stem cells. *J. Biomed. Nanotechnol.* **2020**, *16*, 965–974. [[CrossRef](#)] [[PubMed](#)]
116. Eapen, V.V.; Waterman, D.P.; Lemos, B.; Haber, J.E. *Autophagy: Cancer, Other Pathologies, Inflammation, Immunity, Infection, and Aging*; Elsevier: Amsterdam, The Netherlands, 2017; pp. 213–236.
117. Szabo, P.; Zelko, R. Formulation and stability aspects of nanosized solid drug delivery systems. *Curr. Pharm. Des.* **2015**, *21*, 3148–3157. [[CrossRef](#)]
118. Ema, M.; Gamo, M.; Honda, K. A review of toxicity studies on graphene-based nanomaterials in laboratory animals. *Regul. Toxicol. Pharmacol.* **2017**, *85*, 7–24. [[CrossRef](#)]
119. Hinzmann, M.; Jaworski, S.; Kutwin, M.; Jagiello, J.; Kozinski, R.; Wierzbecki, M.; Grodzik, M.; Lipinska, L.; Sawosz, E.; Chwalibog, A. Nanoparticles containing allotropes of carbon have genotoxic effects on glioblastoma multiforme cells. *Int. J. Nanomed.* **2014**, *9*, 2409–2417.

120. Krasteva, N.; Keremidarska-Markova, M.; Hristova-Panusheva, K.; Andreeva, T.; Speranza, G.; Wang, D.Y.; Draganova-Filipova, M.; Miloshev, G.; Georgieva, M. Aminated graphene oxide as a potential new therapy for colorectal cancer. *Oxid. Med. Cell. Longev.* **2019**, *2019*, 3738980. [[CrossRef](#)]
121. Hashemi, E.; Akhavan, O.; Shamsara, M.; Rahighi, R.; Esfandiar, A.; Tayefeh, A.R. Cyto and genotoxicities of graphene oxide and reduced graphene oxide sheets on spermatozoa. *RSC Adv.* **2014**, *4*, 27213–27223. [[CrossRef](#)]
122. Liu, M.; Zhao, H.M.; Chen, S.; Yu, H.T.; Quan, X. Salt-controlled assembly of stacked-graphene for capturing fluorescence and its application in chemical genotoxicity screening. *J. Mater. Chem.* **2011**, *21*, 15266–15272. [[CrossRef](#)]
123. Chatterjee, N.; Eom, H.-J.; Choi, J. A systems toxicology approach to the surface functionality control of graphene-cell interactions. *Biomaterials* **2014**, *35*, 1109–1127. [[CrossRef](#)] [[PubMed](#)]
124. Sasidharan, A.; Panchakarla, L.S.; Chandran, P.; Menon, D.; Nair, S.; Rao, C.N.R.; Koyakutty, M. Differential nano-bio interactions and toxicity effects of pristine versus functionalized graphene. *Nanoscale* **2011**, *3*, 2461–2464. [[CrossRef](#)]
125. Franqui, L.S.; De Farias, M.A.; Portugal, R.V.; Costa, C.A.R.; Domingues, R.R.; Souza, A.G.; Coluci, V.R.; Leme, A.F.P.; Martinez, D.S.T. Interaction of graphene oxide with cell culture medium: Evaluating the fetal bovine serum protein corona formation towards in vitro nanotoxicity assessment and nanobiointeractions. *Mater. Sci. Eng. C* **2019**, *100*, 363–377. [[CrossRef](#)]
126. Borandeh, S.; Alimardani, V.; Abolmaali, S.S.; Seppala, J. Graphene family nanomaterials in ocular applications: Physicochemical properties and toxicity. *Chem. Res. Toxicol.* **2021**, *34*, 1386–1402. [[CrossRef](#)] [[PubMed](#)]
127. Li, J.; Wang, X.; Mei, K.-C.; Chang, C.H.; Jiang, J.; Liu, X.; Liu, Q.; Guiney, L.M.; Hersam, M.C.; Liao, Y.-P.; et al. Lateral size of graphene oxide determines differential cellular uptake and cell death pathways in Kupffer cells, LSECs, and hepatocytes. *Nano Today* **2021**, *37*, 101061. [[CrossRef](#)]
128. Reina, G.; Ngoc Do Quyen, C.; Nishina, Y.; Bianco, A. Graphene oxide size and oxidation degree govern its supramolecular interactions with siRNA. *Nanoscale* **2018**, *10*, 5965–5974. [[CrossRef](#)]
129. Syama, S.; Mohanan, P.V. Safety and biocompatibility of graphene: A new generation nanomaterial for biomedical application. *Int. J. Biol. Macromol.* **2016**, *86*, 546–555. [[CrossRef](#)]
130. Volkov, Y.; McIntyre, J.; Prina-Mello, A. Graphene toxicity as a double-edged sword of risks and exploitable opportunities: A critical analysis of the most recent trends and developments. *2D Mater.* **2017**, *4*, 022001. [[CrossRef](#)]
131. Yao, J.; Wang, H.; Chen, M.; Yang, M. Recent advances in graphene-based nanomaterials: Properties, toxicity and applications in chemistry, biology and medicine. *Microchim. Acta* **2019**, *186*, 395. [[CrossRef](#)]
132. Akhavan, O.; Ghaderi, E. Toxicity of graphene and graphene oxide nanowalls against bacteria. *ACS Nano* **2010**, *4*, 5731–5736. [[CrossRef](#)]
133. Hu, Q.; Jiao, B.; Shi, X.; Valle, R.P.; Zuo, Y.Y.; Hu, G. Effects of graphene oxide nanosheets on the ultrastructure and biophysical properties of the pulmonary surfactant film. *Nanoscale* **2015**, *7*, 18025–18029. [[CrossRef](#)] [[PubMed](#)]
134. Roth, G.A.; Tahiliani, S.; Neu-Baker, N.M.; Brenner, S.A. Hyperspectral microscopy as an analytical tool for nanomaterials. *Wiley Interdiscip. Rev. Nanomed. Nanobiotechnol.* **2015**, *7*, 565–579. [[CrossRef](#)] [[PubMed](#)]
135. Schroeder, K.L.; Goreham, R.V.; Nann, T. Graphene quantum dots for theranostics and bioimaging. *Pharm. Res.* **2016**, *33*, 2337–2357. [[CrossRef](#)]
136. Wu, C.; Wang, C.; Han, T.; Zhou, X.; Guo, S.; Zhang, J. Insight into the cellular internalization and cytotoxicity of graphene quantum dots. *Adv. Healthc. Mater.* **2013**, *2*, 1613–1619. [[CrossRef](#)]
137. Gao, W.; Zhang, J.; Xue, Q.; Yin, X.; Yin, X.; Li, C.; Wang, Y. Acute and subacute toxicity study of graphene-based tumor cell nucleus-targeting fluorescent nanoprobe. *Mol. Pharm.* **2020**, *17*, 2682–2690. [[CrossRef](#)] [[PubMed](#)]
138. Chen, S.; Xiong, C.; Liu, H.; Wan, Q.; Hou, J.; He, Q.; Badu-Tawiah, A.; Nie, Z. Mass spectrometry imaging reveals the sub-organ distribution of carbon nanomaterials. *Nat. Nanotechnol.* **2015**, *10*, 176–182. [[CrossRef](#)]
139. Cardell, C.; Guerra, I. An overview of emerging hyphenated SEM-EDX and Raman spectroscopy systems: Applications in life, environmental and materials sciences. *TrAC Trends Anal. Chem.* **2016**, *77*, 156–166. [[CrossRef](#)]
140. Ganguly, P.; Breen, A.; Pillai, S.C. Toxicity of nanomaterials: Exposure, pathways, assessment, and recent advances. *ACS Biomater. Sci. Eng.* **2018**, *4*, 2237–2275. [[CrossRef](#)]

MDPI  
St. Alban-Anlage 66  
4052 Basel  
Switzerland  
Tel. +41 61 683 77 34  
Fax +41 61 302 89 18  
[www.mdpi.com](http://www.mdpi.com)

*Nanomaterials* Editorial Office  
E-mail: [nanomaterials@mdpi.com](mailto:nanomaterials@mdpi.com)  
[www.mdpi.com/journal/nanomaterials](http://www.mdpi.com/journal/nanomaterials)





MDPI  
St. Alban-Anlage 66  
4052 Basel  
Switzerland

Tel: +41 61 683 77 34

[www.mdpi.com](http://www.mdpi.com)



ISBN 978-3-0365-4810-4